DEVELOPMENT OF ADSORBENTS AND PHOTOCATALYSTS USING NIGERIAN PINDIGA BENTONITIC CLAY

By

STEPHEN OLUMUYIWA FASHOLA

DEPARTMENT OF CHEMICAL ENGINEERING

AHMADU BELLO UNIVERSITY

ZARIA – NIGERIA

OCTOBER, 2014

DEVELOPMENT OF ADSORBENTS AND PHOTOCATALYSTS USING NIGERIAN PINDIGA BENTONITIC CLAY

By

Stephen Olumuyiwa FASHOLA (B. ENG. ABU ZARIA) 2008

MSc/ENG/03621/2010-2011

A THESIS SUBMITTED TO THE SCHOOL OF POSTGRADUATE STUDIES,

AHMADU BELLO UNIVERSITY, ZARIA

IN PARTIAL FULFILMENT OF THE REQUIREMENTS FOR THE AWARD OF A

MASTER OF SCIENCE DEGREE IN CHEMICAL ENGINEERING

DEPARTMENT OF CHEMICAL ENGINEERING

AHMADU BELLO UNIVERSITY, ZARIA

NIGERIA

OCTOBER, 2014

DECLARATION

I declare that the work in this thesis entitled "Development of Adsorbents and Photocatalysts Using Nigerian Pindiga Bentonitic Clay" has been carried out by me in the Department of Chemical Engineering Ahmadu Bello University, Zaria. The information derived from the literature has been duly acknowledged in the text and list of references provided. No part of this thesis was previously presented for another degree or diploma at this or any other Institution.

Stephen Olumuyiwa FASHOLA _____ _____

Signature Date

CERTIFICATION

This thesis entitled "DEVELOPMENT OF ADSORBENTS AND PHOTOCATALYSTS USING NIGERIA PINDIGA BENTONITIC CLAY" by Stephen Olumuyiwa FASHOLA meets the regulations governing the award of Master of Science in Chemical Engineering of the Ahmadu Bello University, Zaria and is approved for its contribution to knowledge and literacy presentation.

Dr. A. Hamza Chairman Supervisory Committee	_____ Signature	_____ Date
Dr. S.M. Waziri Member Supervisory Committee	_____ Signature	_____ Date
Dr. I.A. Mohammed-Dabo Head, Department of Chemical Engineering, A.B.U Zaria	_____ Signature	_____ Date
Professor A.A. Joshua Dean, School of Postgraduate Studies, A.B.U Zaria	_____ Signature	_____ Date

ACKNOWLEDGEMENT

I thank God Almighty for giving me the strength and grace to finish this project.

I take this opportunity to express my profound gratitude and deep regards to my guide Dr. A. Hamza for his exemplary guidance, monitoring and constant encouragement throughout the course of this thesis. The blessing, help and guidance given by from him time to time shall carry me a long way in the journey of life. I cannot express enough thanks to Dr. S.M. Waziri, for his unique intellectual guidance. I offer my sincere appreciation to Dr. O.A. Ajayi, for being an outstanding advisor and excellent contributor to the success of this work.

I am obliged to staff members of Department of Chemical Engineering A. B. U. Zaria, for the valuable information provided by them in their respective fields. I am grateful for their cooperation during the period of this project.

I thank Almighty, my parents, brothers and sisters for their constant encouragement without which this assignment would not be possible.

Lastly, my completion of this project could not have been accomplishedwithout the support of my classmates and friends, Johnson Fat, Jessy, Hajji Alhaji, Saliu, Nonso, Oche, Kizzo, Gabriel, Deji and Meshel.

ABSTRACT

The potential of Pindiga bentonitic clay for phenol adsorption from aqueous solution and photocatalytic degradation was studied. Pindiga bentonic clay was treated with oxalic acid and calcined at a temperature of 1000^{o}C and was successfully used as an adsorbent and for the degradation of phenol under visible light illumination. The processes were investigated by X-Ray Fluorescence (XRF), X-Ray diffraction (XRD), and surface area analysis. The clay treated with acid for 60 min (PB-60) and 5 min (PB-5) gave higher surface areas of 363.61 m^2/g and 265.99 m^2/g respectively compared with the raw (PB) and the raw calcined (PBC) with surface areas of 151.69 m^2/g and 47.13 m^2/g respectively. The adsorptions of phenol by the acid treated clays were studied using pseudo-first order, pseudo-second order kinetic models and intra-particle diffusion model. The adsorption data does not fit well with pseudo-second order kinetic model. The Freundlich and Langmuir adsorption models were used for the mathematical description of adsorption equilibrium and it was found that the experimental data fitted very well to the Freundlich model. The clay treated with acid for 60 minutes (PB-60) showed a better monolayer coverage capacity and greater affinity for phenol compared with the PB, PBC and PB-5. The increase in pH values from 5 – 11 was observed to hinder adsorption processes. Better adsorption was observed at lower pH value. Increase in catalyst dosage increases the adsorption rate. Langmuir-Hinshelwood kinetic model was employed for photocatalysis processes and the values of $k_r$and K_{LH} were calculated as 6.8483 $mgl^{-1}min^{-1}$ and 0.0034$l$$mg^{-1}$ for PB-60. PB-60 degraded phenol better than PB, PBC and PB-5 under visible light illumination. Catalyst dosages of 1.5, 2.0, 2.5 and 3.0g were used and the optimum catalyst dosage was found to be 2.5g/l for the photocatalytic degradation.

TABLE OF CONTENT

Cover Page ..... **Error! Bookmark not defined.**

Title Page ..... **Error! Bookmark not defined.**

Declaration iii

Certification iv

Acknowledgement v

Abstract vi

Table of content vii

List of Figures xii

List of Tables xiv

List of Abbreviations xv

CHAPTER ONE: INTRODUCTION 1

1.1 Preamble 1

1.2 Statement of Research Problem 3

1.3 Scope of Research 3

1.4 Aim and Objectives 3

1.5 Justification of Research 4

CHAPTER TWO: LITERATURE REVIEW 5

2.1 Introduction 5

2.2 Properties of Bentonites 6

2.2.1 Bentonite synonyms 6

2.2.2 Bentonite designations 6

2.2.3 Bentonite description 7

2.2.4 Typical bentonite chemical properties (wt. %) 8

2.3 Types of Bentonite 8

2.3.1 Sodium bentonite 9

2.3.2 Calcium bentonite 10

2.3.3 Potassium bentonite 10

2.4 Applications of Bentonite 10

2.4.1 Medical 13

2.4.2 Bentonite slurry walls in modern construction 13

2.4.3 Foundry 13

2.4.4 Cat Litter 14

2.4.5 Pelletizing of iron ore pellets 14

2.4.6 Construction and civil engineering 14

2.4.7 Adsorption 15

2.4.8 Drilling 15

2.4.9 Agriculture 15
2.4.10 Pharmaceuticals, Cosmetics and Medical Application 15
2.4.11 Detergents 16
2.4.12 Paints, Dyes and Polishes 16
2.4.13 Paper Productions 16
2.4.14 Catalysis 17
2.5 Pindiga Bentonite Clay 17
2.6 Adsorption 18
2.6.1 Adsorption applications 19
2.6.2 Sorption dynamics 19
2.6.3 Freundlich isotherm 20
2.6.4 Langmuir isotherm 21
2.6.5 Equilibrium isotherm studies 22
2.7 Photocatalysis 23
2.7.1 Mechanism of Photocatalysis 24
2.7.2 Application of photocatalysis 25
2.8 Specific Surface Area of Solids 28
2.8.1 Brunauer Emmet Teller (BET) surface area measurement 29
2.8.2 X-Ray Diffraction 32
2.8.3 Scherrer's equation 32

2.8.4 X-Ray fluorescence spectroscopy 33

2.9 Langmuir–Hinshelwood Kinetic Model of Photocatalytic Processes 34

2.10 Related Works 35

CHAPTER THREE: MATERIALS AND METHODS 37

3.1 Materials 37

3.1.1 Chemicals 37

3.1.2 Apparatus 37

3.1.3 Equipment 39

3.2 Methodology 39

3.2.1 Leaching of Pindiga bentonite clay by oxalic acid solutions 39

3.2.2 Adsorption experiments 40

3.2.3 Effect of pH 40

3.2.4 Effect of initial phenol concentration 41

3.2.5 Effect of adsorbent dose 41

3.2.6 Photocatalytic experiments 41

3.2.7 Determination of specific surface area of the clay 42

3.2.8 Detailed block diagram of the methodology 43

CHAPTER FOUR: RESULTS AND DISCUSSION 44

4.1 Leaching of clay 44

4.2 Specific Surface Areas and Crystallite Sizes of the Raw and Treated Clays 44

4.3 Characterization of the Catalysts 45

4.4 Preliminary Photocatalytic Degradation of Phenol before Adsorption Equilibrium was Established 47

4.5 Adsorption of Phenol on PB, PBC, PB-5 and PB-60 48

4.5.1 Adsorption dynamics 51

4.5.2 Equilibrium Isotherm Studies 60

4.5.3 Effect of Adsorbent Dosage 62

4.5.4 Effect of solution pH 63

4.6 Photocatalytic Degradation of Phenol Using PB, PBC, PB-5 and PB-60 64

4.6.1 Effect of pH 65

4.6.2 Effect of catalyst dosage 66

CHAPTER FIVE: CONCLUSIONS AND RECOMMENDATIONS 67

5.1 Conclusions 67

5.2 Recommendations 68

REFERENCES 69

APPENDICES

LIST OF FIGURES

Fig. 2.1 Mechanism of Photocatalysis 25

Fig. 3.1 Block Diagram of the Research Methodology 43

Fig. 4.1 Cascaded XRD patterns of (a) PB, (b) PBC, (c) PB-5 and (d) PB-60 47

Fig. 4.2 Effect of irradiation time on the photocatalytic degradation of phenol by PB, PBC, PB-5 and PB-60 48

Fig. 4.3 Percentage adsorption of phenol by PB-60 51

Fig. 4.4 Pseudo-first order kinetics of the raw and treated Pindiga clays with phenol concentration of 500mg/l 52

Fig. 4.5 Pseudo-second order kinetics of the raw and treated Pindiga clays with phenol concentration of 500mg/l 52

Fig. 4.6 Intra-particle diffusion model of the raw and treated Pindiga clays with phenol concentration of 500mg/l 53

Fig. 4.7 Pseudo-first order kinetics of the raw and treated Pindiga clays with phenol concentration of 250mg/l 54

Fig. 4.8 Pseudo-second order kinetics of the raw and treated Pindiga clays with phenol concentration of 250 mg/l 54

Fig. 4.9 Intra-particle diffusion model of the raw and treated Pindiga clays with phenol concentration of 250mg/l 55

Fig. 4.10 Pseudo-first order kinetics of the raw and treated Pindiga clays with phenol concentration of 125mg/l 56

Fig. 4.11 Pseudo-second order kinetics of the raw and treated Pindiga clays with phenol concentration of 125mg/l 56

Fig. 4.12 Intra-particle diffusion model of the raw and treated Pindiga clays with phenol concentration of 125mg/l 57

Fig. 4.13 Pseudo-first order kinetics of the raw and treated Pindiga clays with phenol concentration of 62.5mg/l 58

Fig. 4.14 Pseudo-second order kinetics of the raw and treated Pindiga clays with phenol concentration of 62.5mg/l 58

Fig. 4.15 Intra-particle diffusion model of the raw and treated Pindiga clays with phenol concentration of 62.5mg/l 59

Fig. 4.18 Percentage uptake of phenol by various dose of PB-60 at phenol concentration of 500mg/l 62

Fig. 4.19 Percentage uptake of phenol at various pH values of PB-60 at phenol concentration of 500 mg//..... 64

LIST OF TABLES

Table 3.1: List of equipment used and their specifications 39

Table 4.1: Labelling of raw Pindiga clay and developed catalysts 44

Table 4.2: Specific surface areas and particle sizes of PB, PBC, PB-5 and PB-60 44

Table 4.3 Composition of the PB, PBC, PB-5, and PB-60 46

Table 4.4 Concentration measurement for the adsorption of phenol by catalyst PB 49

Table 4.5 Concentration measurement for the adsorption of phenol by catalyst PBC 49

Table 4.6 Concentration measurement for the adsorption of phenol by catalyst PB-5 50

Table 4.7 Concentration measurement for the adsorption of phenol by catalyst PB-60 50

Table 4.8 Kinetic parameters for the adsorption of phenol by the raw and treated Pindiga clays at phenol concentration of 500mg//l 53

Table 4.9. Kinetic parameters for the adsorption of phenol by the raw and acid treated clays at phenol concentration of 250mg//l 55

Table 4.10 Kinetic parameters for the adsorption of phenol by the raw and acid treated clays at phenol concentration of 125mg//l 57

Table 4.11 Kinetic parameters for the adsorption of phenol by the raw and acid treated clays at phenol concentration of 62.5mg//l 59

Table 4.12 Equilibrium isotherm parameters for the adsorption of phenol by the raw and acid treated clays 60

Table 4.13 Percentage uptake of phenol by various dose of PB-60 at phenol concentration of 500mg/l 62

Table 4.14 Percentage uptake of phenol at various pH values of PB-60 at phenol concentration of 500 mg//l 63

Table 4.15 Derived Langmuir-Hinshelwood kinetic parameters. 65

Table 4.16 Effect of solution pH on the photocatalytic degradation of phenol by PB-60 at phenol concentration of 500mg/l 65

Table 4.17 Effect of catalyst dosage on the photocatalytic degradation of phenol with phenol concentration of 500mg/l by PB-60. 66

LIST OF ABBREVIATIONS

PCA	Photocatalytic Activity
HPO	Heterogeneous Photocatalytic Oxidation
UV	Ultraviolet
I_{max}	Maximum Intensity
XRD	X- Ray Diffraction
XRF	X- Ray Fluorescence
BET	Brunauer Emmet Teller
RMRDC	Ram Materials Research and Development Council
ChEd	Chemical Engineering Department
NGRL	Nigeria Geological Research Laboratories
PB	Raw Pindiga clay
PBC	Raw Pindiga clay calcined @1000^{o}C
PB-5	Pindiga clay treated with 0.5 M oxalic acid for 5 min and calcined @ 1000^{o}C
PB-60	Pindiga clay treated with 0.5 M oxalic acid for 60 min and calcined @ 1000^{o}C

CHAPTER ONE

INTRODUCTION

1.1 Preamble

Bentonite is an absorbent aluminium phyllosilicate, impure clay consisting mostly of montmorillonite. The absorbent clay was given the name bentonite by Wilbur C. Knight in 1898, after the Cretaceous Benton Shale near Rock River, Wyoming (Hosterman and Patterson, 1992).

There are different types of bentonite, each named after the respective dominant element, such as potassium (K), sodium (Na), calcium (Ca), and aluminium (Al). Experts debate a number of nomenclatorial problems with the classification of bentonite clays. Bentonite usually forms from weathering of volcanic ash, most often in the presence of water. However, the term bentonite, as well as similar clay called tonstein, has been used to describe clay beds of uncertain origin. For industrial purposes, two main classes of bentonite exist: sodium and calcium bentonite.

Photocatalysis, one of the advanced physico-chemical technology applicable in photodegradation of organic pollutants, has attracted much attention in recent years. Photocatalysis can generally be described as a process in which light is used to activate a substance.The photocatalyst that aid this process is itself not involved in the chemical transformation. Photocatalytic reactions are classified into homogeneous photocatalysis in which both the photocatalyst and the substrate are of the same phase and the heterogeneous photocatalysis in which both the both the photocatalyst and the substrate are of different phases. Heterogeneous photocatalysis is mainly used in cases where a light-absorbing

semiconductor is utilized, which is in contact with either a liquid or a gas phase. (Beydoun*et. al.*, 1999).

However, some obstacles hinder the wide application of iron oxide for the photocatalysis of toxic compounds. Considerable efforts have been made to enhance photocatalytic activity, such as decreasing photocatalyst size to increase surface area, combining photocatalyst with some novel metal nanoparticles, and increasing hole concentration through doping. On the other hand, improved charge separation and inhibition of charge carrier recombination are essential in improving the overall quantum efficiency for interfacial charge transfer. Iron oxide can be a good photocatalyst absorbing visible light. Compared with commonly applied TiO_2, which mainly absorbs UV light with wavelengths of <380 nm (covering only 5% of the solar spectrum).Due to TiO_2 wide band-gap of 3.2 eV, Fe_2O_3 with band-gap of 2.2 eV is an interesting n-type semi conducting material and a suitable candidate for photodegradation under visible light condition. The better photocatalytic performance of iron oxide than TiO_2 can be attributed to considerablegeneration of electron–hole pairs through the narrow band-gap illumination (Piao *et. al*., 2012).

A bentonite deposit of a probable reserve of about 700 million tonnes has been found in North-EasternNigeria.The clay in its natural form is mostly Ca-based and has properties below the standard required for drilling fluid application (RMRDC 1991). Two of the most important factors that affect the value of this raw materials are its iron oxide (Fe_2O_3) concentration and brightness (Martinez-luevanos*et al.*, 2011).Ahmed *et al*. (2012) investigated bentonite clay from Pindiga, Gombe state, Nigeria for its mineral content using X-ray diffraction (XRD) and X-ray fluorescence (XRF) techniques. They observed that the

chemical composition of Pindiga bentonite sample fromGombe State showed high contents of iron oxides of 26.54wt%.

Mohapatra*et.al.*,(2010) and Bakardjieva*et. al.*, (2006), reported that of about 16 pure phases (polymorphs) of iron oxides known, hematite (α-Fe_2O_3) which is obtained at calcination temperature of 1000^{o}C exhibits the highest photocatalytic activity.

In this work, the iron oxides in Pindiga bentonite was exploited and at calcination temperatures of 1000^{o}Cto produce a visible light active photocatalyst which was used to degrade aqueous solution of phenol.

1.2 Statement of Research Problem

Iron oxide rich bentonite clay such as Pindiga bentonitic, clay is difficult and expensive to beneficiate.Iron rich bentonitic clays have less industrial applications due to their high iron concentration and brownish/reddish colour. (Martinez-Luevanos*et. al.*, 2011).Hence, the need to find other usage for iron rich bentonitic clay.

1.3 Scope of Research

Varying the composition of Pindiga bentonite clay with oxalic acid leaching, calcination,characterization of the raw and treated clays and the evaluation of the potential of the raw and treated clays as adsorbents and visible light active photocatalysts for phenol degradation.

1.4 Aim and Objectives

The aim of this research work was to investigate the potential of iron rich bentonite as an adsorbent and visible light active photocatalysts for the degradation of phenol.

The specific objectives include:

1. To vary α-Fe_2O_3 concentration in the Pindiga bentonitic clay via oxalic acid ($H_2C_2O_4.2H_2O$) leaching followed by calcination.
2. To characterize Pindiga bentonitic clay before and after leaching and calcination using XRF, XRD, modified BET and UV-Vis techniques.
3. To study the adsorption of phenol on the raw and treated bentonites.
4. To test for the photocatalytic activities of the raw and treated bentonitesusing phenol as substrate.
5. To study the effects of time, initial concentration of phenol, pH and the clay loading on the adsorption and photocatalytic degradation of phenol.

1.5 Justification of Research

The following validates the essence of this research work:

1. Bentonite is in abundance in Nigeria (estimated reserve of over 700 million tonnes) (RMRDC, 2010).
2. Oxalic acid to be used in leaching of the clay is relatively cheap and very selective for the removal of iron from clays.
3. Visible light is easy to access.
4. This research work may make the bentonite clay under investigation find more industrial usage as adsorbent and photocatalyst.

CHAPTER TWO

LITERATURE REVIEW

2.1 Introduction

The term Bentonite was first used for a clay found in about 1890 in upper cretaceous tuff near Fort Benton, Wyoming. The main constituent, which is the determinant factor in the clay's properties, is the clay mineral montmorillonite. This in turn, derives its name from a deposit at Montmorillon, in Southern France. (http://www.20nano.com/bentonite.php).

Bentonite is a clay generated frequently from the alteration of volcanic ash, consisting predominantly of smectite minerals, usually montmorillonite. Other smectite group minerals include hectorite, saponite, beidelite and nontronite. Smectites are clay minerals, i.e. they consist of individual crystallites the majority of which are <2μm in largest dimension. Smectite crystallites themselves are three-layer clay minerals. They consist of two tetrahedral layers and one octahedral layer. In montmorillonite tetrahedral layers consisting of [SiO_4] - tetrahedrons enclose the [M (O_5,OH)]-octahedron layer (M = and mainly Al, Mg, but Fe is also often found). The silicate layers have a slight negative charge that is compensated by exchangeable ions in the intercrystallite region. The charge is so weak that the cations (in natural form, predominantly Ca^{2+}, Mg^{2+} or Na^{+} ions) can be adsorbed in this region with their hydrate shell. The extent of hydration produces intercrystalline swelling. Depending on the nature of their genesis, bentonites contain a variety of accessory minerals in addition to montmorillonite. These minerals may include quartz, feldspar, calcite and gypsum. The presence of these minerals can impact the industrial value of a deposit, reducing or increasing its value depending on the application. Bentonite presents strong colloidal properties and its volume increases several times when

coming into contact with water, creating a gelatinous and viscous fluid. The special properties of bentonite (hydration, swelling, water absorption, viscosity, thixotropy) make it a valuable material for a wide range of uses and applications(http://www.pranavsaiimpex.com/other-files/bentonite-details-photos.pdf).

Bentonite deposits are normally exploited by quarrying. Extracted bentonite is distinctly solid, even with a moisture content of approximately 30%. The material is initially crushed and, if necessary, activated with the addition of soda ash (Na_2CO_3). Bentonite is subsequently dried (air and/or forced drying) to reach a moisture content of approximately 15%. According to the final application, bentonite is either sieved (granular form) or milled (into powder and super fine powder form) (Odom, 1984).

2.2 Properties of Bentonites

2.2.1 Bentonite synonyms

These are: Sodium montmorillonite, calcium montmorillonite, saponite,taylorite, fuller's earth, wyoming sodium bentonite, hectorite, hormite clay, bentonite magma, southern bentonite, tixoton, volclay, volclay bentonite BC, wilkinite.(http://www.reade.com/products/29-minerals-and-ores-powder).

2.2.2 Bentonite designations

a) Chemical Formula: $Al_2O_34SiO_2H_2O$.

b) Chemical Name: Naturally occurring hydrated aluminum silicate.

2.2.3 Bentonite description

a. A rock composed essentially of a crystalline clay-like mineral formed by devitrification and the accompanying chemical alteration of a glassy igneous material, usually a tuff or volcanic ash.

b. **Smectite refers to a family of non-metallic clays primarily composed of hydrated sodium calcium aluminum silicate. Common names for smectite include montmorillonite or sodium montmorillonite ("sodium bentonite" or "Wyoming bentonite") and swelling bentonite ("Western bentonite").**

c. There are three types of bentonite:

   i. Natural Calcium Bentonite or Calcium Montmorillonite

   ii. Natural Sodium Bentonite or Sodium Montmorillonite

   iii. Sodium Activated Bentonites or Sodium Activated Montmorillonites

d. Bentonite minerals occur as lenses or seams containing up to 50% moisture. They are rocklike in nature and usually extracted by opencast mining (quarrying).

e. Natural sodium bentonite as the name suggests occurs with sodium as the predominant exchange cation. The name originates from its discovery near Fort Benton, USA. Sodium bentonites are characterized by high swelling, high liquid limit and high thermal durability.

f. The vast majority of the montmorillonites occurring in abundance worldwide are of the calcium type and referred to as calcium bentonites. The name montmorillonite originates from a discovery made at Montmorillon in France. Calcium bentonites are often characterized by much lower swelling and liquid limit values compared to natural sodium bentonite.

g. Sodium activated bentonites are produced by the substitution of calcium ions by sodium ions. This transformation can be achieved by the addition of a soluble sodium salt to calcium bentonite.(http://www.reade.com/products/29-minerals-and-ores-powder)

2.2.4 Typical bentonite chemical properties (wt. %)

a) Commercial Grade: SiO_2= 61.3 and Al_2O_3= 19.8

b) Food Grade: SiO_2 = 58-61, CaO= 2.0-2.5, Al_2O_3=21-22, MgO= 3-4, Na_2O= 3.7-4.2, As= 5 ppm max., and Pb= 40 ppm max.(www.reade.com/bentonite-1997)

2.3 Types of Bentonite

Bentonite is an absorbentaluminiumphyllosilicate, impure clay consisting mostly of montmorillonite. The absorbent clay was given the name bentonite by Wilbur C. Knight in 1898, after the Cretaceous Benton Shale near Rock River, Wyoming. (Hosterman and Patterson, 1992).

There are different types of bentonite, each named after the respective dominant element, such as potassium (K), sodium (Na), calcium (Ca), and aluminium (Al). Experts debate a number of nomenclatorial problems with the classification of bentonite clays. Bentonite usually forms from weathering of volcanic ash, most often in the presence of water. However, the term bentonite, as well as a similar clay called tonstein, has been used to describe clay beds of uncertain origin. For industrial purposes, two main classes of bentonite exist: sodium and calcium bentonite. In stratigraphy and tephrochronology, completely devitrified (weathered volcanic glass) ash-fall beds are commonly referred to as K-bentonites when the dominant clay species is illite. Other common clay species, and sometimes dominant, are montmorillonite and kaolinite. Kaolinite-dominated clays are

commonly referred to as tonsteins and are typically associated with coal. (Hosterman and Patterson, 1992).

2.3.1 Sodium bentonite

Sodium bentonite expands when wet, absorbing as much as several times its dry mass in water. Because of its excellent colloidal properties, it is often used in drilling mud for oil and gas wells and for geotechnical and environmental investigations.

The property of swelling also makes sodium bentonite useful as a sealant, since it provides a self-sealing, low permeability barrier. It is used to line the base of landfills to prevent migration of leachate, for quarantining metal pollutants of groundwater, and for the sealing of subsurface disposal systems for spent nuclear fuel. Similar uses include making slurry walls, waterproofing of below-grade walls, and forming other impermeable barriers, e.g., to seal off the annulus of a water well, to plug old wells. It is also used to form a barrier around newly planted trees to constrain root growth so as to prevent damage to nearby pipes, footpaths and other infrastructure.

Sodium bentonite can also be "sandwiched" between synthetic materials to create geo-synthetic clay liners (GCL) for the aforementioned purposes. This technique allows for more convenient transport and installation, and it greatly reduces the volume of sodium bentonite required.

Various surface modifications to sodium bentonite improve some rheological or sealing performance in geo-environmental applications, for example, the addition of polymers (Odom, 1984).

2.3.2 Calcium bentonite

Calcium bentonite is a useful adsorbent of ions in solution, as well as fats and oils, being a main active ingredient of fuller's earth, probably one of the earliest industrial cleaning agents. Calcium bentonite may be converted to sodium bentonite (termed sodium beneficiation or sodium activation) to exhibit many of sodium bentonite's properties by a process known as "ion exchange" (patented in 1935 by Germans U. Hofmann and K.Endell). In common usage, this means adding 5–10% of a soluble sodium salt such as sodium carbonate to wet bentonite, mixing well, and allowing time for the ion exchange to take place and water to remove the exchanged calcium. Some properties, such as viscosity and fluid loss of suspensions, of sodium-beneficiated calcium bentonite (or sodium-activated bentonite) may not be fully equivalent to those of natural sodium bentonite. For example, residual calcium carbonates (formed if exchanged cations are insufficiently removed) may result in inferior performance of the bentonite in geosyntheticliners(Odom, 1984).

2.3.3 Potassium bentonite

Also known as potash bentonite or K-bentonite, potassium bentonite is a potassium-rich illitic clay formed from alteration of volcanic ash.

2.4 Applications of Bentonite

Much of bentonite's usefulness in the drilling and geotechnical engineering industry comes from its unique rheological properties. Relatively small quantities of bentonite suspended in water form a viscous, shear thinning material. Most often, bentonite suspensions are also

thixotropic, although rare cases of rheopectic behavior have also been reported. At high enough concentrations (~60 grams of bentonite per liter of suspension), bentonite suspensions begin to take on the characteristics of a gel (a fluid with a minimum yield strength required to make it move). For these reasons it is a common component of drilling mud used to curtail drilling fluid invasion by its propensity for aiding in the formation of mud cake(http://intersac.com/bentonite/).

Bentonite can be used in cement, adhesives, ceramic bodies, and cat litter. Bentonite is also used as a binding agent in the manufacture of taconite pellets used in the steelmaking industry. Fuller's earth, an ancient dry-cleaning substance, is finely ground bentonite, typically used for purifying transformer oil. Bentonite, in small percentages, is used as an ingredient in commercially designed clay bodies and ceramic glazes. Bentonite clay is also used in pyrotechnics to make end plugs and rocket engine nozzles.

The ionic surface of bentonite has a useful property in making a sticky coating on sand grains. When a small proportion of finely ground bentonite clay is added to hard sand and wetted, the clay binds the sand particles into a moldable aggregate known as green sand used for making molds in sand casting. Some river deltas naturally deposit just such a blend of clay silt and sand, creating a natural source of excellent molding sand that was critical to ancient metalworking technology. Modern chemical processes to modify the ionic surface of bentonite greatly intensify this stickiness, resulting in remarkably dough-like yet strong casting sand mixes that stand up to molten metal temperatures.

The same effluvial deposition of bentonite clay onto beaches accounts for the variety of plasticity of sand from place to place for building sand castles. Beach sand consisting of

only silica and shell grains does not mold well compared to grains coated with bentonite clay. This is why some beaches are much better for building sand castles than others.

The self-stickiness of bentonite allows high-pressure ramming or pressing of the clay in molds to produce hard, refractory shapes, such as model rocket nozzles. Indeed, to test whether a particular brand of cat litter is bentonite, simply ram a sample with a hammer into a sturdy tube with a close-fitting rod; bentonite will form a very hard, consolidated plug that is not easily crumbled.

Bentonite also has the interesting property of adsorbing relatively large amounts of protein molecules from aqueous solutions. Therefore, it is uniquely useful in the process of winemaking, where it is used to remove excessive amounts of protein from white wines. Were it not for this use of bentonite, many or most white wines would precipitate undesirable flocculent clouds or hazes upon exposure to warmer temperatures, as these proteins denature. It also has the incidental use of inducing more rapid clarification of both red and white wines.

Bentonite can also be used as a desiccant due to its adsorption properties. Bentonite desiccants have been successfully used to protect pharmaceutical and diagnostic products from moisture degradation and extend shelf life. In fact, in the most common package environments, Bentonite Desiccants offer a higher adsorption capacity than silica gel desiccants. Bentonite complies with the FDA for contact with food and drugs(http://intersac.com/bentonite/).

Find here some uses of bentonite clay:

2.4.1 Medical

Bentonite has been prescribed as a bulk laxative, and it is also used as a base for many dermatologic formulas.Granular bentonite called Woundstat TM is now being studied for use in battlefield wound dressings.

Bentoquatam is a bentonate-based topical medication intended to act as a shield against exposure to urushiol, the oil found in plants such as poison ivy or poison oak(Bentonite from oregonstate.edu/bentonite).

2.4.2 Bentonite slurry walls in modern construction

Bentonite slurry walls are used in construction, where the slurry wall is a trench filled with a thick colloidal mixture of Bentonite and water. A trench that would collapse due to the hydraulic pressure in the surrounding soil does not collapse as the slurry balances the hydraulic pressure. Forms for concrete, and rebar, can be assembled in a slurry filled trench, and then have concrete poured into the form. The liquid concrete is heavier than the bentonite slurry, and displaces it, and the bentonite slurry can subsequently be re-used in a new trench elsewhere on the construction site.

In addition, because the colloid is relatively impervious to water, a slurry wall can prevent the seepage of groundwater, which is useful in preventing the further spread of ground-water that has been contaminated by toxic material like industrial waste(Gutberle, 1994).

2.4.3 Foundry

Bentonite is used as a bonding material in the preparation of molding sand for the production of iron, steel and non-ferrous casting. The unique properties of bentonite yield

green sand moulds with good flowability, compactability and thermal stability for the production of high quality castings (http://www.ima-na.org).

2.4.4 Cat Litter

Bentonite is used for cat litter, due to its advantage of absorbing refuse by forming clumps (which can be easily removed) leaving the remaining product intact for further use.(http://www.ima-na.org).

2.4.5 Pelletizing of iron ore pellets

Bentonite is used as a binding agent in the production of iron ore pellets. Through this process, iron ore fines are converted into spherical pellets, suitable as feed material in blast furnaces for pig iron production, or in the production of direct reduction iron (DRI).(http://www.ima-na.org).

2.4.6 Construction and civil engineering

Bentonite in civil engineering applications is used traditionally as a thixotropic, support and lubricant agent in diaphragm walls and foundations, in tunneling, in horizontal directional drilling and pipe jacking. Bentonite, due to its viscosity and plasticity, also is used in Portland cement and mortars(http://www.ima-na.org).

2.4.7 Adsorption

Bentonite's sorption properties are very useful for wastewater purification. Common environmental directives recommend low permeability soils, which naturally should containbentonite, as a sealing material in the construction and rehabilitation of landfills to ensure the protection of groundwater from the pollutants. Bentonite is the active protective layer of geosynthetic clay liners.Bentonite is also utilized in the removal of impurities in oils where its adsorptive properties are crucial in the processing of edible oils and fats (Soya/palm/canola oil). In drinks such as beer, wine and mineral water, and in products like sugar or honey, bentonite is used as a clarification agent(http://www.ima-na.org).

2.4.8 Drilling

Another conventional use of bentonite is as a mud constituent for oil and water well drilling. Its roles are mainly to seal the borehole walls, to remove drill cuttings and to lubricate the cutting head(http://www.ima-na.org).

2.4.9 Agriculture

Bentonite is used as an animal feed supplement, and as a pelletizing aid in the production of animal feed pellets, as well as a flowability aid for unconsolidated feed ingredients such as soy meal. It also is used as an ion exchange for improvement and conditioning of the soil. When thermally treated, it can be used as a porous ceramic carrier for various herbicides and pesticides(http://www.ima-na.org).

2.4.10 Pharmaceuticals, Cosmetics and Medical Application

Bentonite is used as filler in pharmaceuticals, and due to its absorption/adsorption functions, it allows paste formation. Such applications include industrial protective creams,

calamine lotion, wet compresses, and anti-irritants for eczema. In medicine, bentonite is used as an antidote in heavy metal poisoning. Personal care products such as mud packs, sunburn paint, baby and facepowders, and face creams may all contain bentonite (http://www.ima-na.org).

2.4.11 Detergents

Laundry detergents and liquid hand cleansers/soaps rely on the inclusion of bentonite, in order to remove the impurities in solvents and to soften the fabrics (http://www.ima-na.org).

2.4.12 Paints, Dyes and Polishes

Due to its thixotropic properties, bentonite and organoclays function as a thickening and/or suspension agent in varnishes, and in water and solvent paints. Its adsorption properties are appreciated for the finishing of indigo dying cloth, and in dyes (lacquers for paints & wallpapers) (http://www.ima-na.org).

2.4.13 Paper Productions

Bentonite is crucial to paper making, where it is used in pitch control, i.e. absorption of wood resins that tend to obstruct the machines and to improve the efficiency of conversion of pulp into paper as well as to improve the quality of the paper. Bentonite also offers useful de-inking properties for paper recycling. In addition, acid-activated bentonite is used as the active component in the manufacture of carbonless copy paper (http://www.ima-na.org).

2.4.14 Catalysis

Chemically-modified clay catalysts find application in a diverse range of duties where acid catalysis is a key mechanism. Most particularly, they are employed in the alkylation processes to produce fuel additives(http://www.ima-na.org).

2.5 Pindiga Bentonite Clay

Bentonite clay from Pindiga, Gombe State, Nigeria was investigated for its mineral content using X-ray diffraction technique. The chemical composition was also determined using X-ray fluorescence (XRF) technique. These determinations were carried out on the raw clay, wet beneficiated samples, calcined at 700^{o}C, 750^{o}C and 800^{o}C as well as calcined samples acidified using sulphuric acid. The Pindiga raw bentonite was found to contain Ca-, K-, Na- and Mg-montmorillonite minerals with the calcium type being the predominant mineral. The calcium type also appeared to be the most thermally stable. Accessory minerals such as graphite, carbon, quartz and iron (III) oxide were detected. The quartz was completely removed by wet beneficiation while the carbonaceous matters burnt off completely on calcination to 800^{o}C.The iron (III) oxide in the beneficiated sample calcined at 700^{o}C appeared to react with the sulphuric acid treatment (Ahmed *et. al.*, 2012).

Ahmed *et. al.,* made the following conclusions based on their investigation of Pindiga bentonite clay;

a) The chemical composition of Pindiga raw bentonite samplefrom Gombe State showed moderate contents of Al_2O_3, $SiO_2$and CaO, while the Fe_2O_3 content was very high at 26.54wt%. Wet acid treatment of the bentonite with sulphuric acid caused dealumination of the clay.

b) XRD investigation showed that the bentonite sample contained the Ca-, K-, Na-and the Mg-montmorillonites minerals with the calcium type being the dominant mineral. The calcium type also appeared to be more thermally stable than the rest.

c) The ferric oxide content was significantly attacked by sulphuric acid treatment on the bentonite sample calcined at 700^{o}C(Ahmed *et. al*., 2012).

2.6 Adsorption

Adsorption is the adhesion of atoms, ions, or molecules from a gas, liquid, or dissolved solid to a surface.This process creates a film of the adsorbate on the surface of the adsorbent. This process differs from absorption, in which a fluid (the absorbate) permeates or is dissolved by a liquid or solid (the absorbent). Adsorption is a surface-based process while absorption involves the whole volume of the material. The term sorption encompasses both processes, while desorption is the reverse of it. Adsorption is a surface phenomenon.

Similar to surface tension, adsorption is a consequence of surface energy. In a bulk material, all the bonding requirements (be they ionic, covalent, or metallic) of the constituent atoms of the material are filled by other atoms in the material. However, atoms on the surface of the adsorbent are not wholly surrounded by other adsorbent atoms and therefore can attract adsorbates. The exact nature of the bonding depends on the details of the species involved, but the adsorption process is generally classified as physisorption (characteristic of weak van der Waals forces) or chemisorption (characteristic of covalent bonding). It may also occur due to electrostatic attraction(Ferrari*et. al.,* 2010).

2.6.1 Adsorption applications

Adsorption is present in many natural, physical, biological, and chemical systems, and is widely used in industrial applications such as activated charcoal, capturing and using waste heat to provide cold water for air conditioning and other process requirements (adsorption chillers), synthetic resins, increase storage capacity of carbide-derived carbons, and water purification. Adsorption, ion exchange, and chromatography are sorption processes in which certain adsorbates are selectively transferred from the fluid phase to the surface of insoluble, rigid particles suspended in a vessel or packed in a column. Lesser known, are the pharmaceutical industry applications as a means to prolong neurological exposure to specific drugs or parts thereof.The word "adsorption" was coined in 1881 by German physicist Heinrich Kayser (1853-1940) (Czepirski, *et. al.*, 2000)

2.6.2 Sorption dynamics

In order to study the mechanism of sorption and potential rate determining steps, different kinetic models have been used to test experimental data obtained. The sorption dynamics of the adsorption by the raw and acid treated clays were tested with the Lagergrenpseudo-first order, the chemisorption pseudo-second order and the intra-particle diffusion model.

The linearized form of the pseudo-first orderequation of Lagergren is generally expressed as depicted in equation 2.1:

$$\log[q_e - q_t] = \log[q_e] - \left[{k_1}/{2.303}\right] t \qquad (2.1)$$

where$q_e$and $q_t$are the sorption capacity at equilibriumand at time t, respectively (mg/g). k_1 is therate constant of pseudo first-order adsorption.

The plot of log (q_e-q_t) versus t should give a linearrelationship; k_1 and $q_e$can be calculated from the slope and intercept of the plot, respectively.

The pseudo second order kinetic model is representedby the following linear equation:

$$t/q_e = 1/kq_e + 1/q_e t \qquad (2.2)$$

whereq_e, q_t, and t, have the same meaning asexplained above. k_2 is the overall rate constantsof pseudo second order sorption [g/mg/min]. Ifpseudo–second order kinetics is applicable, the plot of t/q_t against t of equation 2.2 should give a linear relationship;*qeand*k_2 can be determined from the slopeand intercept of the plot.

The initial sorption rate can be obtained from thepseudo second order linear plots as q_t/t approacheszero.

Several steps are involved in the sorption of sorbateby a sorbent. These involve transport of thesolute molecules from the aqueous phase to the surfaceof the solid particulates and diffusion of the solutemolecules into the interior of the pores, which isusually a slow process. The intra-particle diffusionrate constant (k_{id}) is given by the following equation:

$$q_t = k_{id} t^{0.5} \qquad (2.3)$$

When intra-particle diffusion plays a significant rolein controlling the kinetics of the sorption process, the plots of q_t versus $t^{0.5}$ yield straight lines and the slope gives the rateconstant k_{id}.

2.6.3 Freundlich isotherm

The first mathematical fit to an isotherm was published by Freundlich and Küster (1894) and is a purely empirical formula for gaseous adsorbates,

$$\frac{x}{m} = kP^{\frac{1}{n}} \qquad (2.4)$$

where **x**is the quantity adsorbed in *mg*, **m**is the mass of the adsorbent in *g*, **p**is the pressure of adsorbate and **k**and **n**are empirical constants for each adsorbent-adsorbate pair at a given temperature. The function is not adequate at very high pressure because in reality **x/m** has an asymptotic maximum as pressure increases without bound. As the temperature increases, the constants **k**and **n**change to reflect the empirical observation that the quantity adsorbed rises more slowly and higher pressures are required to saturate the surface(Czepirski, *et. al.*, 2000).

2.6.4 Langmuir isotherm

Irving Langmuir was the first to derive a scientifically based adsorption isotherm in 1918.The model applies to gases adsorbed on solid surfaces. It is a semi-empirical isotherm with a kinetic basis and was derived based on statistical thermodynamics. It is the most common isotherm equation to use due to its simplicity and its ability to fit a variety of adsorption data. It is based on four assumptions:

a) All of the adsorption sites are equivalent and each site can only accommodate one molecule.
b) The surface is energetically homogeneous and adsorbed molecules do not interact.
c) There are no phase transitions.
d) At the maximum adsorption, only a monolayer is formed. Adsorption only occurs on localized sites on the surface, not with other adsorbates.

These four assumptions are seldom all true: there are always imperfections on the surface, adsorbed molecules are not necessarily inert, and the mechanism is clearly not the same for the very first molecules to adsorb to a surface as for the last. The fourth condition is the most troublesome, as frequently more molecules will adsorb to the monolayer; this problem is addressed by the BET isotherm for relatively flat (non-microporous) surfaces. The Langmuir isotherm is nonetheless the first choice for most models of adsorption, and has many applications in surface kinetics (usually called Langmuir–Hinshelwood kinetics) and thermodynamics.

Langmuir-Hinshelwood adsorption isotherm model in linearized form is given in equation 2.2

$$\frac{Ce}{q_e} = \frac{1}{K_l q_m} + \frac{Ce}{q_m} \qquad (2.5)$$

Where Ce is equilibrium concentration after adsorption (*mg/l*)and

$$qe = \frac{(Co - Ce) * V}{M} \qquad (2.6)$$

qe is the amount of adsorbate per unit mass of adsorbent (*mg/g*); $q_m$is the maximum amount of adsorbate that an adsorbent can adsorb at the maximum concentration (*mg/g*);K_l(*l/mg*)*V* is the volume of solution (*l*), M is the mass of the adsorbent (*g*) (Czepirski, *et. al.*, 2000).

2.6.5 Equilibrium isotherm studies

Equilibrium isotherm is described by a sorptionisotherm, characterized by certain constants whosevalues express the surface properties and affinity ofthe sorbent sorption equilibrium

is established whenthe concentration of sorbate in the bulk solution is indynamic balance with that at the sorbent interface. In order to quantify the affinity of bentonite for the phenol studied, two widely used isotherm models (Langmuir and Freundlich, isotherm models) were used to analyze the data obtained from thesorption process.

The monolayer coverage of the sorbate on a sorbentsurface at a constant temperature is representedby the Langmuir isotherm. The basic assumption isthat the forces exerted by chemically unsaturatedsurface atoms do not extend further than the diameterof one sorbed molecule. The Langmuir isothermhints towards surface homogeneity (Eq. 2.7).

Langmuir Isotherm: $\left[{}^{1}/_{q_e}\right] + \left[{}^{1}/_{q_o K_L}\right] \times {}^{1}/_{C_e}$ (2.7)

Where*qe*is the amount of phenol sorbed at equilibrium per mass of catalysts (mg/g); *Ce*is the concentration of the phenol in aqueous phase at equilibrium; $K_L$isthe sorption equilibrium constant; q_o (mg/g) is themonolayer capacity.

The monolayer coverage is obtained from a plot of$1/q_e$versus $1/C_e$. The slope and the intercept of thelinear graph obtained from this plot give the valueof $q_o$and K_L.

The Freundlich Isotherm: $q_e = K_f C_e^{\,1/n}$ (2.8)

The Freundlich isotherm is an empirical equationthat encompasses the heterogeneity of sites and theexponential distribution of sites and their energies (Eq.2.8). The Freundlich coefficients $1/n$ and $K_f$areobtained from the plots of Lnq_eversus LnC_e.

2.7 Photocatalysis

Photocatalysis is of Greek origin composing of two parts: the prefix “photo’’ means light and the ‘’catalysis’’ means break apart or decompose. Hence, photocatalysis can generally

be describe as a process in which light is used to activate a substance, the photo catalyst that aid this process is itself not involved in the chemical transformation. Photocatalytic reactions are classified into homogeneous photo catalysis in which both the photo catalyst and the substrate are of the same phase and the heterogeneous photocatalysis in which both the photocatalyst and the substrate are of different phases. However, heterogeneous photocatalysis is by far more intensively studied in recent years because of its potential use in a variety of environmental and energy- related application as well as in organic synthesis. The reaction scheme in heterogeneous involve the previous formation of an interface between a solid photocatalyst (metal or semiconductor) and a fluid containing the reactants and products of the reaction. Therefore, heterogeneous photocatalysis is mainly used in cases where a light-absorbing semiconductor is utilized, which is in contact with either a liquid or a gas phase. (Beydoun*et. al.*, 1999).

2.7.1 Mechanism of Photocatalysis

When a photocatalyst such as iron (III) Oxide (Fe_2O_3) absorbs Ultraviolet (UV) or Visible (Vis) radiation from sunlight or illuminated light source (lamps), it will produce pairs of electrons and holes. The electron of the valence band of iron (III) oxide becomes excited when illuminated by light. The excess energy of this excited electron promoted the electron to the conduction band of iron (III) oxide therefore creating the negative-electron (e-) and positive-hole (h+) pair. This stage is referred as the semiconductor's 'photo-excitation' state. The energy difference between the valence band and the conduction band is known as the 'Band Gap'. Wavelength of the light necessary for photo-excitation is: 1240 (Planck's constant, h) / 3.2 eV (band gap energy) = 388 nm

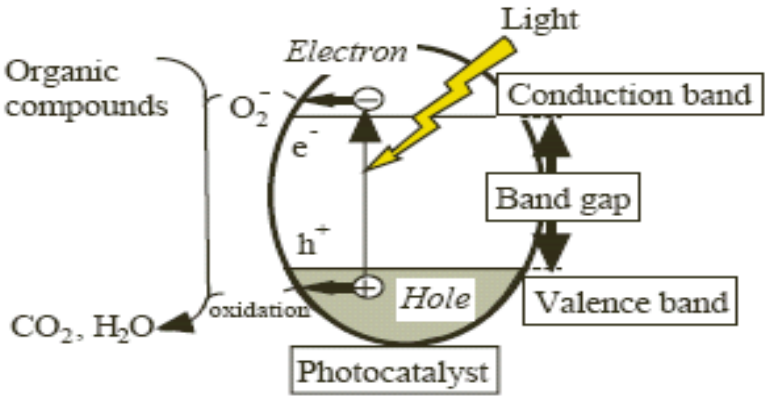


Fig. 2.1 Mechanism of Photocatalysis

The positive-hole of iron oxide breaks apart the water molecule to form hydrogen gas and hydroxyl radical. The negative-electron reacts with oxygen molecule to form super oxide anion. This cycle continues when light is available.

(www.mch-nano solutions.com/mechanism of photocatalysis-2012)

2.7.2 Application of photocatalysis

Both the technological and economic importance of photocatalysis has considerably increased over the past decades .Improvement in performance have been strongly correlated to advances in nanotechnology. For example, the introduction of nano-particulate photocatalysts has tremendously enhanced the catalytic efficiency of specific materials. A variety of application ranging from anti-fogging, anti-microbial and self-cleaning surfaces through to water and air purification and solar induced hydrogen production have been developed and many of these have made their way into commercial products. However, extensive research continues to further optimize this technology and to widen the spectrum of potential applications (Serpone and Pellizette, 2000).

a. Self-Cleaning Surfaces

This support the light induced destruction of adherent organic molecules and is of particular importance for anti- bacterial, anti-viral and fungicidal applications. Particular relevance is given to surface sterilization in areas such as biomedical engineering and food preparation.

Photo-induced hydrophilicity is generated by the exposure of a TiO_2- treated surface to intense UV light. Water is prevented from forming droplets and instead covers the surface with a homogeneous thin wetting layer, which penetrates below dirt particles. Hydrophilic surfaces are thus easy to clean by pure water sprinkling and demonstrate considerable anti-fogging effects. Wet vehicle rear-view mirrors will therefore impact on the user´s view to a lesser extent.

A combination of both effects generates considerable self-cleaning properties. Organic dirt can easily be washed off, for example by the next rain shower, surfaces remain clean, and moreover possess anti-microbial properties. Photocatalytically active surfaces of glass, metals or ceramics are also widely established. (Bräuer*et. al*., 2009)

b. Air Purification

Photocatalytic surfaces have the potential to act against a variety of air pollutants and odours such as microbes, volatile organic carbons (VOC), formaldehyde, ammonia and inorganic gaseous substances such as nitrogen- or sulphur-oxides (NO_X,SO_X). Meanwhile a variety of technical products are commercially available. Applications include photocatalytic components for air filters, ventilation, and air conditioning systems via active decomposition of cigarette smoke or

automotive and industrial exhaust to general air purifying effects of larger photoactive building elements. (Bräuer*et. al*., 2009)

c. Destruction of Warfare Agents

Photocatalysts have the potential to decompose various hazardous substances at least in mild conditions. Researchers have examined the photocatalytic degradation of chemical warfare agents (CWAs), and the results indicated that photocatalysts can support the detoxification of hazardous compounds. However, they must be applied as an additional component within larger decontamination measures (Serpone *et. al.*,2000).

d. Conversion of Carbon dioxide to gaseous hydrocarbons

Another application is in the conversion of carbon dioxide into gaseous hydrocarbons using titanium dioxide in the presence of water. As an efficient absorber in the UV range, titanium dioxide nanoparticles in the anatase and rutile phases are able to generate excitations by promoting electrons across the band gap. The electrons and holes react with the surrounding water vapor to produce hydroxyl radicals and protons. At present, proposed reaction mechanisms usually suggest the creation of a highly reactive carbon radical from carbon monoxide and carbon dioxide which then reacts with the photogenerated protons to ultimately form methane. Although the efficiencies of present titanium dioxide based photocatalysts are low, the incorporation of carbon based nanostructures such as carbon nanotubes and metallicnanoparticleshave beenshown to enhance the efficiency of these photocatalysts. (Bräuer*et. al*., 2009)

e. Conversion of Water to Hydrogen

Conversion of water to hydrogen gas by photocatalytic water splitting is another important application of photocatalysis. An efficient photocatalyst in the UV range is based on a sodium tantalite ($NaTaO_3$) doped with La and loaded with a co-catalyst nickel oxide. The surface of the sodium tantalite crystals is grooved with so called nano-steps that is a result of doping with lanthanum (3–15 nm range). The N_iO particles which facilitate hydrogen gas evolution are present on the edges, the oxygen gas evolves from the grooves(Bräuer *et. al*., 2009)

2.8 Specific Surface Area of Solids

Specific surface area is one of the most important and effective geometrical parameters in defining and interpreting petro-physical relationships, textural framework, and fluid–solid interactions in porous media. It is defined as the interstitial surface area of the pores and pore channels for each unit of bulk volume, grain volume, or pore volume, or for a unit of weight of a material.

Surface area is important in chemical kinetics. Increasing the surface area of a substance generally increases the rate of a chemical reaction. For example, iron in a fine powder will combust, while in solid blocks it is stable enough to use in structures. For different applications a minimal or maximal surface area may be desired.Specific surface area (S_s) is one of the most important and effective geometrical parameters in defining and interpreting petro-physical relationships, textural framework, and fluid–solid interactions in porous media. It is defined as the interstitial surface area of the pores and pore channels for each unit of bulk volume, grain volume, or pore volume, or for a unit of weight of a material (George, 1999).

2.8.1 Brunauer Emmet Teller (BET) surface area measurement

BrunauerEmmet Teller was the first method to measure the specific surface area of finely divided and porous solids. BET named after Stephen Brunauer, P.H. Emmet and Edward Teller was developed in 1938 when they were working on ammonia catalysts**.** Theymade the following assumptions for BET surface area measurement:

a) Homogeneous surface.

b) No lateral interactions between molecules.

c) Uppermost layer is in equilibrium with vapor phase.

d) First layer: heat of adsorption; higher layers; heat of condensation.

e) At saturation pressure, the number of layers becomes infinite.

The surface area of the catalyst can be determined using adopted BET method developed by Adefila *et. al.*, (2003) which employs adsorption of adsorbate (water molecules) on the surface of the adsorbent (samples of catalyst to characterize) using the BET theory. The concept of the theory is an extension of the Langmuir theory, which is a theory of monolayer molecular adsorption, to multilayer adsorption with the following hypothesis (a) Gas molecules physically adsorb on a solid in layers indefinitely; (b) There is no interaction between each adsorption layer and (c) the Langmuir theory can be applied to each layer (Adefila, 2003). The resulting BET equation is expressed by

$$\frac{\mathrm{P/Po}}{\mathrm{V}(1-{}^{\mathrm{P}}/_{\mathrm{Po}})} = \frac{1}{\mathrm{VmC}} + \frac{\mathrm{C}-1}{\mathrm{VmC}}\left(\frac{\mathrm{P}}{\mathrm{Po}}\right) \qquad (2.9)$$

P and Po are the equilibrium and the saturation pressure of the adsorbate at the temperature of adsorption, v is the adsorbed quantity of the adsorbate,Vm is the monolayer adsorbed gas quantity, C is the BET constant

Equation (2.9) is an adsorption isotherm and can be plotted as a straight line with $(\frac{P}{Po})/V\{1-{}^{P}/_{Po}\}$ *on the x-axis according to experimental results. This plot is called a BET plot. The linear relationship of this equation is maintained only in the range of 0.05 <* $\frac{P}{Po}$ *< 0.35. The value of the slope S and the y-intercept I of the line are used to calculate the monolayer adsorbed gas quantity* Vm and *the BET constant c. The following equation can be used to find intercept, I and slope S*

$$I = \frac{1}{VmC} \text{ and } S = \frac{C-1}{VmC} \quad (2.10)$$

Upon mathematical manipulations, it follows that:

$$Vm = \frac{1}{1+S} \quad (2.11)$$

Employing room temperature and assuming ideal situation,

$$PV = nRT \quad (2.12)$$

$$n = \frac{Vm}{M} \quad (2.13)$$

Hence, $Vml = \frac{VmRT}{MP}$ (2.14)

Where, R = 8.314 J/gmol.K

T = Room temperature (298K)

M = Molecular mass of the adsorbate (18g/gmole, for water)

V = Standard volume at STP (0.0224 m^3)

P = Atmospheric pressure (1.01325* $10^5 Nm^{-2}$)

Area occupied by one volume of adsorbent, α can be derived from first principle:

Assuming, the geometry of the α molecule of the adsorbent is spherical

Then, cross sectional area of a molecule

$$\alpha = \pi R^2 \tag{2.15}$$

Volume of a molecule, $\gamma = \frac{M}{No\rho}$ (2.16)

Where ρ = density of the adsorbate in g/cm^3

No = Avogadro's constant = 6.023* 10^{23}mol^{-1}

Also, $\gamma = \frac{4}{3}\pi r^3$ (2.17)

Equating equations (2.14) and (2.15), we have

$$r = (\frac{3M}{4\pi\rho N_O})^{\frac{1}{3}} \tag{2.18}$$

But r = R, Hence, substitute equation (2.16) into (2.17), it follows that

$$\alpha = 1.209(\frac{M}{\rho N_O})^{\frac{2}{3}} \tag{2.19}$$

However, the surface area of the adsorbent is calculated as thus

$$Sg = \left(\frac{VmlN_O}{V}\right)\alpha \tag{2.20}$$

Substituting equations (2.18) and (2.19) into (2.20), S_g can be calculated as thus,

$$Sg = (\frac{VmRT}{MP} * \frac{N_O}{V})\ \alpha \tag{2.21}$$

Equation (2.19) can be used to evaluate Sg in m^2 /g (Adefila *et. al.*, 2003)

2.8.2 X-Ray Diffraction

When crystallites are less than approximately 1,000Å in size, appreciable broadening in the x-ray diffraction lines will occur. These regions may in fact correspond to the actual size of the particles. At other times, however, these regions form "domains" in the larger particle and may be a distinguishing and important feature. In either case, the observed line broadening can be used to estimate the average size. In the simplest case where the particles are stress-free, the size is estimated from a single diffraction peak. But in those cases where stress may be present, a more robust method involving several diffraction peaks is required.X-Ray diffraction has found applicationincorrosion products, forensic analysis, intermetallic contaminants pharmaceuticals, amorphous/crystalline contents, quality control, phase transformations, catalysts, and fiber analysis (Klug*et. al.*, 2004).

2.8.3 Scherrer's equation

X-ray diffraction is a convenient method for determining the mean pore size of nanocrystallites in nano crystalline bulk materials. Paul Scherrer, published his results in a paper that included what became known as the Scherrer equation (Langford *et. al.*, 1981).Crystalline size is not synonymous with particle size. X-Ray diffraction is sensitive to the crystallite size inside the particles. From the well-known Scherrer formula the average crystallitesize, L, is expressed in equation 2.22

$$L = \frac{K\lambda}{\beta COS\theta} \qquad (2.22)$$

Where λ is the X-ray wavelength in nanometre (*nm*), β is the peak width of the diffraction peak profile at half maximum height resulting from small crystallite size in radians and K is a constant related to crystallite shape, normally taken as 0.9. The value of β in 2θ axis of

diffraction profile must be in radians. The θ can be in degrees or radians (Dinilichenko, *et. al.*,2002)

2.8.4 X-Ray fluorescence spectroscopy

An X-ray fluorescence (XRF) spectrometer is an x-ray instrument used for routine, relatively non-destructive chemical analyses of rocks, minerals, sediments and fluids. It works on wavelength-dispersive spectroscopic principles that are similar to an electron microprobe. However, an XRF cannot generally make analyses at the small spot sizes typical of 2-5 microns, so it is typically used for bulk analyses of larger fractions of geological materials. The relative ease and low cost of sample preparation, and the stability and ease of use of x-ray spectrometers make this one of the most widely used methods for analysis of major and trace elements in rocks, minerals, and sediment (Fitton, 1997).

The XRF method depends on fundamental principles that are common to several other instrumental methods involving interactions between electron beams and x-rays with samples, including: X-ray spectroscopy, X-ray diffraction, and wavelength dispersive spectroscopy. The analysis of major and trace elements in geological materials by x-ray fluorescence is made possible by the behavior of atoms when they interact with radiation. When materials are excited with high-energy, short wavelength radiation (e.g., X-rays), they can become ionized. If the energy of the radiation is sufficient to dislodge a tightly-held inner electron, the atom becomes unstable and an outer electron replaces the missing inner electron. When this happens, energy is released due to the decreased binding energy of the inner electron orbital compared with an outer one. The emitted radiation is of lower energy than the primary incident X-rays and is termed fluorescent radiation. Because the energy of the emitted photon is characteristic of a transition between specific electron

orbitals in a particular element, the resulting fluorescent X-rays can be used to detect the abundances of elements that are present in the sample (Potts, 1987).

X-Ray fluorescence is used in a wide range of applications, including research in igneous, sedimentary, and metamorphic petrology, soil surveys, mining (e.g., measuring the grade of ore),cement production, ceramic and glass manufacturing, metallurgy (e.g. quality control),environmental studies (e.g., analyses of particulate matter on air filters),petroleum industry (e.g., sulfur content of crude oils and petroleum products),field analysis in geological and environmental studies (using portable, hand-held XRF spectrometers). X-Ray fluorescence is particularly well-suited for investigations that involve bulk chemical analyses of major elements (Si, Ti, Al, Fe, Mn, Mg, Ca, Na, K, P) in rock and sediment, bulk chemical analyses of trace elements (in abundances >1 ppm; Ba, Ce, Co, Cr, Cu, Ga, La, Nb, Ni, Rb, Sc, Sr, Rh, U, V, Y, Zr, Zn) in rock and sediment - detection limits for trace elements are typically on the order of a few parts per million. X-ray fluorescence is limited to analysis of relatively large samples, typically > 1 gram, materials that can be prepared in powder form and effectively homogenized, materials for which compositionally similar, well-characterized standards are available, materials containing high abundances of elements for which absorption and fluorescence effects are reasonably well understood. (Rollinson, 1993).

2.9 Langmuir–Hinshelwood Kinetic Model of Photocatalytic Processes

Langmuir-Hinshelwood modified to accommodate reactions occurring at a solid-liquid interface is given in equation 2.18:

$$r_o = -\frac{dc}{dt} = \frac{K_r K_e Co}{1 + K_e Co} \qquad (2.23)$$

Therefore, Equation (2.23) can be linearized as follow

$$r_o(1 + K_e Co) = K_r K_e Co \tag{2.24}$$

$$\frac{1 + K_e Co}{K_r K_e Co} = \frac{1}{r_o} \tag{2.25}$$

$$\frac{1}{r_o} = \frac{1}{K_r K_e Co} + \frac{1}{K_r} \tag{2.26}$$

Equation (2.26) is the linearized form of Langmuir-Hinshelwood kinetic model for adsorption involving photocatalytic reactions.

Where r_o *is* the initial rate of reaction in mg/lmin and is calculated as thus

$$r_o = \frac{Co - Ce}{time} \tag{2.27}$$

K_r the rate constant for photocatalysis in lmin/mg, K_e the rate constant for adsorption in l/mg, Co the initial concentration of bulk solution in mg/l at adsorption equilibrium C_e is the equilibrium concentration

Experimental data on $1/r_o$can be plotted against 1/ Co for the given parameters and a straight line graph can be obtained from which the values for K_r and $K_e$can be evaluated.

2.10 Related Works

Ahmed *et.al.*, (2012), reported the properties of raw, beneficiated and acid modified Pindiga bentonite clay using X-ray diffraction and X-ray fluorescence techniques. They reported that raw Pindiga bentonite clay contains 27%wt Fe_2O_3.

Bakardjieva *et. al.*, (2006), studied the photocatalytic efficiency of iron oxides in the degradation of 4-chlorophenol and were able to establish that Fe_2O_3 is photocatalytic in the heamatite polymorph at calcination temperature of 1000^oC.

Banet *et. al*., (2000), studied the adsorption of phenol by bentonite and established the adsorption equilibrium time of phenol by bentonite clays to be 6hours.

Martinez-Luevanos *et. al*., (2011), studied the leaching kinetics of iron from low grade kaolin by oxalic acid solution and were able to leach iron oxide from kaolinite clay using oxalic acid.

CHAPTER THREE

MATERIALS AND METHODS

3.1 Materials

The following are the list of materials used during the course of this work. All materials listedwith the exception of bentonite clay, were obtained from Jossy Chemical Stores in Zaria, Nigeria and manufactured by BDH Chemicals England. The chemicals were of analytical grade.

3.1.1 Chemicals

1. Bentonite clay from Pindiga, Gombe State.
2. 0.5M Oxalic acid.
3. Distilled water.
4. Deionised water
5. Phenol
6. NaCl
7. $KMnO_4$
8. HCl
9. NaOH

3.1.2 Apparatus

The following are some of the apparatus and glass wares used during this study:

1. Beakers (Pyrex), 1000ml and 500ml
2. Conical flasks (500ml), Pyrex
3. Measuring cylinders (1000ml, 500ml, 10ml), Pyrex
4. Crucibles

5. Laboratory mortar and pestle
6. Sieves
7. Spatula
8. Plastic spoons
9. Buchner flask (1 litre)
10. Sinta glass filter
11. Plastic bucket
12. Glass rod stirrer
13. Desiccators
14. Sample bottles (glass and plastic)
15. Petri dishes,
16. Stainless steel thongs
17. Halogen lamp (500W)

3.1.3 Equipment

Table 3.1 shows a list of the equipment used and their models.

Table 3.1: List of equipment used and their specifications

S/N	EQUIPMENT	MODEL	AVAILABILTY
1	X-Ray Diffractometer (XRD)	Empyrean Panalytical BV	NGRL, Kaduna.
2	X-Ray Fluorescence Machine (XRF)	Minipal4 Energy Dispersive	NGRL, Kaduna.
3	UV/Vis Spectrophotometer	Jenway 6405	CHEMISTRY Dept., A.B.U Zaria.
4	Ball mill machine	Kera BV	ChED, A.B.U Zaria.
5	Weighing Balance	Adam 22	ChED, A.B.U Zaria.
6	Sieves	N/A	Geology Dept., A.B.U Zaria.
7	pH meter	Jenway	CHEMISTRY Dept., A.B.U Zaria.
8	Magnetic Stirrer		ChED, A.B.U Zaria.
9	Constant Temperature Water bath		CHEMISTRY Dept., A.B.U Zaria.
10	Vacuum Pump filtration set up		ChED, A.B.U Zaria.
11	Deionizer		ChED, A.B.U Zaria.
12	Refrigerator		ChED, A.B.U Zaria.
13	Electric Oven	Haraeus	ChED, A.B.U Zaria.

3.2 Methodology

3.2.1 Leaching of Pindiga bentonite clay by oxalic acid solutions

Leaching experiments were carried out in 1 litre round-bottom glass flask at a temperature of 100^{o}C.The flask (equipped with a thermometer and a reflux condenser) was heated with a thermostatically controlled heating mantle. Stirring was done magnetically. All leaching experiments were done at atmospheric pressure. For each run, 500ml of oxalic acid solution ($C_2H_2O_4$, reagent grade) of 0.5M concentration was added to the flask and the temperature was set to 100^{o}C. Then, 5.0g of clay was added to the flask while under magnetic stirring. After the desired period of leaching, the slurry was filtered hot using vacuum filtration

pump then centrifuged immediately and then dried at 110^{o}C for 24 hours. The dried residue was calcined at 1000^{o}C for 4 hours to obtain iron oxides in hematitepolymorphs state (α-Fe_2O_3) that exhibit the highest photocatalytic activity. (Martinez-Luevanos *et. al*., 2011, Mohapatra *et. al.,* 2010 and Bakardjieva *et. al.,* 2006).

3.2.2 Adsorption experiments

Adsorption experiments were carried out by allowing an accurately weighted amount of raw or leached bentonites to reach equilibrium with phenol solutions of known concentrations. Initial concentrations of phenol were held between 62.5 and 500mg/l. 2.5g bentonite was added toconical flasks, each containing 100ml solution of phenol. This was stirred continuously with magnetic stirrer for up to ten hours, during which aliquot were collected at various intervals of time, filtered, then taken for UV/Vis spectrophotometric analysis (Banat *et. al.*, 1999).

3.2.3 Effect of pH

2.5g of bentonite was added to narrow-neck bottle containing 100ml solution of phenol of 500mg/l concentration. The pH was adjusted using dilute HCl or NaOH solutions. The pH values employed were 5, 9 and 12. This was stirred continuously with magnetic stirrer for 10 hours.

3.2.4 Effect of initial phenol concentration

100ml of initial concentrations of phenol (62.5,125,250 and 500mg/l) with 2.5g of bentonite were added to narrow-neck bottles respectively and stirred continuously in the dark for 12 hours.

3.2.5 Effect of adsorbent dose

100ml of phenol was measured and placed in a beaker, 1.5g of the catalyst was then measured and added to content of the beaker, which was then placed on a hot plate. A magnetic stirrer was introduced into the beaker and the content was continuously stirred in the dark for 10 hours after which aliquot was collected for analysis. The same procedure was repeated for 2.0g, 2.5g and 3.0g of catalysts.

3.2.6 Photocatalytic experiments

All photocatalytic experiments were carried out using the same procedure. Stock solution of concentration 500 mgl^{-1} of the phenol (substrate) was prepared in deionized water for all the experiments. 100 m*l* of solution was put in the reactor and 2.5g catalyst was added to it. Dark adsorption pH of the solution was noted. The suspension was then irradiated under 500W halogen lamp with continuous stirring using a magnetic stirrer for two hours. Aliquot was taken from the reactor at regular intervals of time with the help of a syringe. The catalyst was filtered from the sample using a filter paper. These samples were analyzed using a UV-Vis spectrophotometer. The pH of the final solution was noted. Experiments were repeated in duplicate to ascertain reproducibility of the results.

For degradation of phenol with the above procedure, the various experiments were conducted for optimizing parameters like initial concentration, pH and catalyst loading.

Before photocatalytic treatment (with optimized conditions), the solution of phenol and the catalyst were stirred continuously for 6hrs to achieve adsorption-desorption equilibrium.

3.2.7 Determination of specific surface area of the clay

In this method an adsorbate constant relative humidity was established as a relative humidity of water vapour obtained from a saturated salt solution in water. This relative humidity was proved to be equal to $\frac{P}{PO}$, as in equation 2.9.

First and foremost, two saturated solutions of four different kind of salts were prepared, one of each salt was kept in a desiccator and the other left open in the laboratory, the two were left for 24hrs, while their respective weight at the beginning and at the end of 24hrs were noted. The relative humidity of the saturated salt solution for each of the salt were then evaluated as the ratio of the weight differences of salt solution in the desiccator (at initial point and after 24hrs) to the weight differences of salt solution left open (at initial point and after 24hrs). The salts used are $CaSO_4$, K_2SO_4, CH_3COONa, and $MgCl_2$. After the determination of value of $\frac{P}{PO}$ for each salt, a saturated solution of the salt of each salt were then prepared and kept in a desiccator with 1g of the adsorbent (synthesized catalyst) evenly spread on a petri dish and kept together with the saturated salt solution in the air tight desiccator for 24hrs while maintaining the laboratory temperature at room temperature. The weight gain of the catalyst was determined at the end of 24hrs to represent v in equation 2.5.The procedure was repeated for the remaining catalysts and equations (2.4 to 2.16) were used to determine the specific surface area of the catalyst synthesized (Adefila *et. al.,* 2003).

3.2.8 Detailed block diagram of the methodology

Figure 3.1 shows a detailed block diagram of the processes employed during the course of this work.

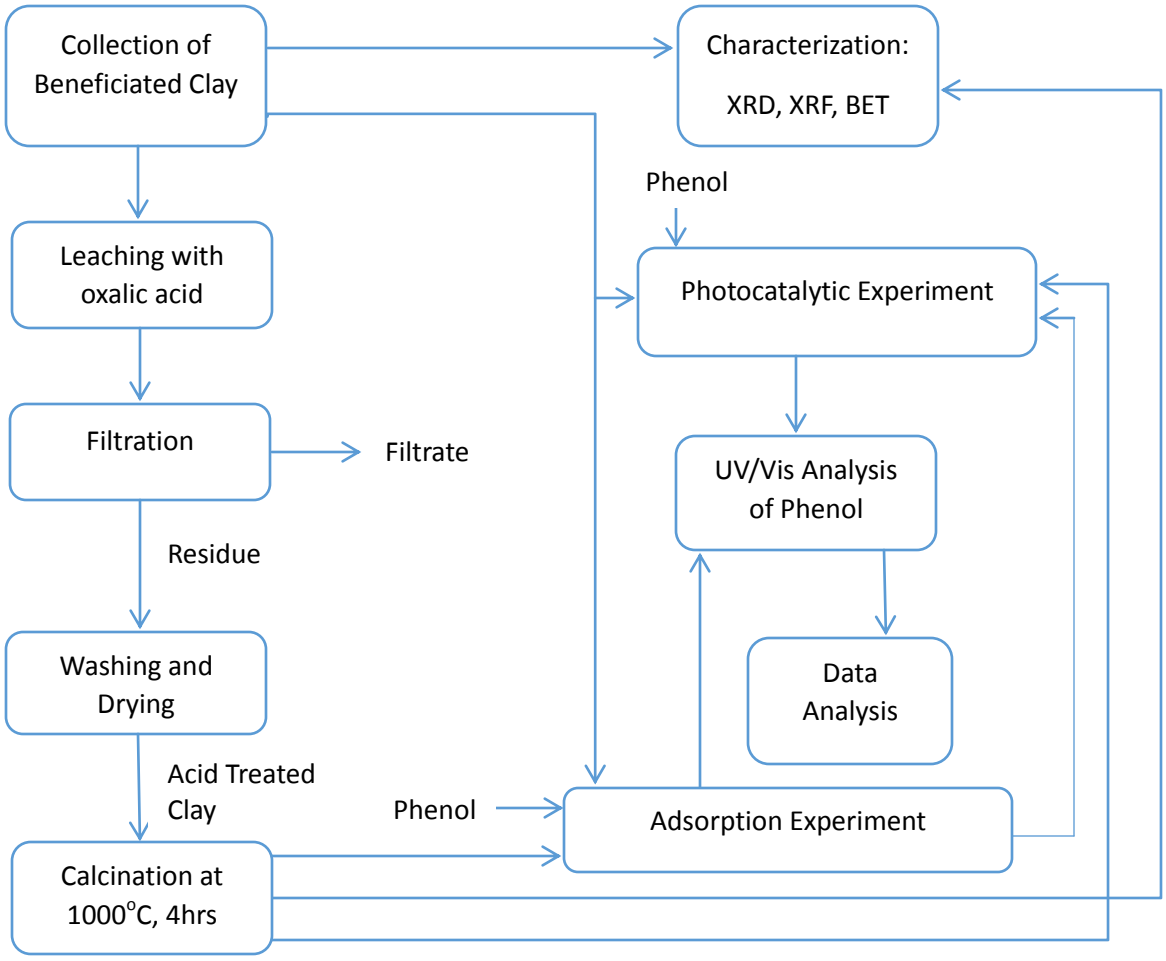


Fig. 3.1 Block Diagram of the Research Methodology

CHAPTER FOUR

RESULTS AND DISCUSSION

4.1 Leaching of clay

Pindiga bentonite clay was treated with0.5M solution oxalic acid at a temperature of 100^{o}C and varying the leaching time (0,5, and 60 minutes).Theraw and acid leached clays were activated by calcination at 1000^{o}C. The raw and treated clays obtained were labeled based on leaching time as; PB, PBC, PB-5 and PB-60 as shown in Table 4.1.

Table 4.1: Labelling of raw Pindiga clay and developed catalysts

Label	Description
PB	Raw Clay
PBC	Raw clay calcined at1000^{o}C
PB-5	Raw clay treated for 5 mins with 0.5 M oxalic acid then calcined at1000^{o}C
PB-60	Raw clay treated for 60mins with 0.5 M oxalic acid then calcined at1000^{o}C

4.2 Specific Surface Areas and Crystallite Sizes of the Raw and Treated Clays

Appendices A and B gives detailed water adsorption method used in determining the surface area and Scherrer's equation for the determination of the particle sizes of PB, PBC, PB-5 and PB-60, respectively. Table 4.2 shows the specific surface areas and particle sizes as determined.

Table 4.2: Specific surface areas and particle sizes of PB, PBC, PB-5 and PB-60

Catalysts	Surface area(m^2/g)	Particle size(nm)

PB	47.13	14.76
PBC	151.69	65.84
PB-5	265.99	57.06
PB-60	363.61	51.25

The surface areas of the raw and treated clays are listed in Table 4.2 and of the raw and treated clays, PB-60 was found to have the highest surface area of 363.61m^2/g, followed by PB-5 which has a surface area of 265.99m^2/g, then PBC which has a surface area of 151.69m^2/g and lastly PB which has a surface area of 47.13m^2/g. PB-60 has a better surface area because the leaching time with acid which has effect on the surface area was more than the other catalyst (Martinez-Luevanos *et al*., 2011).

Table 4.2 also gives the particle size of the clays.

4.3 Characterization of the Catalysts

Table 4.3 shows the X-ray fluorescence of raw Pindiga clay and the developed catalysts and their structures is depicted in Figure 4.1.

X-ray fluorescence (XRF) results presented in Table 4.3 shows that Pindigabentonite clay from Gombe State Nigeria contains high amount of iron oxide (26.24 wt. %) and this is the driving force behind this research project.The X-ray diffraction (XRD) pattern shown in Figure 4.1 shows the hematite peaks, Ca-montmorillonite peaks and other relevant peaks which conform with standard peaks for bentonite clays. These analyses shows that it's a bentonitic clay with other compositions which shows that it's consistent with typical literature XRF and XRD results for bentonite clays (Mekatel *et. al.,* 2012 and Ahmed *et. al.,* 2012).

Table 4.3Composition of the PB,PBC, PB-5, and PB-60

	Concentration (wt%)			
Component	**PB**	**PBC**	**PB-5**	**PB-60**
A_2O_3	14	15.94	16.8	17.6
SiO_2	43.6	47.66	56.1	57.3
K_2O	3.52	3.68	3.92	3.86
CaO	2.46	1.71	1.33	1.44
TiO_2	2.06	2.09	2.15	2.37
V_2O_5	N/A	0.15	0.11	0.11
Cr_2O_3	N/A	0.05	0.04	0.039
MnO	N/A	N/A	0.08	0.1
Fe_2O_3	**26.54**	**21.47**	**17.33**	**15.71**
NiO	N/A	N/A	0.01	0.06
CuO	N/A	0.03	0.03	N/A
ZnO	0.03	0.05	0.07	0.14
Ag_2O	N/A	3.4	2.46	2.8
BaO	N/A	N/A	0.22	0.26
SO_3	1	N/A	N/A	N/A
CaO	2.46	N/A	N/A	N/A
Eu_2O_3	N/A	N/A	0.19	0.16
Yb_2O_3	0.03	0.03	0.02	0.01
Re_2O_7	0.14	0.11	0.1	0.1

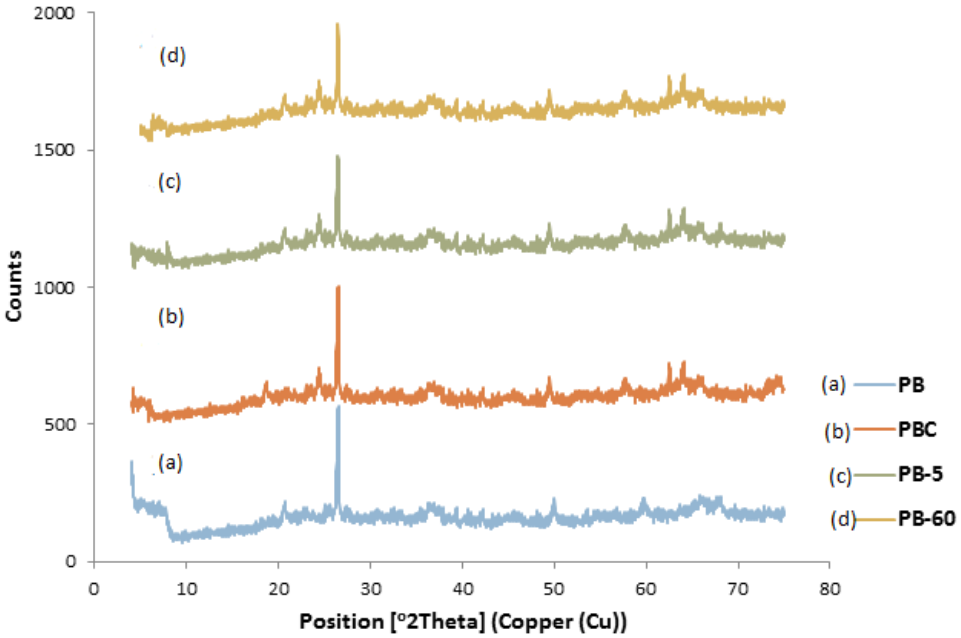


Fig. 4.1 Cascaded XRD patterns of (a) PB, (b) PBC, (c) PB-5 and (d) PB-60

4.4 Preliminary Photocatalytic Degradation of Phenol beforeAdsorptionEquilibrium was Established

Figure 4.2 shows the photocatalytic phenol degradation by various catalyst; PB, PBC, PB-5and PB-60. This experiment was carried out before adsorption equilibrium was established.

Percentage degradation was calculated using equation 4.1.

$$\%\, degradation = \frac{Co - C}{Co} X\ 100 \qquad (4.1)$$

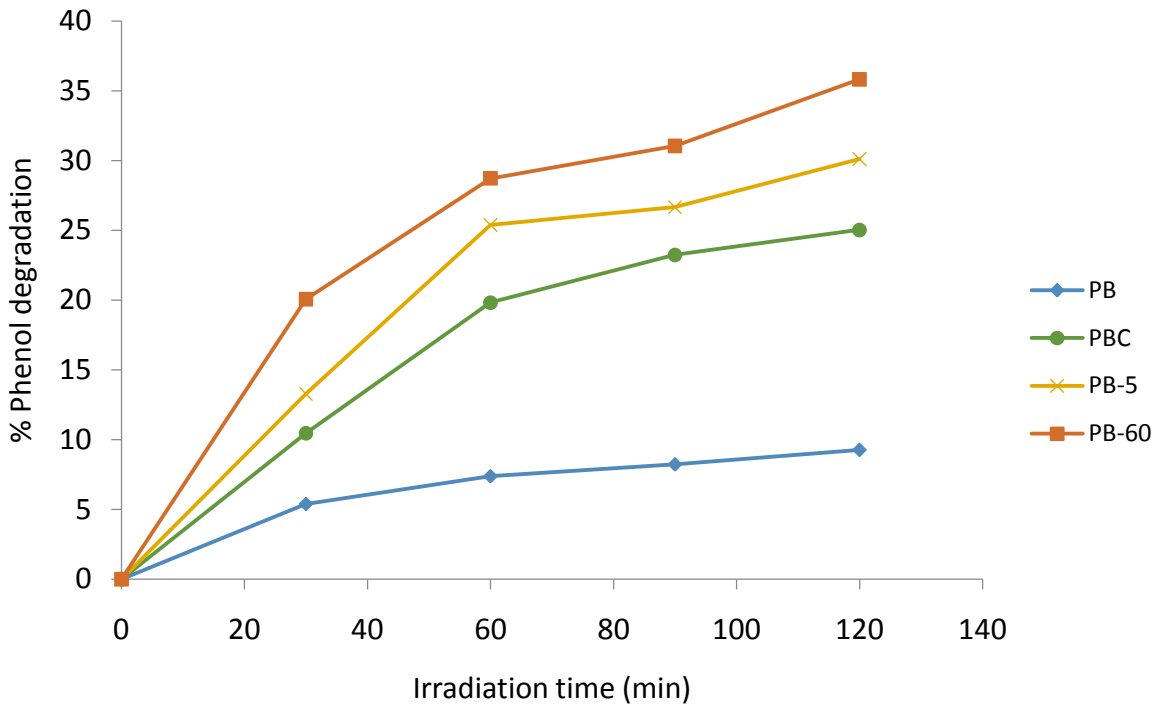


Fig. 4.2 Effect of irradiation time on the photocatalytic degradation of phenol by PB, PBC, PB-5 and PB-60

Figure 4.2 shows that PB has a very poor degradation capacity for phenol, which is just 5% in 2 hours. PBC has better photocatalytic activity of 25%, followed by PB-5 which is 30% and the best photocatalyst is PB-60 which was able to photo degrade phenol by 35% in 2 hours. The overall degradation by the clays is poor. This is probably because adsorption equilibrium was not established before photodegradation was carried out.

4.5 Adsorption of Phenol on PB, PBC, PB-5 and PB-60

Theadsorption data for the uptake of phenol versus contact time at different initial concentrations of phenol for PB, PBC, PB-5 and PB-60 is presented inTables 4.4 – 4.7. The data was analyzed usingpseudo-first order kinetics, pseudo-second order kinetics, intra-particle diffusion, Langmuir adsorption model and Freundlich adsorption models.

Table 4.4 Concentration measurement for the adsorption of phenol by catalyst PB

	Concentration			
Ad. Time(hrs)	**500mg/l**	**250mg/l**	**125mg/l**	**62.5mg/l**
0	429.714	243.286	129.714	68.286
1	420.857	236.286	123.714	63.429
2	413.429	229.429	119.286	61.143
4	399.429	219.714	115.000	59.143
6	393.286	216.571	112.143	58.286
8	393.286	216.571	112.286	58.286
10	393.429	216.571	112.143	58.286

Table 4.5 Concentration measurement for the adsorption of phenol by catalyst PBC

	Concentration			
Ad. Time(hrs)	**500mg/l**	**250mg/l**	**125mg/l**	**62.5mg/l**
0	429.714	243.286	129.714	68.286
1	405.143	224.857	117.000	59.429
2	396.286	218.429	112.571	56.857
4	382.143	208.286	106.429	52.571
6	370.714	199.286	101.429	51.143
8	370.714	199.286	101.429	51.143
10	370.714	199.286	101.429	51.143

Table 4.6 Concentration measurement for the adsorption of phenol by catalyst PB-5

Ad. Time(hrs)	Concentration			
	500mg/l	**250mg/l**	**125mg/l**	**62.5mg/l**
0	429.714	243.286	129.714	68.286
1	376.571	206.857	102.714	52.000
2	359.143	193.571	96.857	49.286
4	334.000	181.857	92.143	45.857
6	322.571	173.571	86.286	43.571
8	322.571	173.571	86.286	43.571
10	322.571	173.571	86.286	43.571

Table 4.7 Concentration measurement for the adsorption of phenol by catalyst PB-60

Ad. Time(hrs)	Concentration			
	500mg/l	**250mg/l**	**125mg/l**	**62.5mg/l**
0	429.714	243.286	129.714	68.286
1	354.000	179.714	85.000	36.857
2	321.571	154.429	71.714	33.000
4	261.286	132.571	56.429	26.857
6	236.857	111.714	50.571	23.571
8	236.857	111.714	50.571	23.571
10	236.857	111.714	50.571	23.571

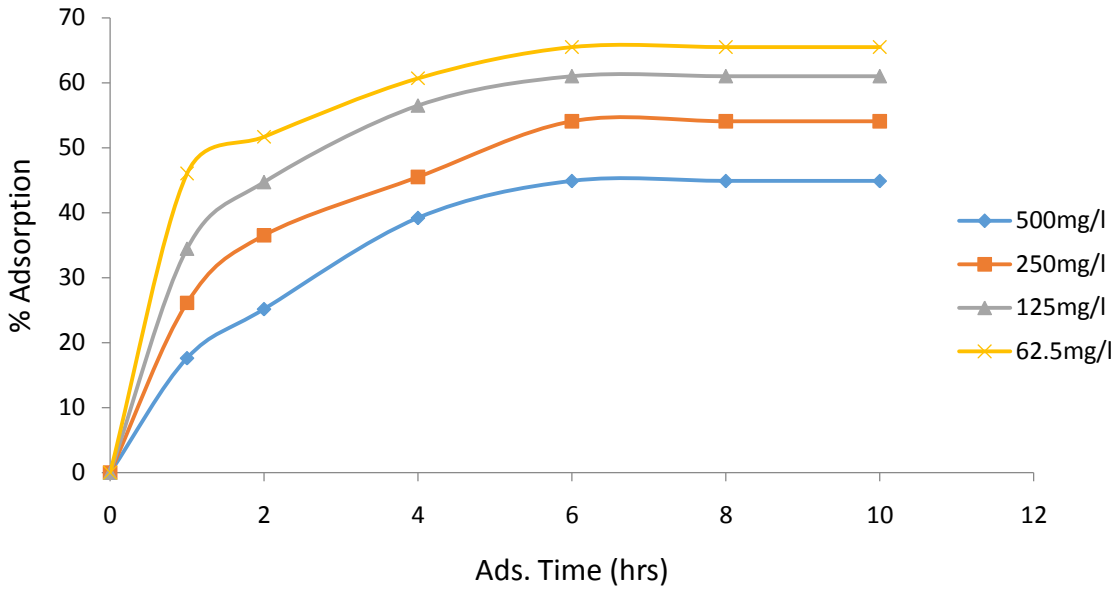


Fig. 4.3 Percentage adsorption of phenol by PB-60

Figure 4.3 shows that the time required for the equilibrium adsorption of phenol on the clays was six hours. The adsorption of phenol by the clays increases as the initial phenol concentration increased. Increasing the initial phenol concentration would increase the mass transfer driving force and therefore the rate at which phenol molecules pass from the bulk solution to the particle surface. This would result in higher phenol adsorption. On a relative basis, however, the percentage adsorption of phenol decreases (Figure 4.3) as the initial phenol concentration increases (Oladoja *et. al.*, 2008).

4.5.1 Adsorption dynamics

The effect of initial phenol concentration at different phenol concentrations of 500, 250, 125 and 62.5mg/*l* on the kinetics was studied.Kinetics of adsorption, a standard analysis in defining adsorption efficiency, describes the solute uptake rate, which in turn governs the residence time of adsorption process.From Equation 2.1, a plot of *log* $(q_e - q_t)$ versus *t* shown in Fig. 4.4 gave a linear relationship; hence, k_1 and q_e were calculated from the slope

and intercept of the plot, respectively. Also, from Equation 2.2, t/qt was plotted against t(Fig.4.5) which also gave a linear relationship; $q_e$and k_2 were determined from the slop and intercept of the plot. A plot of q_t against $t^{1/2}$ was also generated using Equation 2.3; here the slope gave the rate constant, k_{id}(Fig.4.6). These were summarized in Tables 4.8 to 4.11.

1. *Effect of initial phenol concentration-phenol concentration of 500mg/l*

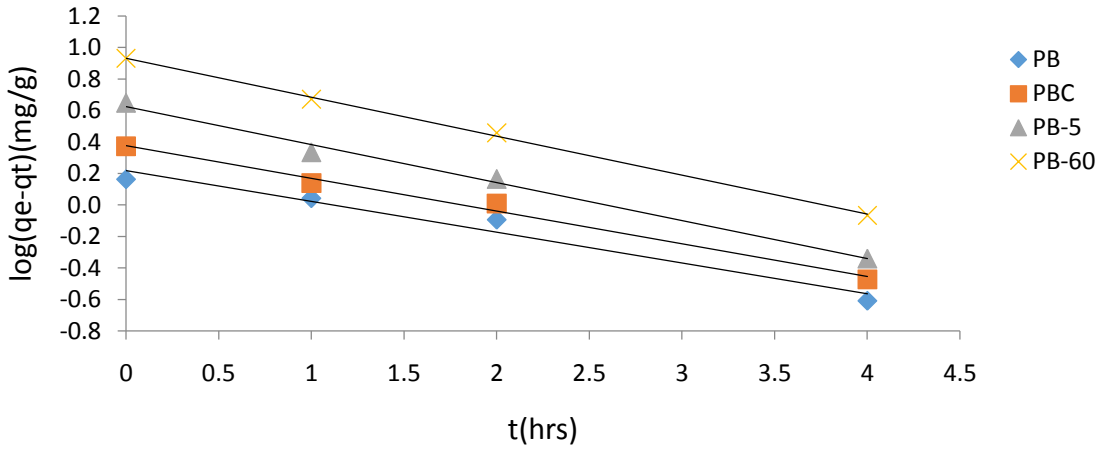


Fig. 4.4 Pseudo-first order kinetics of the raw and treated Pindiga clays with phenol concentration of 500mg/*l*

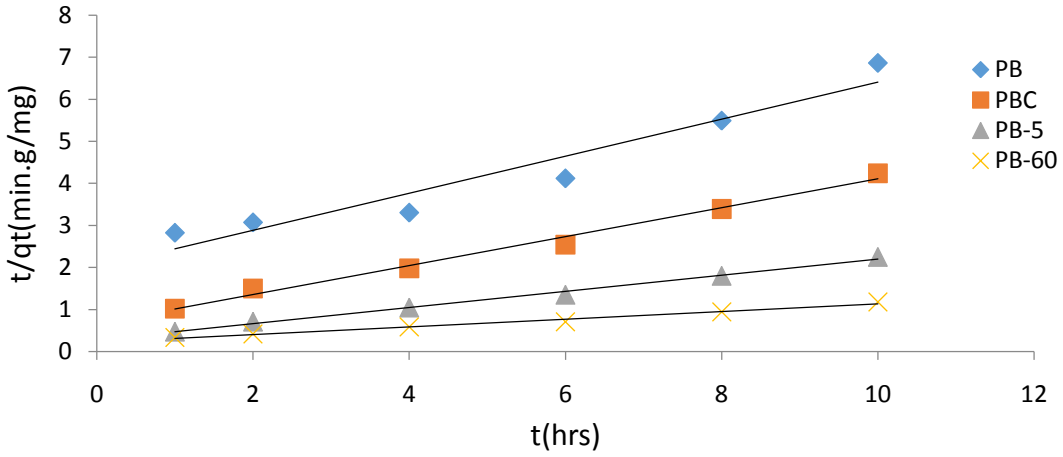


Fig. 4.5 Pseudo-second order kinetics of the raw and treated Pindiga clays with phenol concentration of 500mg/*l*

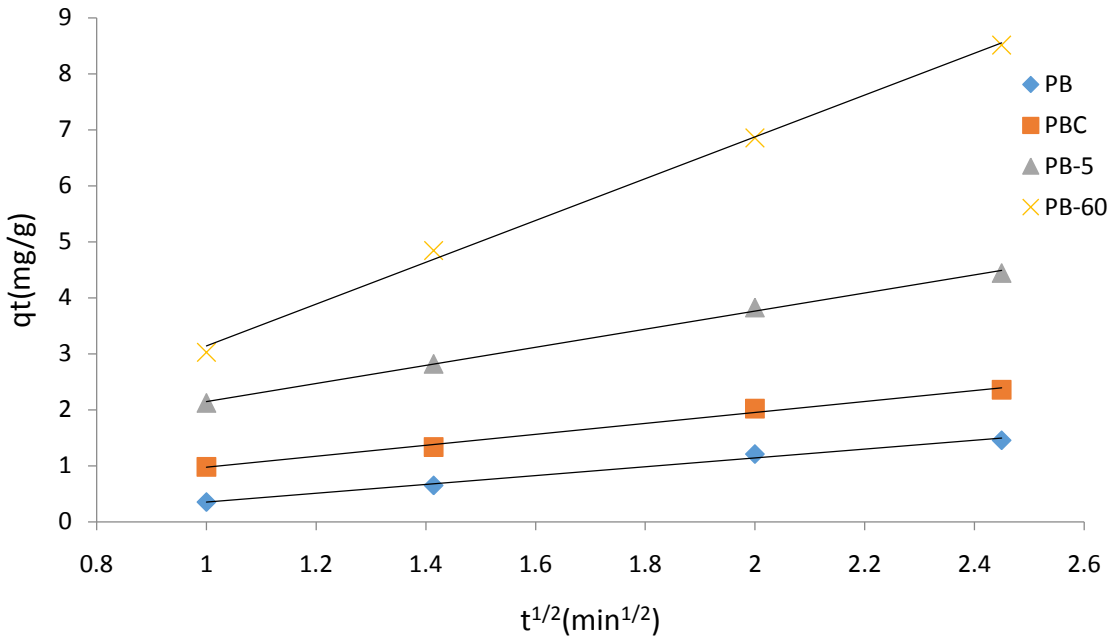


Fig. 4.6 Intra-particle diffusion model of the raw and treated Pindiga clays with phenol concentration of 500mg/*l*

Table 4.8Kinetic parameters for the adsorption of phenol by the raw and treated Pindiga clays at phenol concentration of 500mg/*l*

	1st Order Kinetics				**2nd Order Kinetics**				**Intra-Particle Diffusion**	
Catalysts/Ads. parameters	k_1 (min^{-1})	q_{ee} (mg/g)	q_{em} (mg/g)	R^2	k_2 (g/mg .min)	q_{ee} (mg/g)	q_{em} (mg/g)	R^2	k_{id} (mg/g. $min^{1/2}$)	R^2
PB	0.451	1.457	1.653	0.966	0.097	1.457	2.268	0.930	0.787	0.990
PBC	0.478	2.360	2.375	0.990	0.177	2.360	2.908	0.989	0.980	0.993
PB-5	0.555	4.286	4.203	0.993	0.132	4.286	4.941	0.994	1.615	0.997
PB-60	0.570	7.714	8.537	0.998	0.060	7.714	10.94	0.987	3.733	0.997

2. *Effect of initial phenol concentration-phenol concentration of 250mg/l*

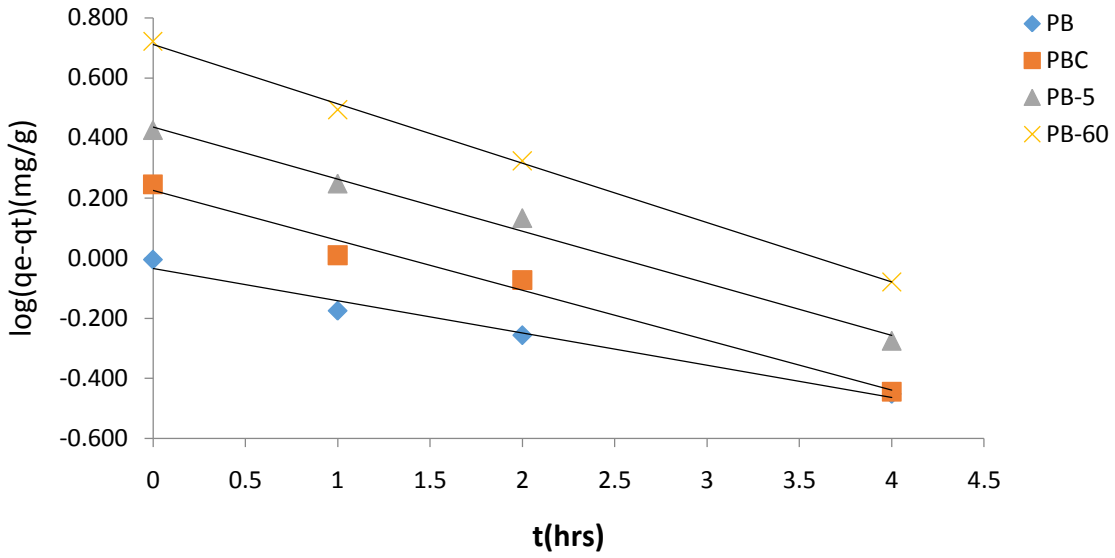


Fig. 4.7 Pseudo-first order kinetics of theraw and treated Pindiga clays with phenol concentration of 250mg/*l*

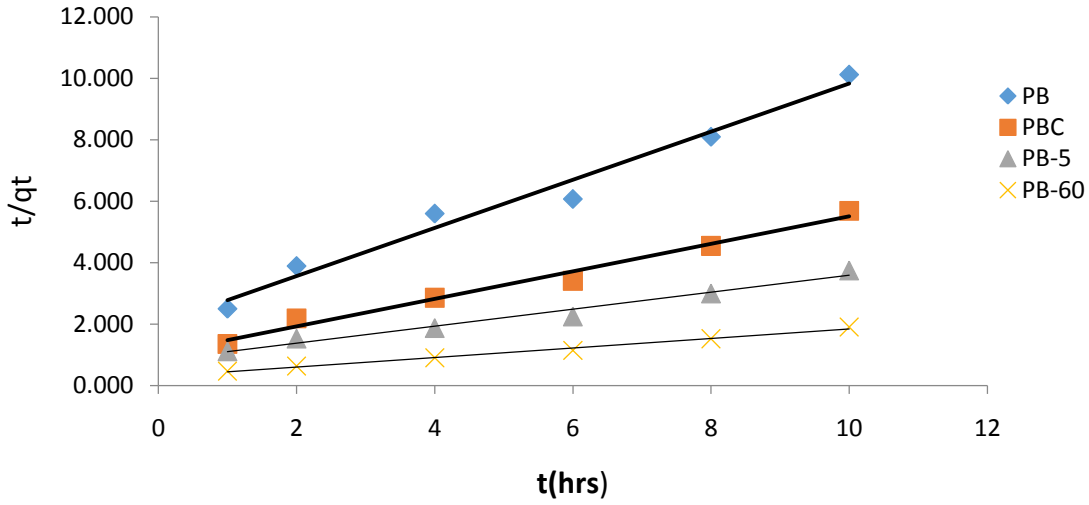


Fig. 4.8 Pseudo-second order kinetics of the raw and treated Pindiga clays with phenol concentration of 250 mg/*l*

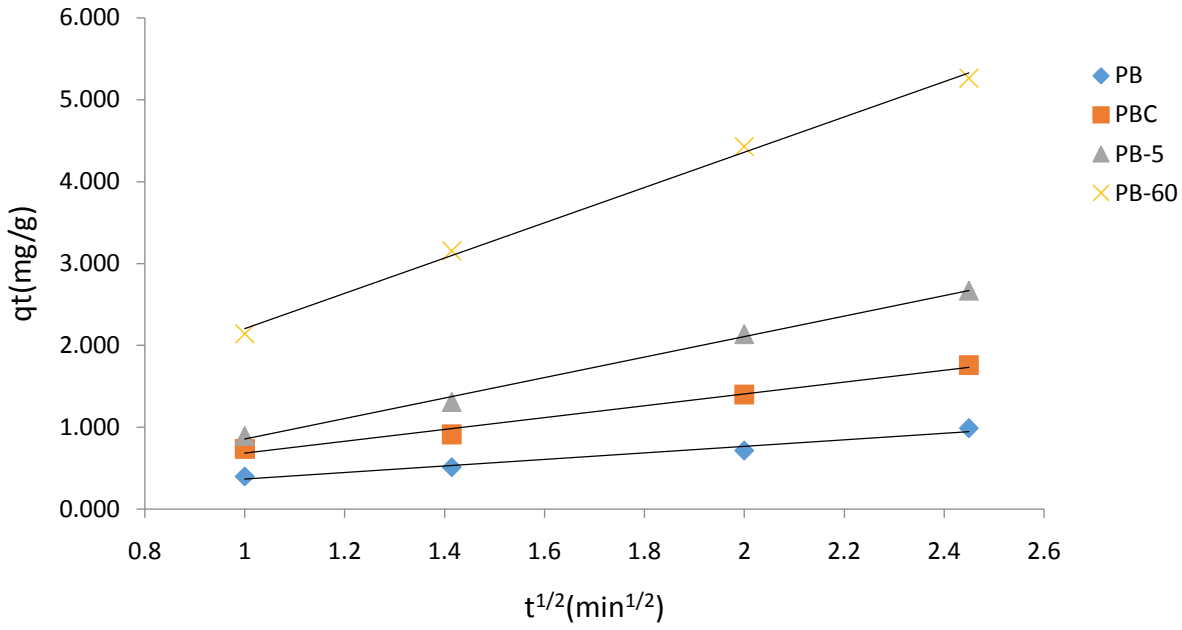


Fig. 4.9 Intra-particle diffusion model of the raw and treated Pindiga clayswith phenol concentration of 250mg/*l*

Table 4.9 Kinetic parameters for the adsorption of phenol by the raw and acid treated claysat phenol concentration of 250mg/*l*

	1st Order Kinetics				2nd Order Kinetics				Intra-Particle Diffusion	
Catalysts /Ads. parameters	k_1 (min^{-1})	q_{ee} (mg/g)	q_{em} (mg/g)	R^2	k_2 (g/mg .min)	q_{ee} (mg/g)	q_{em} (mg/g)	R^2	k_{id} (mg/g. $min^{1/2}$)	R^2
PB	0.247	1.069	1.081	0.979	0.306	1.069	1.277	0.976	0.398	0.970
PBC	0.383	1.760	1.68	0.984	0.196	1.760	2.23	0.982	0.724	0.987
PB-5	0.400	2.669	2.733	0.990	0.092	2.669	3.618	0.977	1.249	0.996
PB-60	0.455	5.263	5.139	0.998	0.082	5.263	6.447	0.992	2.154	0.997

3. *Effect of initial phenol concentration-phenol concentration of 125mg/l*

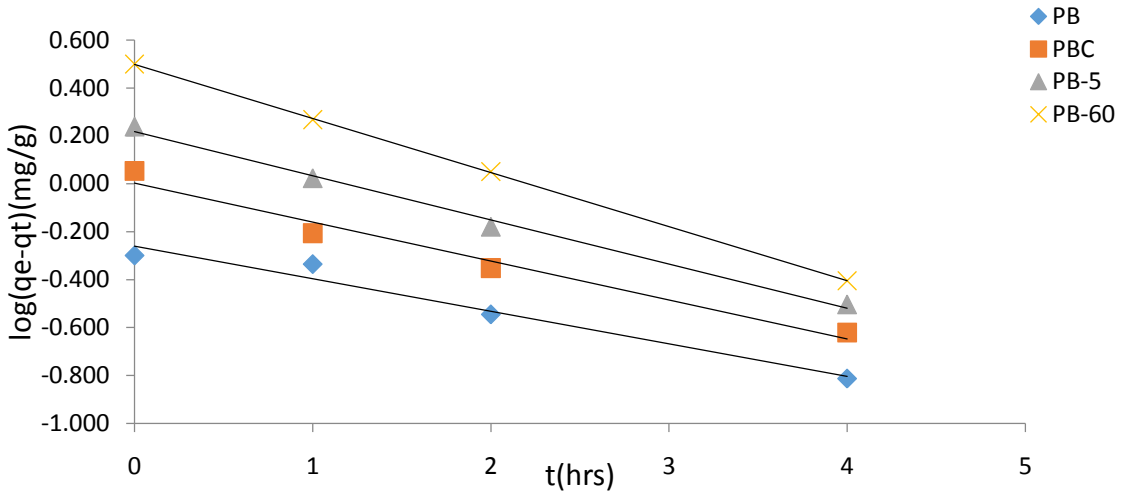


Fig. 4.10 Pseudo-first order kinetics of theraw and treated Pindiga clays with phenol concentration of 125mg/*l*

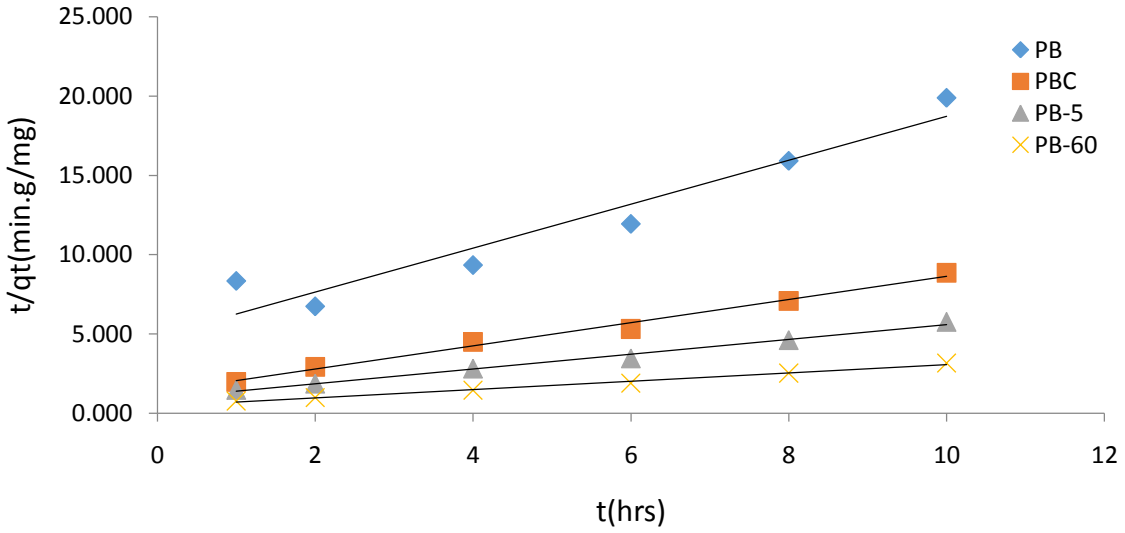


Fig. 4.11Pseudo-second order kinetics of the raw and treated Pindiga clays with phenol concentration of 125mg/*l*

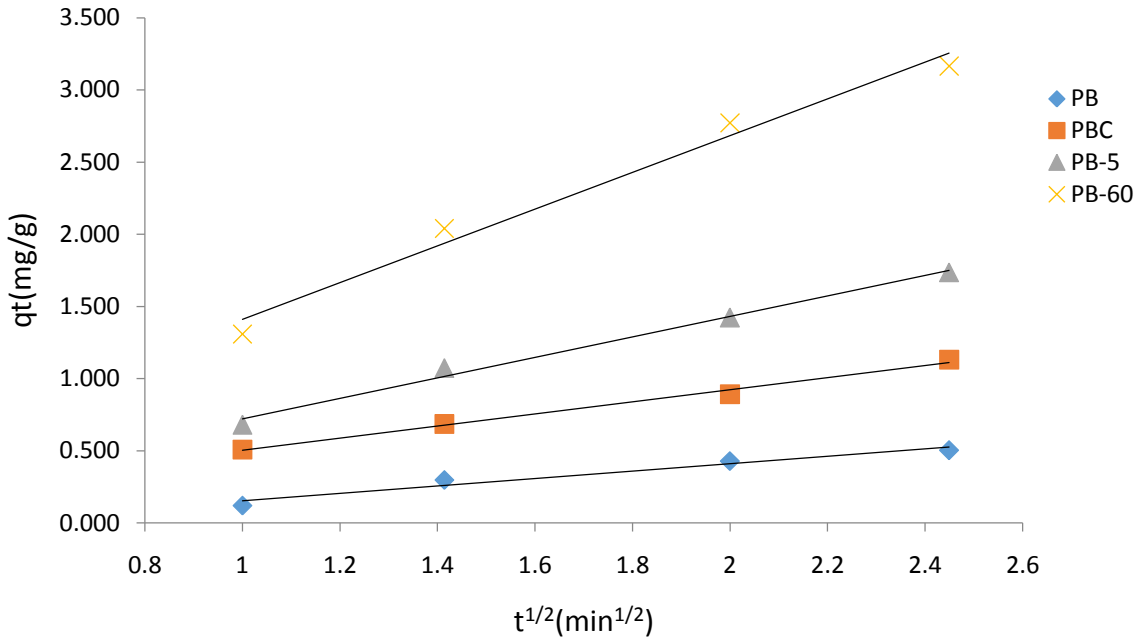


Fig. 4.12 Intra-particle diffusion model of the raw and treated Pindiga clays with phenol concentration of 125mg/*l*

Table 4.10 Kinetic parameters for the adsorption of phenol by the raw and acid treated claysat phenol concentration of 125mg/*l*

	1st Order Kinetics				**2nd Order Kinetics**				**Intra-Particle Diffusion**	
Catalysts/ Ads. parameters	k_1 (min^{-1})	q_{ee} (mg/g)	q_{em} (mg/g)	R^2	k_2 (g/mg.min)	q_{ee} (mg/g)	q_{em} (mg/g)	R^2	k_{id} (mg/g.$min^{1/2}$)	R^2
PB	0.313	0.583	0.550	0.967	0.393	0.583	0.722	0.926	0.257	0.960
PBC	0.374	1.131	1.009	0.974	0.406	1.131	1.366	0.990	0.419	0.993
PB-5	0.425	1.737	1.654	0.995	0.240	1.737	2.138	0.991	0.709	0.991
PB-60	0.520	3.166	3.154	0.999	0.160	3.166	3.793	0.993	1.273	0.981

4. *Effect of initial phenol concentration-phenol concentration of 62.5mg/l*

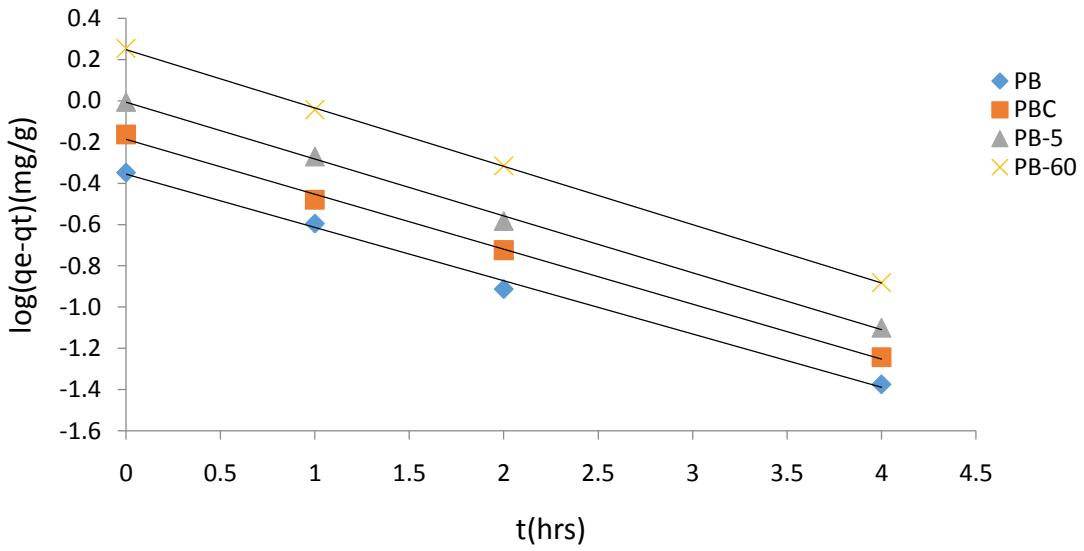


Fig. 4.13 Pseudo-first order kinetics of the raw and treated Pindiga clays with phenol concentration of 62.5mg/*l*

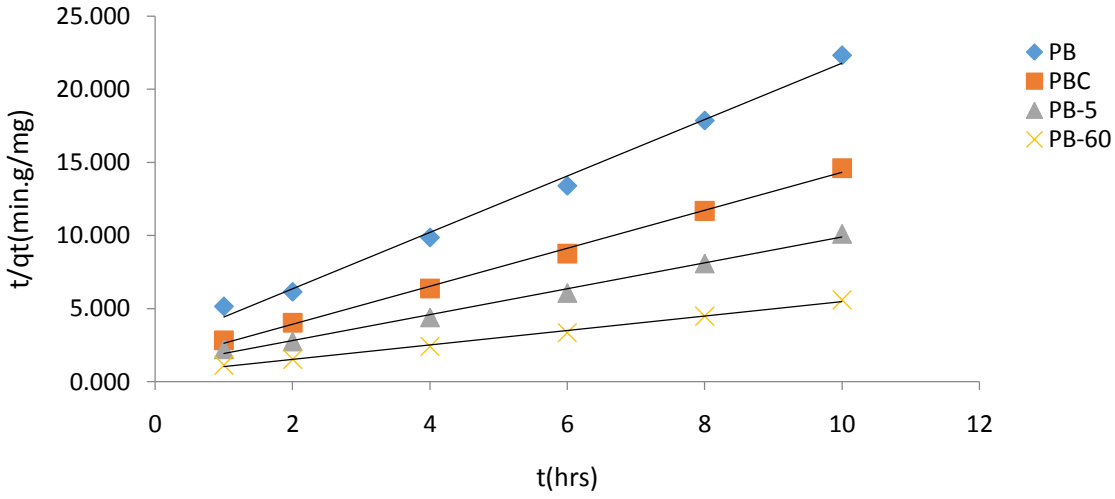


Fig. 4.14 Pseudo-second order kinetics of the raw and treated Pindiga clays with phenol concentration of 62.5mg/*l*

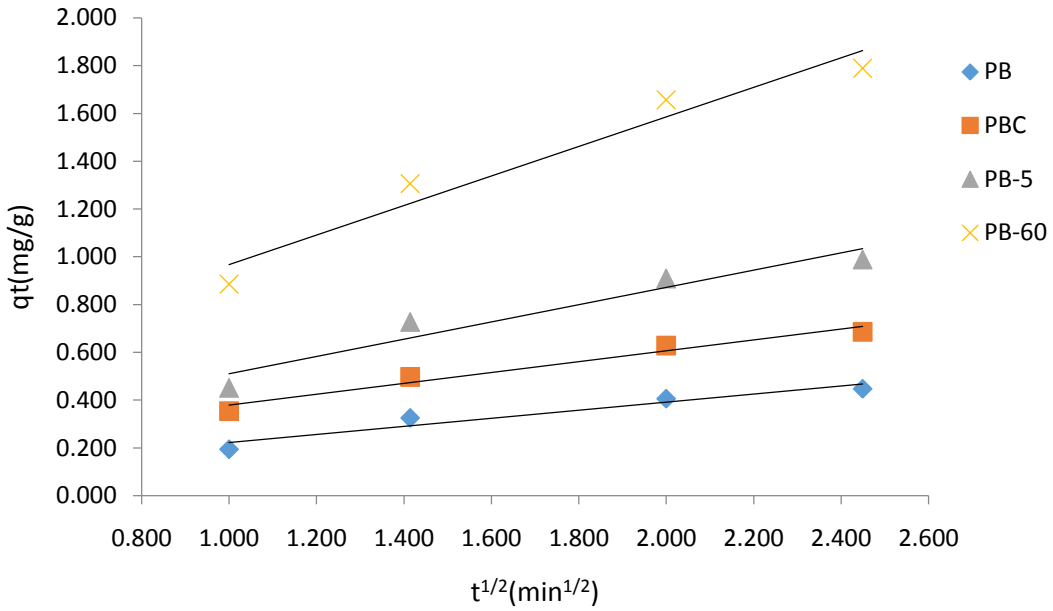


Fig. 4.15 Intra-particle diffusion model of the raw and treated Pindiga clays with phenol concentration of 62.5mg/*l*

Table 4.11Kinetic parameters for the adsorption of phenol by the raw and acid treated claysat phenol concentration of 62.5mg/*l*

	1st order kinetics				**2nd order kinetics**				**Intra-particle Diffusion**	
Catalysts/ Ads. Parameters	k_1 (min^{-1})	q_{ee} (mg/l)	q_{em} (mg/g)	R^2	k_2 (g/mg.min)	q_{ee} (mg/g)	q_{em} (mg/g)	R^2	k_{id} ($mg/g.min^{1/2}$)	R^2
PB	0.595	0.448	0.441	0.996	1.489	0.448	0.519	0.993	0.168	0.993
PBC	0.614	0.686	0.651	0.998	1.262	0.686	0.771	0.997	0.227	0.997
PB-5	0.634	0.989	0.983	0.999	0.754	0.989	1.131	0.994	0.36	0.994
PB-60	0.650	1.789	1.765	1.000	0.468	1.789	2.02	0.996	0.617	0.996

The study of the adsorption kinetics of phenol uptake by PB, PBC, PB-5 and PB-60 was carried out for phenol concentrations of 500, 250, 125 and 62.5 mg/*l* respectively. The data presented in Figures 4.4 to 4.15 and Tables 4.8 to 4.11 indicates that the adsorption process

obeys pseudo-first order kinetic model. At 500 mg/*l* phenol concentration, PB-60 was found to have the highest rate constant of k_1= 0.570 $min^{-1}$by pseudo-first order model followed by PB-5 (k_1= 0.555 min^{-1}), PBC (k_1= 0.478 min^{-1}) and PB (k_1= 0.451 min^{-1}). The kinetic model was not well described by pseudo-second order kinetics. PB-60 has higher intra-particle diffusion constant k_{id} of 3.733mg/g.$min^{1/2}$ as compared to PB-5 (1.616 mg/g.$min^{1/2}$), PBC (0.981 mg/g. $min^{1/2)}$ and PB (0.788 mg/g. $min^{1/2}$).

The same order as above was observed at phenol concentrations of 250, 125 and 62.5 mg/*l*as shown in Tables 4.9, 4.10 and 4.11 respectively.

4.5.2 Equilibrium Isotherm Studies

In order to determine the adsorption potential of the adsorbents (PB, PBC, PB-5 and PB-60) for the removal of phenol, the adsorption data was tested using the Freundlich and Langmuir isotherm models. (Rengaraj *et. al.*, 2002 and Aksu *et. al.*, 2001).

Table 4.12 Equilibrium isotherm parameters for the adsorption of phenol by the raw and acid treated clays

	Langmuir			**Freundlich**		
Catalyst/Adsorption Parameters	K_L (g/l)	q_o (mg/g)	R^2	K_f (mg/g)	1/n	R^2
PB	0.00424	2.169	0.929	0.0328	0.696	0.945
PBC	0.00457	3.551	0.989	0.0553	0.663	0.982
PB-5	0.00594	5.587	0.996	0.0619	0.640	0.991
PB-60	0.00688	12.69	0.996	0.2006	0.614	0.999

The results reveal that the adsorption of phenol on PB, PBC, PB-5 and PB-60 is best described by the Freundlich adsorption isotherm, as indicated by R^2 values (>92%). As shown in Table 4.12, higher K_f-value of PB-60(0.2006 mg/g) indicates greater affinity for phenol compared to that of PB-5 (0.0619 mg/g), PBC (0.0553 mg/g) and PB (0.03228 mg/g). The adsorption intensity, 1/n was found to be 0.614, 0.640, 0.663 and 0.696 for catalysts PB-60, PB-5, PBC and PB respectively. It was observed that, in this system, the n-values satisfy the condition of heterogeneity, i.e. $0<1/n<1$ (Khalid *et. al.*, 2000). In the Langmuir adsorption model, the higher adsorption capacity (q_o) for PB-60 (12.69 mg/g) indicates that the amount of phenol per unit weight of sorbent (to form a complete monolayer on the surface) is higher than for PB-5 (5.587 mg/g), PBC (3.551 mg/g) and PB (2.169 mg/g). A relatively lower K_L-value (<0.007) implies low surface energy for all the adsorbents, thus, indicating a probable stronger bonding between phenol and sorbents (Aksu *et. al.*, 2001). In fact, fairly low to moderate K_L–values have been reported in many of the sorbent-phenol systems, involving palm-seed-coat-activated-carbon, bentonite, and rice husk (Rengaraj*et. al.*, 2002 and Mahvi *et. al.*, 2004). The K_L –values for PB-60, PB-5, PBC and PB are 0.00688 g/l, 0.00594 g/l, 0.00457 g/l and 0.00424 g/l respectively. PB-60 was found to have fit well with kinetic models and had better equilibrium isotherm parameters, hence, it was chosen for further study.

4.5.3 Effect of Adsorbent Dosage

Table 4.13 Percentage uptake of phenol by various dose of PB-60 at phenol concentration of 500mg/l

Adsorption Time(hrs)/Sorbent dose	1.5g	2.0g	2.5g	3.0g
0	0.000	0.000	0.000	0.000
1	7.547	13.697	17.620	25.332
2	17.453	20.080	25.166	30.386
4	24.302	32.380	39.195	44.415
6	32.713	38.830	44.880	49.202
8	32.713	38.830	44.880	49.202
10	32.713	38.830	44.880	49.202

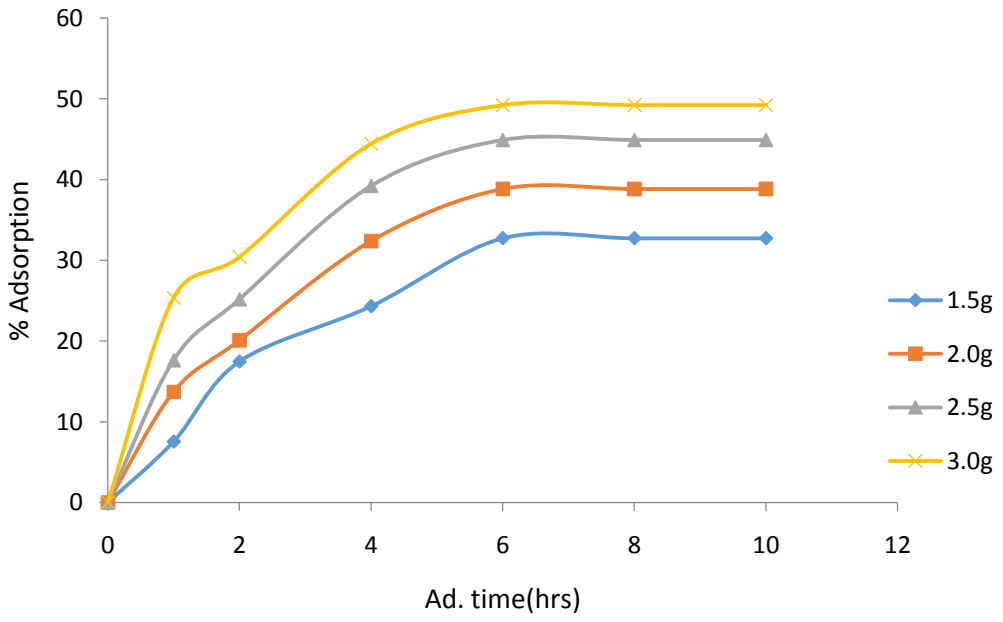


Fig. 4.18Percentage uptake of phenol by various dose of PB-60 at phenol concentration of 500mg/l

Figure 4.18 shows the amount of phenol removed as a function of adsorbent dosage from the solution at neutral pH and at 500 mg/l of phenol concentration. PB-60 dosage was varied from 1.5 g to 3.0 g and equilibrated for 10 hours. The percentage removal of phenol increased with the increase in adsorbent dosage. This can be attributed to increased adsorbent surface area and availability of more adsorption sites resulting from the increase adsorbent dosage. Equilibrium was achieved at 6 hrs so there was no further adsorption after 6 hrs.

4.5.4 Effect of solution pH

Table 4.14 Percentage uptake of phenol at various pH values of PB-60 at phenol concentration of 500mg/*l*

Adsorption Time (hrs)/Solution pH	pH=5	pH=9	pH=11
0	0.0	0.0	0.0
1	25.9	22.9	20.7
2	29.3	25.1	23.4
4	32.7	29.0	27.0
6	39.6	35.4	29.6
8	39.6	35.4	29.6
10	39.6	35.4	29.6

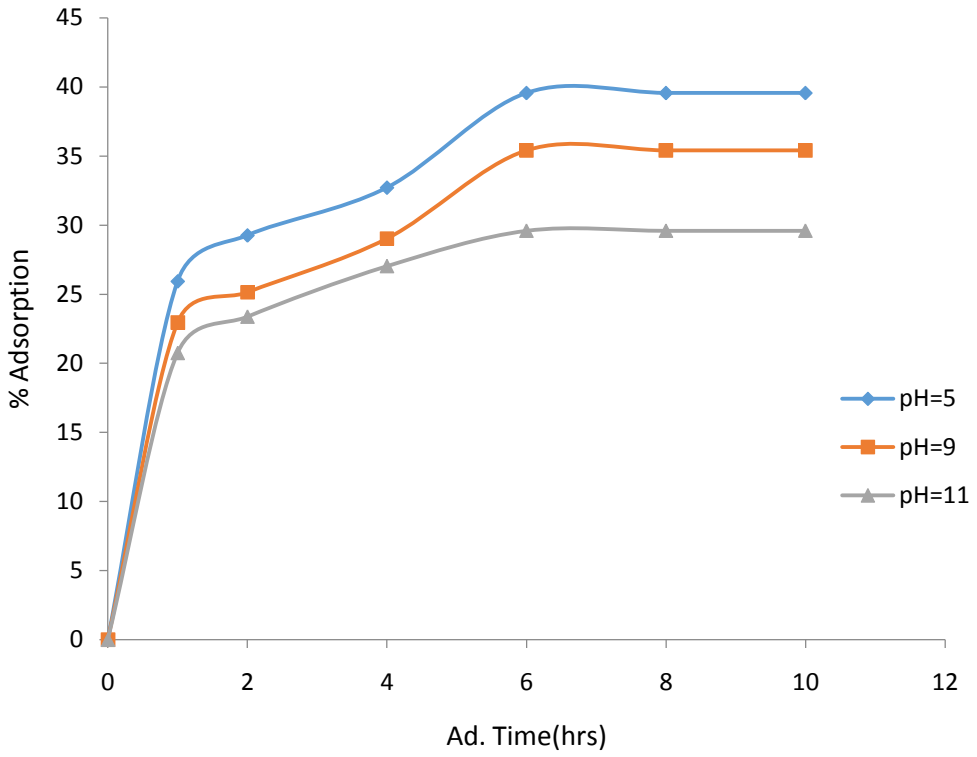


Fig. 4.19Percentage uptake of phenol at various pH values of PB-60 at phenol concentration of 500mg/*l*

The adsorption of phenol by PB-60 was studied at pH values of 5, 9 and 12. The result as shown in Figure 4.19 shows that the adsorbed amount decreases with increasing pH value. This can be attributed to the dependency of phenol ionization on the pH value (Ashe*et al*., 2003). Accordingly, phenol, which is a weak acid (pK_a = 10), will be adsorbed to a lesser extent at higher pH values. Similar behavior has been reported by Halhouli *et. al.*, (1997) for the adsorption of phenol by activated carbon.

4.6 Photocatalytic Degradation of Phenol Using PB, PBC, PB-5 and PB-60

The kinetic degradation of phenol for PB, PBC, PB-5 and PB-60 was studied using the Langmuir-Hinshelwood (L-H) kinetic model at different initial concentrationsand the results are shown in Table 4.13 and Appendix G (Figure G1). The values of $k_r$were greater

than those of $K_{LH}$for all the catalysts, indicating the phenol adsorption was the controlling step of the process. A similar phenomenon was reported for the photo decolorization of methyl orange over alpha-Fe_2O_3-supported HY photocatalysts (Nur *et. al.,* 2012). PB-60 fits best with the model and hence, chosen for further study.

Table 4.15Derived Langmuir-Hinshelwood kinetic parameters.

Catalysts/kinetic parameters	k_r ($mgL^{-1}min^{-1}$)	K_{LH} (Lmg^{-1})	R^2
PB	0.3777	0.0353	0.954
PBC	0.4852	0.0353	0.980
PB-5	3.8314	0.0035	0.991
PB-60	6.8483	0.0034	0.999

4.6.1 Effect of pH

Table 4.16 Effect of solution pH on the photocatalytic degradation of phenol by PB-60 at phenol concentration of 500mg/l

Kinetic parameter/pH values	pH=11	pH=9	pH=5
K (min^{-1})	0.0001	0.005	0.008
R^2	0.948	0.992	0.997

Lower pH values are observed to be favourable for the photocatalytic degradation of phenol by PB-60 as presentedin Table 4.16. PB-60 was more efficient in photo degrading phenol at a pH of 5 as compare to a pH of 11.

4.6.2 Effect of catalyst dosage

The catalyst dosages were varied from 1.5g to 3.0g and photodegradation of phenol was carried out for 2 hour.

Table 4.17: Effect of catalyst dosage on the photocatalytic degradation of phenol withphenol concentration of 500mg/l by PB-60.

Kinetic parameter /catalyst dose	1.5g	2.0g	2.5g	3.0g
K_{app} (min^{-1})	0.002	0.003	0.007	0.005
R^2	0.91	0.964	0.999	0.999

The effect of photocatalyst concentration on the degradation rate of phenol has been investigated by employing different concentrations of PB-60 varying from 1.5 to 3.0g/*l* under visible light illumination. The result is presented in Table 4.15. It was observed that the initial rate increases with increase in PB-60 concentration, becomes maximum at 2.5g/*l* and then decreases afterwards. The optimum PB-60 concentration for the degradation of phenol is 2.5 g/*l*.This showed that an increase in the amount of PB-60 to 2.5 g/*l*increases the amount of phenol degradation. Any further increase above 2.5g/*l*has negative effect on the photo degradation efficiency. This is because, with increase in the amount of photocatalyst,the particles can create a light screening effect that reduces the surface area of the photocatalyst exposed to light illumination and photocatalytic efficiency.

CHAPTER FIVE

CONCLUSIONS AND RECOMMENDATIONS

5.1 Conclusions

The following are conclusions drawn from this work:

1. Adsorbent and photocatalysts were developed from Pindiga bentonitic clay via oxalic acid leaching and calcinations at 1000^{o}C for four hours.The physicochemical properties of the catalysts were studied via XRF, XRD, and surface area analysis.
2. PB-60 was observed to havethe highest surface area of 363.61m^2/g, followed by PB-5 which has a surface area of 265.99m^2/g, then catalyst PBC which has a surface area of 151.69m^2/g and lastly PB which has a surface area of 47.13m^2/g.
3. Pseudo-first order kinetic model and intra-particle diffusion model were observed to provide a better correlation for the adsorption data while the data does not fit well with pseudo-second order kinetic model.
4. The equilibrium data in aqueous solutions was best described by the Freundlich isotherm.
5. Increase in pH value was observed to hinder adsorption and photocatalytic processes. Better adsorption and photocatalysis was observed at a lower pH value (acidic medium).
6. The kinetics of photocatalytic degradation of phenol was well represented by the Langmuir-Hinshelwood kinetic model.
7. The optimum catalyst dosage required was 2.5g/l for the photocatalytic degradation.

5.2 Recommendations

Here are some recommendations in relation to this thesis work

1. Further works should be carried out by using natural source of light-sunlight as source of visible light in photocatalytic experiments.
2. This work should be pursued further to industrial level.
3. A pilot scale adsorption/photocatalytic reactor should be built for further adsorption/photocatalytic experiments.

REFERENCES

Adefila, S.S., Aderemi, B.O., Ajayi, O.A. and Bederin, D. A. (2003). Comparative Surface Area Determination Using Water Adsorption Method: Nigeria Journal of Engineering, 11(2) 88-95.

Ahmed, A. S., Salahudeen, N., Ajinomoh,C. S., Hamza, H. and Ohikere, A. (2012). *Studies on the Mineral and Chemical Characteristics of PindigaBentonitic Clay:* Petroleum Technology Development Journal, vol. 1, pp. 2-8.

Aksu, Z and Yener, J. (2001).*A Comparative Adsorption/Biosorption Study of Mono-Chlorinated Phenols onto Various Sorbent*.Waste Management,vol. 21, pp. 695-702.

Asheh, S. A., Banat, F. and Aitah, L. A. (2003). *Adsorption of Phenol Using Different Types of Activated Bentonites.* Separation and Purification Technology Vol. 33, pp. 1-10.

Banat F.A., Al-Bashir B., Al-Asheh S. and Hayajneh O. (1999).*Adsorption of Phenol by Bentonite.* Environmental Pollution Journal, vol. 107, pp. 391-398. .

Bakardjieva, S., Stengl, V., Subrt, J., Houskova, V. and Kalenda, P. (2006).Photocatalytic Efficiency of Iron Oxides: Degradation of 4-Chlorophenol.*Journal of Physics and Chemistry of Solids*, vol. 68, pp. 721-724.

Beydoun, D., and Amal, R.(1999). Role of Nanoparticle in Photocatalysis.*Journal Nanoparticles Research*, pp. 439- 458.

Bräuer, G.,Bullinger, H. Springer, J. (2009).*Surface and Coating Technologies: Technology Guide*.

Czepirski, L., Balys, M. R., Komorowska-Czepirska, E. (2000). Some Generalization of Langmuir Adsorption Isotherm.*Internet Journal of Chemistry*, vol. 3(14).

Dinilichenko, S., Kukharenko, O., Moseke, C.,Protsenko, I., Sukhodub, L.and Sulkio-Cleff, B.(2002). Determination of the Bone Mineral Crystallite Size and Lattice Strain from Diffraction Line Broadening.*Research and Technology Crystal*, vol. 37, No. 11, pp. 1234-1240.

Ferrari, L., Kaufmann, J., Winnefeld, F. and Plank, J. (2010). Interaction of Cement Model Systems With Super Plasticizers Investigated by Atomic Force Microscopy, Zeta Potential, and Adsorption Measurements. *Journal Colloid Interface Science*, vol. 347(1), pp. 15–24.

Fitton, G. (1997). X-Ray Fluor*escence Spectrometry and Modern Analytical Geochemistry: An Introduction to Quantitative Chemical Analysis for Earth, Environmental and Material Scientists.* Addison Wesley Longman, UK.

George, V. (1999). *Journal of Petroleum Science and Engineering*, vol. 22(4), pp. 241–252. doi: 10.1016/S0920-4105(98)00084-9

Gutberle (1994). *Slurry Walls*. Virginia Tech. Retrieved 2012-01-05.

Halhouli, K.A., Darwish, N.A., Al-Jahmany, Y. (1997). *Effects of Temperature and Inorganic Salts on the Adsorption of Phenol from Multicomponent System on a Decolorizing Carbon*.Separation Science and Technology,vol. 32, pp. 3027-3036.

Hamza, A., Abdallah, N. M. and Aliyu, A.A. (2011).Photocatalytic Activity of Nigerian Ilmenite. *Nigerian Journal of Engineering*, vol. 18, pp. 111-114.

Hosterman, J.W. and Patterson, S. H. (1992). *Bentonite and Fuller's Earth Resources of the United States*. U.S. Geological Survey Professional Paper 1522. United States Government Printing Office, Washington D.C., USA

Khalid, N., Ahmad, S.and Toheed, S. (2000).A Potential of Rice Husk for Antimony Removal. *Applied Radiation and Isotopes*, vol. 52, pp. 30-38.

Klug, H.and Alexander, L. (2004).*X-Ray Diffraction Procedure for Polycrystalline and Amorphous Materials.*2nd Edition, John Wiley and Sons, New York.

Langford, J. and Wilson, A.(1981).Scherrer after Sixty Years: A Survey and Some New Results in the Determination of Crystallite Size.*Journal of Applied Crystallography,* vol. 11, pp. 102-103.

Mahvi, A.H., Maleki, A. and Eslami, A. (2004).Potential of Rice Husk and Rice Husk Ash for Phenol Removal in Aqueous Systems.*American Journal of Applied Sciences*, vol. 1(4), pp. 321-326.

Martinez-Luevanos, A., Rodriguez-Delgado, M.G., Uribe-Salas, A. and Carrillo-Pedroza, F.R., (2011).Leaching Kinetics of Iron from Low Grade Kaolin by Oxalic Acid Solutions.*Applied Clay Science Journal*, vol. 51, pp. 473-477.

Mohapatra, M. and Anand, S. (2010).Synthesis and Application of Nano-Structured Iron Oxides/Hydroxides-A Review.*International Journal of Engineering, Science and Technology,* vol. 2, pp. 127-146.

Odom, I. E. (1984). Smectite clay Minerals: Properties and Uses. Philosophical Transactions of the Royal Society.*A Mathematical, Physical and Engineering Sciences,* vol. 5, pp. 231-240.

Oladoja, N. A., Aboluwoye C. O. and Oladimeji Y. B. (2008). Kinetics and Isotherm Studies on Methylene Blue Adsorption onto Ground Palm Kernel Coat.*Turkish Journal of Engineering, Environment and Science,*vol. 32, pp 303-312.

Piao, X., Guang, M. Z., Dan, L. H. and Chong, L. F. (2012).Use of Iron Oxide Nanomaterial in Wastewater Treatment: A Review: *Science of the Total Environment Journal*, vol. 424, pp. 1-10.

Potts, P.J. (1987).*A Handbook of Silicate Rock Analysis*.Chapman and Hall, pp. 234-235.

Rengaraj, S., Seuny-Hyeon, M. and Sivabalan, R. (2002).Agricultural Solid Waste for the Removal of Organics: Adsorption of Phenol from Water and Wastewater by Palm Seed Coat Activated Carbon. *Waste Management*,vol. 22, pp. 543-548.

Raw Material Research and Development Council,RMRDC (1991).*Raw Materials Sourcing for Manufacturing in Nigeria*, 3rdedition, Abuja.

Rollinson, H.(1993).*Using Geochemical Data: Evaluation, Presentation and Interpretation*.John Wiley, NY, pp. 43-47.

Serponeand Pellizette (2000). Photocatalysis Fundamental and Applications.*Journal of Photochemistry and Photobiology*, vol.2, pp. 130.

http://www.20nano.com/bentonite.php

http://www.pranavsaiimpex.com/other-files/bentonite-details-photos.pdf

http://www.reade.com/products/29-minerals-and-ores-powder

http://www.reade.com/bentonite-1997

http://www.ima-na.org

http://intersac.com/bentonite/

www.mch-nano solutions.com/mechanism of photocatalysis-2012

APPENDIX A

SURFACE AREA DETERMINATION

Appendix A shows the water adsorption method used in determining the surface area of catalysts PB, PBC, PB-5 and PB-60.

Table A1. Data for the determination of Relative Humidity of salts solutions

Salts	$CaSO_4$	$MgCl_2$	K_2SO_4	CH_3COONa
WD1	36.88	70.06	35.3	64.2
WD2	36.63	69.8	34.92	64.01
WA1	38.33	64.71	33.49	51.34
WA2	34.05	63.57	29.89	49.64
RH	0.0584	0.2281	0.1056	0.1118

Where,

WD1 = Initial weight of salt solution in desiccator

WD2 = Final weight of salt solution in desiccator after 24hrs

WA1 = Initial weight of salt solution opened to atmosphere

WA2 =Final weight of salt solution opened to atmosphere after 24hrs

RH = Relative Humidity of salts

$$RH = \frac{WD2 - WD1}{WA2 - WA1} = {}^{P}/_{Po}$$

Table A2. BET Isotherm of prepared photocatalysts

	$CaSO_4$		K_2SO_4		CH_3COONa		$MgCl_2$	
Sample	**V(g)**	**Y(g^{-1})**	**V(g)**	**Y(g^{-1})**	**V(g)**	**Y(g^{-1})**	**V(g)**	**Y(g^{-1})**
PB	0.0310	1.0909	0.0500	1.2330	0.0470	3.7852	0.0500	3.9875
PBC	0.187	0.1808	0.613	0.1006	0.200	0.8895	0.172	1.1592
PB-5	5.7660	0.0059	3.7520	0.0164	0.3710	0.4795	0.3420	0.5830
PB-60	1.8310	0.0185	1.4820	0.0416	0.4160	0.4277	0.4970	0.4012

Table A3. BET Isotherm and Relative Humidity Data

	PB-0		**PB-5**		**PB-60**		**PB-C**	
Salts	**P/P_o**	**Y(g^{-1})**	**P/P_o**	**Y(g^{-1})**	**P/P_o**	**Y(g^{-1})**	**P/P_o**	**Y(g^{-1})**
$CaSO_4$	0.0350	1.0909	0.0350	0.0059	0.0350	0.0185	0.0350	0.1808
K_2SO_4	0.0660	1.2330	0.0660	0.0164	0.0660	0.0416	0.0660	0.1006
CH_3COONa	0.2315	3.7852	0.2315	0.4795	0.2315	0.4277	0.2315	0.8895
$MgCl_2$	0.2750	3.9875	0.2750	0.5830	0.2750	0.4012	0.2750	1.1592

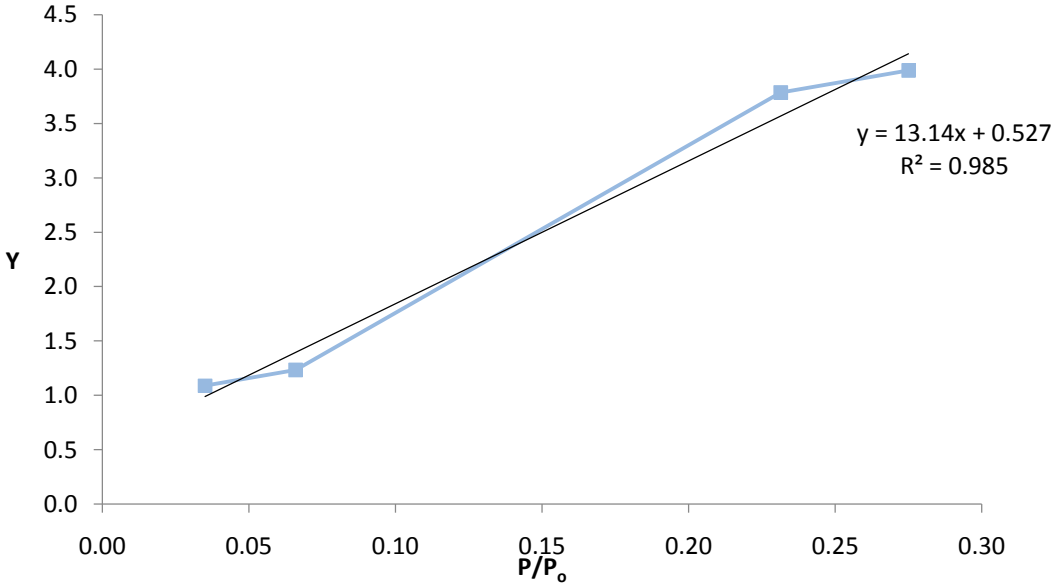


Fig. A1. BET Isotherm plot for catalyst PB

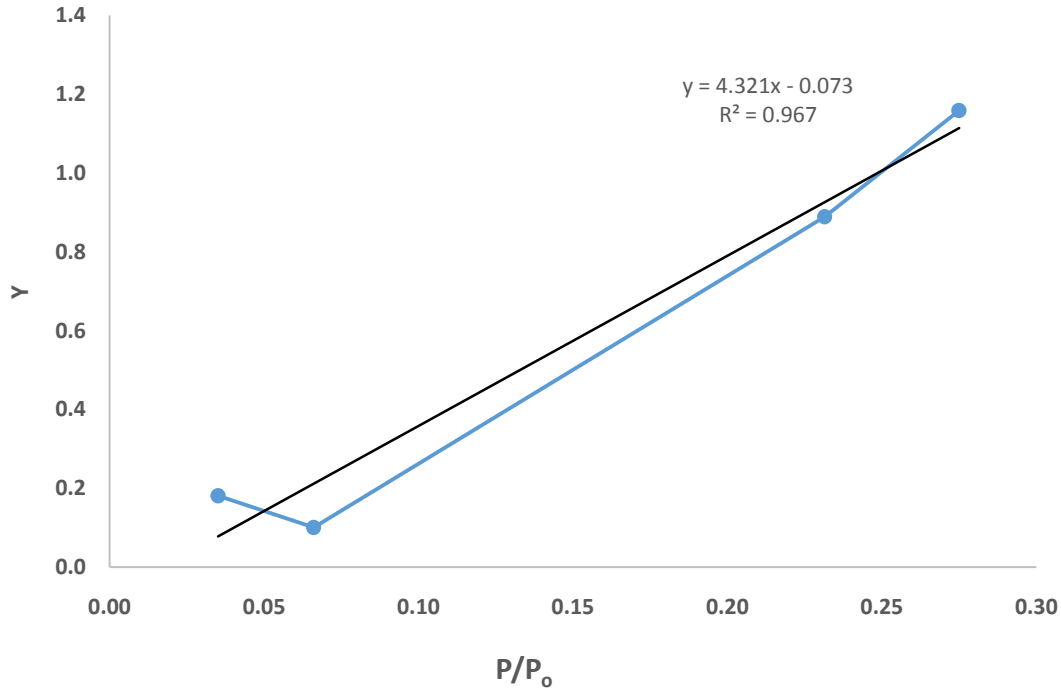


Fig. A2. BET Isotherm plot for catalyst PBC

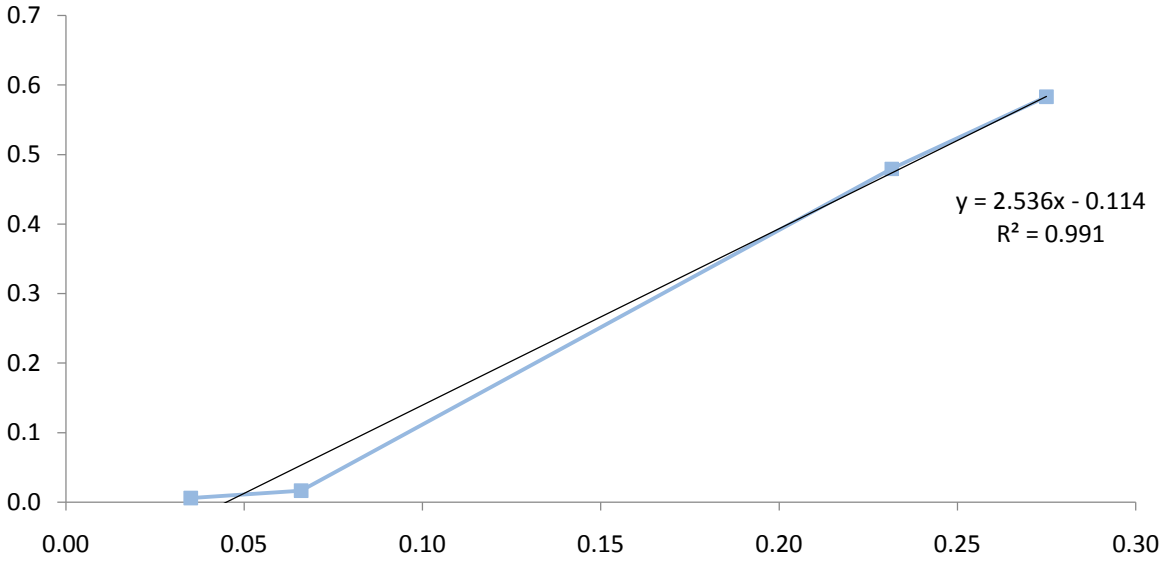


Fig. A3. BET Isotherm plot for catalyst PB-5

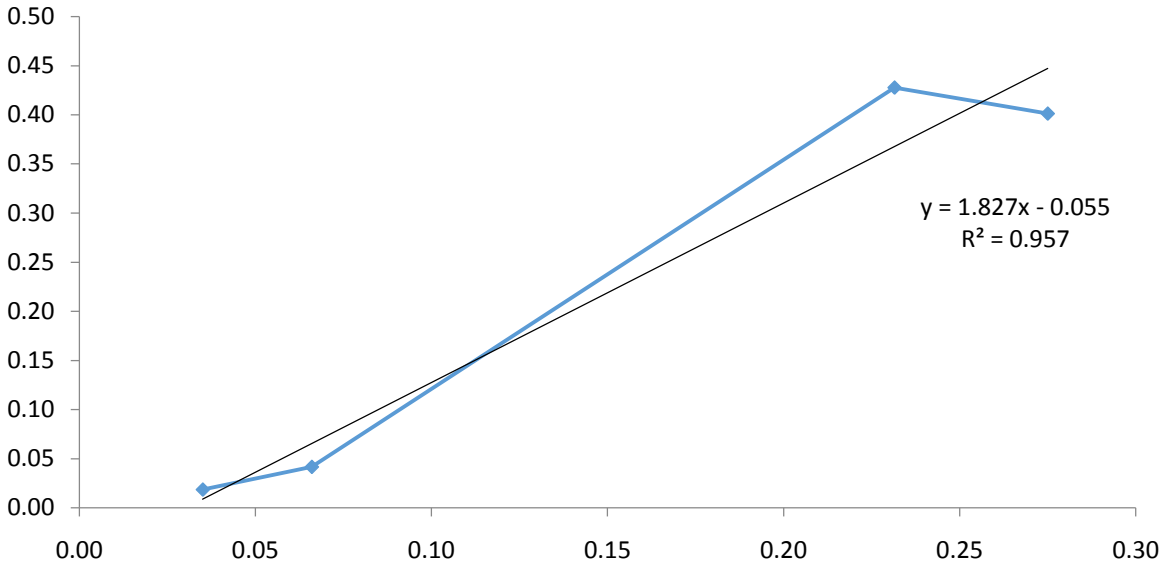


Fig. A4. BET Isotherm plot for catalyst PB-60

Table A4: From equation 2.1 to 2.13 the surface area is calculated and the following results is obtained

	PB	**PB-C**	**PB-5**	**PB-60**
V_m	0.073143	0.235427	0.412814	0.564302
alpha	4.04E-19	4.04E-19	4.04E-19	4.04E-19
$S_G(m^2/g)$	47.13019	151.6985	265.9984	363.6107

APPENNDIX B

CRYSTALLITE SIZE ANALYSIS USING XRD

1. Catalyst PB

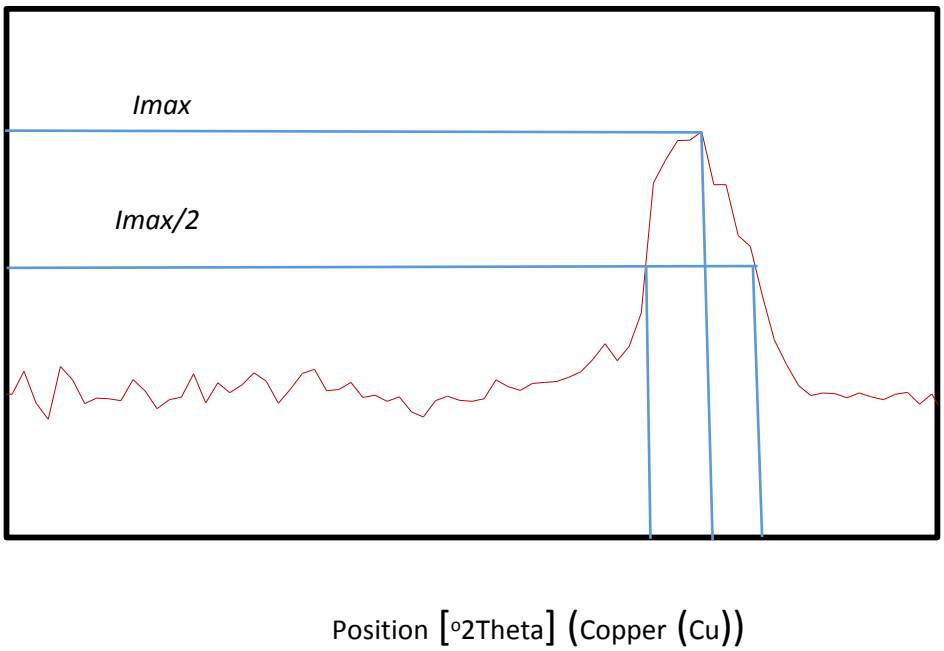


Figure B1: XRD showing the peaks for evaluating β and θ for catalyst PB

Using Scherrer's equation,

$$D = \frac{0.9\lambda}{\beta cos\theta}$$

Where, D=particle size, nm

$$\lambda = 1.54\text{Å}$$

β=width at Full Width at Half Maximum (FWHM) in radians

$cos2\theta$=Bragg angle

$$2\theta = 49.70$$

$$\beta = (49.47 - 48.89) \times {}^{\pi}/_{180} = 0.010124$$

$$D = \frac{0.9 \times 1.54A}{0.010124 \times \cos\left({}^{49.70}/_{2}\right)}$$

$$= 147.577A$$

$$= 14.76nm$$

2. Catalyst PBC

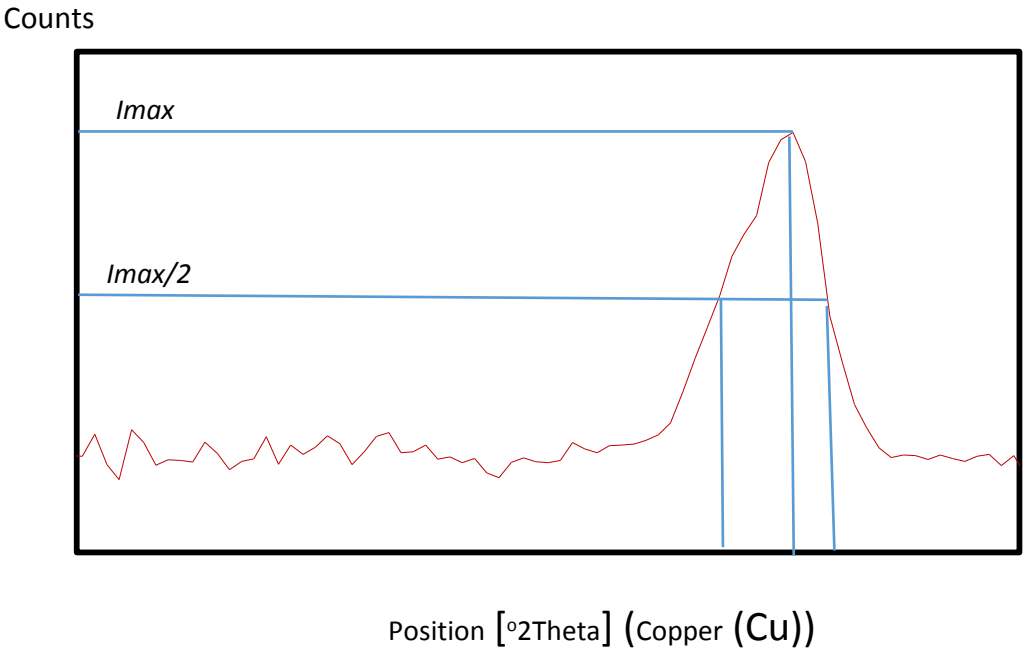


Figure B2: XRD showing the peaks for evaluating β and θ for catalyst PBC

$$2\theta = 49.50$$

$$\beta = (49.84 - 49.71) \times {}^{\pi}/_{180} = 0.002269$$

$$D = \frac{0.9 \times 1.54A}{0.002269 \times \cos\left({}^{49.50}/_{2}\right)}$$

$$= 658.422A$$

$$= 65.84nm$$

3. Catalyst PB-5

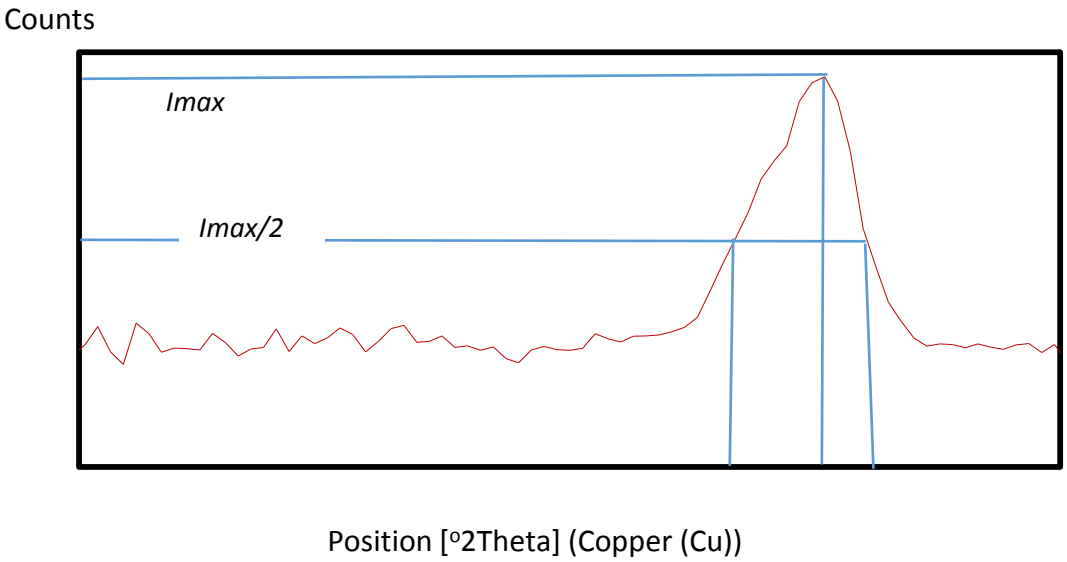


Figure B3: XRD showing the peaks for evaluating β and θ for catalyst PB-5

$$2\theta = 49.51$$

$$\beta = (49.85 - 49.69) \times {}^{\pi}/_{180} = 0.002618$$

$$D = \frac{0.9 \times 1.54A}{0.002618 \times \cos\left({}^{49.51}/_{2}\right)}$$

$$= 570.633A$$

$$= 57.10nm$$

4. Catalyst PB-60

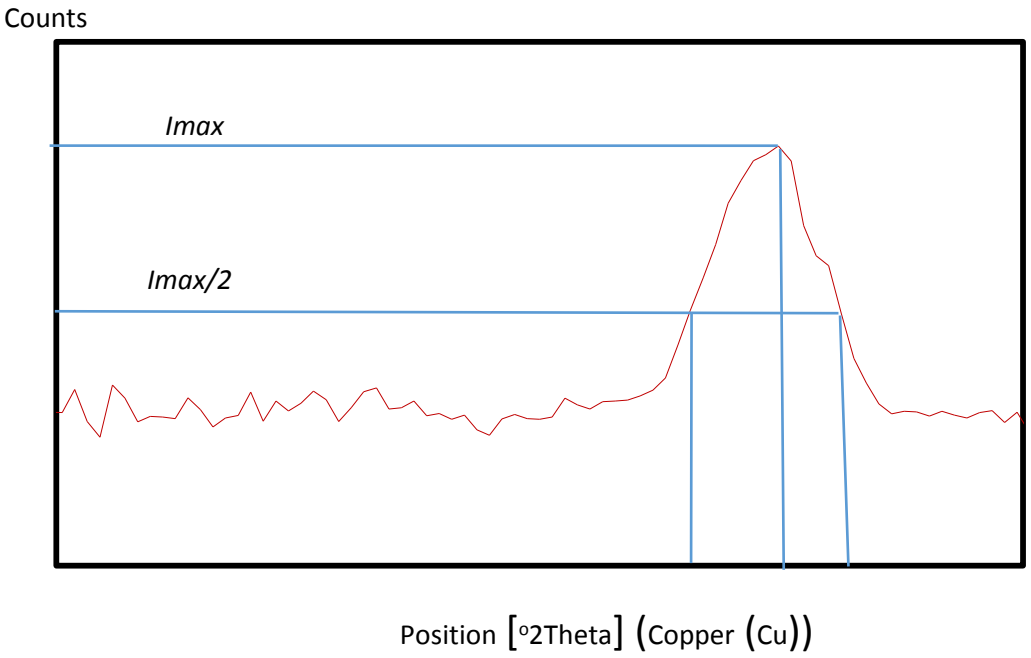


Figure B4:XRD showing the peaks for evaluating β and θ forcatalyst PB-60

$$2\theta = 49.51$$

$$\beta = (49.85 - 49.69) \times {}^{\pi}/_{180} = 0.002915$$

$$D = \frac{0.9 \times 1.54A}{0.002915 \times \cos\left({}^{49.51}/_{2}\right)}$$

$$= 512.544A$$

$$= 51.25nm$$

APPENDIX C

Calibration of absorbance measurement in relations to concentration of phenol in mg/l

Table C1 Conversion of absorbance to concentration in mg/l

Phenol Conc.	Absorbance	Wavelength, nm	Conc, mol/dm^3	Conc,mg/l
Phenol 10mg in 50ml	1.559	270	0.021251727	200.0
Phenol 10mg in 100ml	0.805	270	0.010625863	100.0
Phenol 10mg in 150ml	0.503	270	0.007083909	66.7
Phenol 10mg in 200ml	0.345	270	0.005312932	50.0

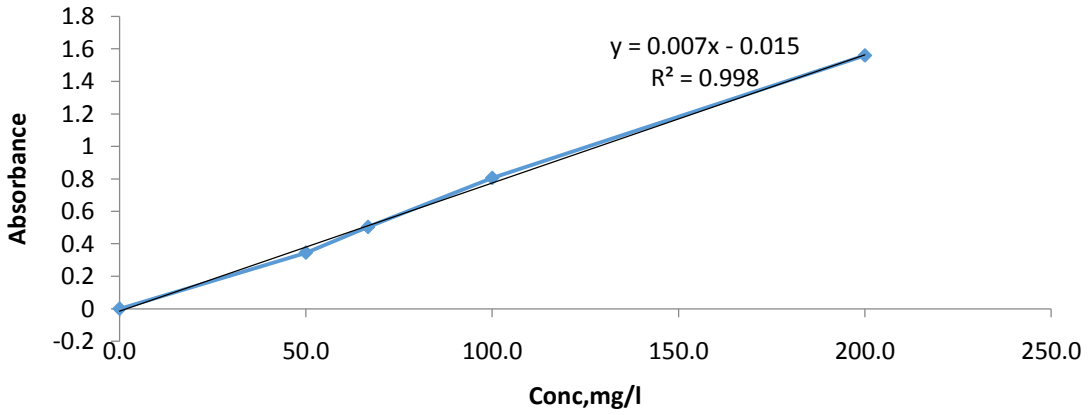


Figure C1: Conversion of absorbance to concentration in mg/l

Hence the resulting equation for the conversion of absorbance to concentration in mg/l is given as below;

C=A+0.017/0.007 (mg/l)

C=Concentration in mg/l

A=Absorbance

APPENDIX D

Data for the adsorption of phenol by sorbents

Table D1: Absorbance measurement for the adsorption of phenol by catalyst PB

Ad. Time(hrs)/Phenol conc.	500mg/l	250mg/l	125mg/l	62.5mg/l
0	2.991	1.686	0.891	0.461
1	2.929	1.637	0.849	0.427
2	2.877	1.589	0.818	0.411
4	2.779	1.521	0.788	0.397
6	2.736	1.499	0.768	0.391
8	2.736	1.499	0.769	0.391
10	2.737	1.499	0.768	0.391

Table D2: Concentration measurement for the adsorption of phenol by catalyst PB

Ad. Time(hrs)/Phenol conc.	500mg/l	250mg/l	125mg/l	62.5mg/l
0	429.714	243.286	129.714	68.286
1	420.857	236.286	123.714	63.429
2	413.429	229.429	119.286	61.143
4	399.429	219.714	115.000	59.143
6	393.286	216.571	112.143	58.286
8	393.286	216.571	112.286	58.286
10	393.429	216.571	112.143	58.286

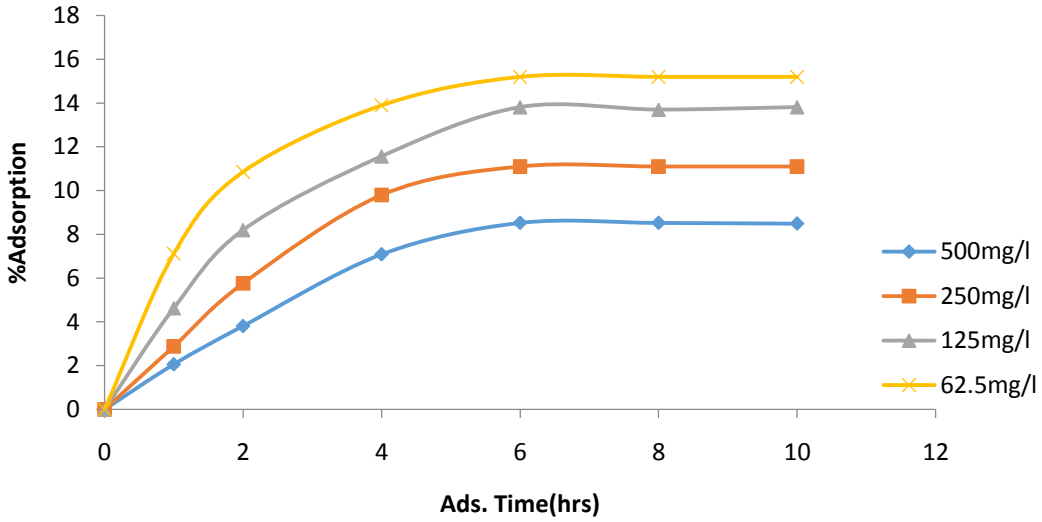


Figure D1: Percentage adsorption by catalyst PB

Table D3: Absorbance measurement for the adsorption of phenol by catalyst PBC

Ad. Time(hrs)/Phenol Conc.	500mg/l	250mg/l	125mg/l	62.5mg/l
0	2.991	1.686	0.891	0.461
1	2.819	1.557	0.802	0.399
2	2.757	1.512	0.771	0.381
4	2.658	1.441	0.728	0.351
6	2.578	1.378	0.693	0.341
8	2.578	1.378	0.693	0.341
10	2.578	1.378	0.693	0.341

Table D4: Concentration measurement for the adsorption of phenol by catalyst PBC

Ad. Time(hrs)/Phenol Conc.	500mg/l	250mg/l	125mg/l	62.5mg/l
0	429.714	243.286	129.714	68.286
1	405.143	224.857	117.000	59.429
2	396.286	218.429	112.571	56.857
4	382.143	208.286	106.429	52.571
6	370.714	199.286	101.429	51.143
8	370.714	199.286	101.429	51.143
10	370.714	199.286	101.429	51.143

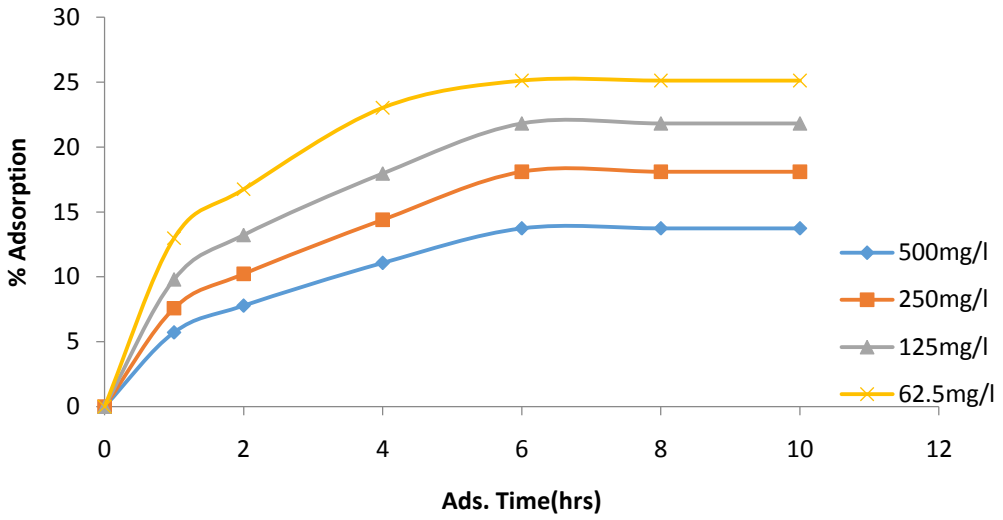


Figure D2: Percentage adsorption by catalyst PBC

Table D5: Absorbance measurement for the adsorption of phenol by catalyst PB-5

Ad. Time(hrs)/Phenol conc.	500mg/l	250mg/l	125mg/l	62.5mg/l
0	2.991	1.686	0.891	0.461
1	2.619	1.431	0.702	0.347
2	2.497	1.338	0.661	0.328
4	2.321	1.256	0.628	0.304
6	2.241	1.198	0.587	0.288
8	2.241	1.198	0.587	0.288
10	2.241	1.198	0.587	0.288

Table D6: Concentration measurement for the adsorption of phenol by catalyst PB-5

Ad. Time(hrs)/Phenol conc.	500mg/l	250mg/l	125mg/l	62.5mg/l
0	429.714	243.286	129.714	68.286
1	376.571	206.857	102.714	52.000
2	359.143	193.571	96.857	49.286
4	334.000	181.857	92.143	45.857
6	322.571	173.571	86.286	43.571
8	322.571	173.571	86.286	43.571
10	322.571	173.571	86.286	43.571

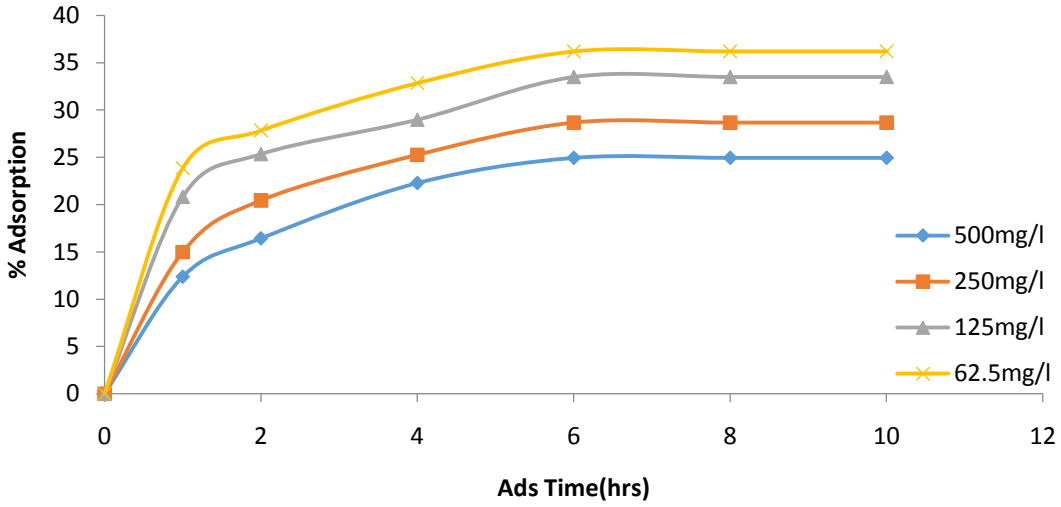


Figure D3: Percentage adsorption by catalyst PB-5

Table D7: Absorbance measurement for the adsorption of phenol by catalyst PB-60

Ad. Time (hrs)/Phenol conc	500mg/l	250mg/l	125mg/l	62.5mg/l
0	2.991	1.686	0.891	0.461
1	2.461	1.241	0.578	0.241
2	2.234	1.064	0.485	0.214
4	1.812	0.911	0.378	0.171
6	1.641	0.765	0.337	0.148
8	1.641	0.765	0.337	0.148
10	1.641	0.765	0.337	0.148

Table D8: Concentration measurement for the adsorption of phenol by catalyst PB-60

Ad. Time(hrs)/Phenol conc	500mg/l	250mg/l	125mg/l	62.5mg/l
0	429.714	243.286	129.714	68.286
1	354.000	179.714	85.000	36.857
2	321.571	154.429	71.714	33.000
4	261.286	132.571	56.429	26.857
6	236.857	111.714	50.571	23.571
8	236.857	111.714	50.571	23.571
10	236.857	111.714	50.571	23.571

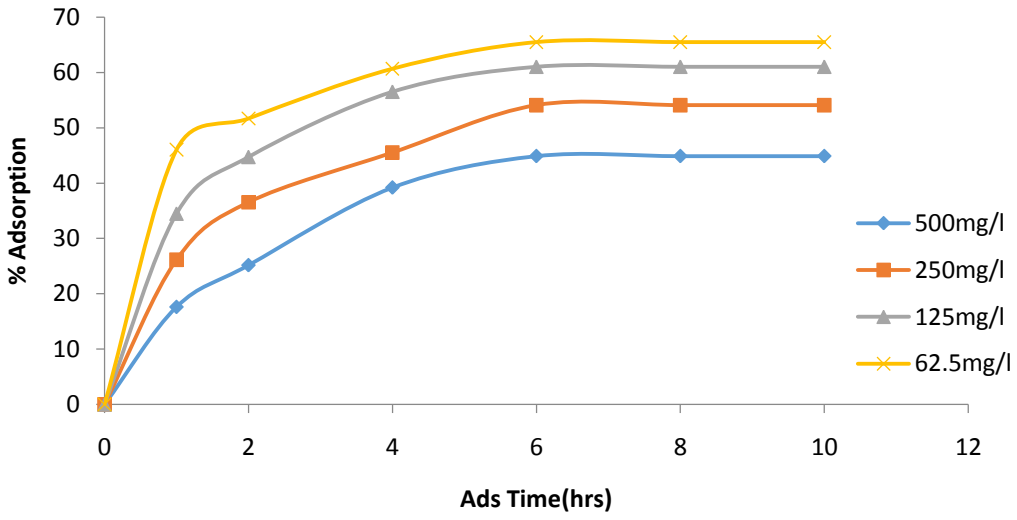


Figure D4: Percentage adsorption by catalyst PB-60

Table D9: Absorbance measurement for the adsorption of phenol by catalyst PB-60 at various pH values

Ad. Time(hrs)/pH	pH=5	pH=9	pH=11
0	2.991	2.991	2.991
1	2.211	2.301	2.367
2	2.111	2.235	2.288
4	2.007	2.118	2.178
6	1.801	1.926	2.101
8	1.801	1.926	2.101
10	1.801	1.926	2.101

Table D10: Concentration measurement for the adsorption of phenol by catalyst PB-60 at various pH values.

Ad. Time(hrs)/pH	pH=5	pH=9	pH=11
0	429.714	429.714	429.714
1	318.286	331.143	340.571
2	304.000	321.714	329.286
4	289.143	305.000	313.571
6	259.714	277.571	302.571
8	259.714	277.571	302.571
10	259.714	277.571	302.571

Table D11: Absorbance measurement for the adsorption of phenol by catalyst PB-60 at various catalyst dosages.

Ad. Time(hrs)/Dosage	1.5g	2.0g	2.5g	3.0g
0	2.991	2.991	2.991	2.991
1	2.764	2.579	2.461	2.229
2	2.466	2.387	2.234	2.077
4	2.260	2.017	1.812	1.655
6	2.007	1.823	1.641	1.511
8	2.007	1.823	1.641	1.511
10	2.007	1.823	1.641	1.511

Table D12: Concentration measurement for the adsorption of phenol by catalyst PB-60 at various catalyst dosages.

Ad. Time(hrs)/Dosage	1.5g	2.0g	2.5g	3.0g
0	429.714	429.714	429.714	429.714
1	397.286	370.857	354.000	320.857
2	354.714	343.429	321.571	299.143
4	325.286	290.571	261.286	238.857
6	289.143	262.857	236.857	218.286
8	289.143	262.857	236.857	218.286
10	289.143	262.857	236.857	218.286

APPENDIX E

Data of the photocatalytic degradation of phenol by sorbents

Table E1: Absorbance measurement for the photocatalytic degradation of phenol by catalyst PB at initial phenol concentrations.

Irrad. Time(mins)/Phenol conc.	500mg/l	250mg/l	125mg/l	62.5mg/l
0	2.737	1.488	0.768	0.332
30	2.701	1.415	0.703	0.282
90	2.611	1.381	0.667	0.263
120	2.589	1.343	0.649	0.249

Table E2: Concentration measurement for the photocatalytic degradation of phenol by catalyst PB at initial phenol concentrations.

Irrad. Time(mins)/Phenol conc.	500mg/l	250mg/l	125mg/l	62.5mg/l
0	393.429	215.000	112.143	49.857
30	388.286	204.571	102.857	42.714
90	375.429	199.714	97.714	40.000
120	372.286	194.286	95.143	38.000

Table E3: Absorbance measurement for the photocatalytic degradation of phenol by catalyst PBC at initial phenol concentrations.

Irrad. Time(mins)/Phenol conc.	500mg/l	250mg/l	125mg/l	62.5mg/l
0	2.578	1.378	0.693	0.341
30	2.412	1.115	0.533	0.222
90	2.111	0.996	0.457	0.181
120	1.825	0.843	0.409	0.149

Table E4: Concentration measurement for the photocatalytic degradation of phenol by catalyst PBC at initial phenol concentrations.

Irrad. Time(mins)/Phenol conc.	500mg/l	250mg/l	125mg/l	62.5mg/l
0	370.714	199.286	101.429	51.143
30	347.000	161.714	78.571	34.143
90	304.000	144.714	67.714	28.286
120	263.143	122.857	60.857	23.714

Table E5: Absorbance measurement for the photocatalytic degradation of phenol by catalyst PB-5 at initial phenol concentrations.

Irrad. Time(mins)/Phenol conc.	500mg/l	250mg/l	125mg/l	62.5mg/l
0	2.241	1.198	0.587	0.288
30	1.812	0.815	0.333	0.122
90	1.613	0.776	0.307	0.101
120	1.225	0.623	0.248	0.089

Table E6: Concentration measurement for the photocatalytic degradation of phenol by catalyst PB-5 at initial phenol concentrations.

Irrad. Time(mins)/Phenol conc.	500mg/l	250mg/l	125mg/l	62.5mg/l
0	322.571	173.571	86.286	43.571
30	261.286	118.857	50.000	19.857
90	232.857	113.286	46.286	16.857
120	177.429	91.429	37.857	15.143

Table E7: Absorbance measurement for the photocatalytic degradation of phenol by catalyst PB-60 at initial phenol concentrations.

Irrad. Time(mins)/Phenol conc.	500mg/l	250mg/l	125mg/l	62.5mg/l
0	1.641	0.765	0.337	0.148
30	1.249	0.415	0.133	0.042
90	1.137	0.356	0.097	0.021
120	0.897	0.283	0.068	0.011

Table E8: Concentration measurement for the photocatalytic degradation of phenol by catalyst PB-60 at initial phenol concentrations.

Irrad. Time(mins)/Phenol conc.	500mg/l	250mg/l	125mg/l	62.5mg/l
0	236.857	111.714	50.571	23.571
30	180.857	61.714	21.429	8.429
90	164.857	53.286	16.286	5.429
120	130.571	42.857	12.143	4.000

Table E9: Absorbance measurement for the effect of pH on the photocatalytic degradation of phenol by catalyst PB-60 at 500mg/l phenol conc.

Irrad. Time(mins)/pH	pH=11	pH=9	pH=5
0	1.801	1.926	2.101
30	1.258	0.858	0.633
90	1.125	0.803	0.572
120	1.017	0.733	0.431

Table E10: Concentration measurement for the effect of pH on the photocatalytic degradation of phenol by catalyst PB-60 at 500mg/l phenol conc.

Irrad. Time(mins)/pH	pH=11	pH=9	pH=5
0	259.714	277.571	302.571
30	182.143	125.000	92.857
90	163.143	117.143	84.143
120	147.714	107.143	64.000

Table E11: Absorbance measurement for the effect of catalyst dosage on the photocatalytic degradation of phenol by catalyst PB-60 at 500mg/l phenol conc.

Irrad. Time(mins)/dosage	1.5g	2.0g	2.5g	3.0g
0	2.207	2.101	1.881	1.811
30	1.649	1.485	1.249	1.242
90	1.535	1.356	1.137	1.131
120	1.402	1.286	1.005	1.051

Table E12: Concentration measurement for the effect of catalyst dosage on the photocatalytic degradation of phenol by catalyst PB-60 at 500mg/l phenol conc.

Irrad. Time(mins)/dosage	1.5g	2.0g	2.5g	3.0g
0	317.714	302.571	271.143	261.143
30	238.000	214.571	180.857	179.857
90	221.714	196.143	164.857	164.000
120	202.714	186.143	146.000	152.571

APENDIX F

Tables for the calculation of adsorption kinetic models for all the catalysts

Table F1: Kinetic adsorption model for catalyst PB at phenol concentration of 500mg/l

t(hrs)	C_t(mg/l)	q_t(mg/g)	q_e(mg/g)	q_e-q_t(mg/g)	log(q_e-q_t)(mg/g)	t/q_t(min.g/mg)	$t^{1/2}$($min^{1/2}$)
0	429.714	0.000	1.457	1.457	0.164	0	0
1	420.857	0.354	1.457	1.103	0.043	2.823	1.000
2	413.429	0.651	1.457	0.806	-0.094	3.070	1.414
4	399.429	1.211	1.457	0.246	-0.610	3.302	2.000
6	393.286	1.457	1.457	0.000	0.000	4.118	2.449
8	393.286	1.457	1.457	0.000	0.000	5.490	2.828
10	393.286	1.457	1.457	0.000	0.000	6.863	3.162

Table F2: Kinetic adsorption model for catalyst PBC at phenol concentration of 500mg/l

t(hrs)	C_t(mg/l)	q_t(mg/g)	q_e(mg/g)	q_e-q_t(mg/g)	log(q_e-q_t)(mg/g)	t/q_t(min.g/mg)	$t^{1/2}$($min^{1/2}$)
0	429.714	0.000	2.360	2.360	0.373	0	0
1	405.143	0.983	2.360	1.377	0.139	1.017	1.000
2	396.286	1.337	2.360	1.023	0.010	1.496	1.414
4	379.143	2.023	2.360	0.337	-0.472	1.977	2.000
6	370.714	2.360	2.360	0.000	0.000	2.542	2.449
8	370.714	2.360	2.360	0.000	0.000	3.390	2.828
10	370.714	2.360	2.360	0.000	0.000	4.237	3.162

Table F3: Kinetic adsorption model for catalyst PB-5 at phenol concentration of 500mg/l

t(hrs)	C_t(mg/l)	q_t(mg/g)	q_e(mg/g)	q_e-q_t(mg/g)	log(q_e-q_t)(mg/g)	t/q_t(min.g/mg)	$t^{1/2}$($min^{1/2}$)
0	429.714	0.000	4.446	4.446	0.648	0	0
1	376.571	2.126	4.286	2.160	0.334	0.470	1.000
2	359.142	2.823	4.286	1.463	0.165	0.708	1.414
4	334.000	3.829	4.286	0.457	-0.340	1.045	2.000
6	318.571	4.446	4.286	-0.160	0.000	1.350	2.449
8	318.571	4.446	4.286	-0.160	0.000	1.799	2.828
10	318.571	4.446	4.286	-0.160	0.000	2.249	3.162

Table F4: Kinetic adsorption model for catalyst PB-60 at phenol concentration of 500mg/l

t(hrs)	C_t(mg/l)	q_t(mg/g)	q_e(mg/g)	q_e-q_t(mg/g)	log(q_e-q_t)(mg/g)	t/q_t(min.g/mg)	$t^{1/2}$($min^{1/2}$)
0	429.714		8.514	8.514	0.930	0	0
1	354.000	3.029	7.714	4.686	0.671	0.330	1.000
2	308.571	4.846	7.714	2.869	0.458	0.413	1.414
4	258.285	6.857	7.714	0.857	-0.067	0.583	2.000
6	216.857	8.514	7.714	-0.800	0.000	0.705	2.449
8	216.857	8.514	7.714	-0.800	0.000	0.940	2.828
10	216.857	8.514	7.714	-0.800	0.000	1.174	3.162

Table F5: Kinetic adsorption model for catalyst PB at phenol concentration of 250mg/l

t(hrs)	C_t(mg/l)	q_t(mg/g)	q_e(mg/g)	q_e-q_t(mg/g)	log(q_e-q_t)(mg/g)	t/q_t(min.g/mg)	$t^{1/2}$($min^{1/2}$)
0	243.286	0.000	0.989	0.989	-0.005	0	0
1	233.286	0.400	1.069	0.669	-0.175	2.500	1.000
2	230.429	0.514	1.069	0.554	-0.256	3.889	1.414
4	225.414	0.715	1.069	0.354	-0.451	5.596	2.000
6	218.571	0.989	1.069	0.080	0.000	6.069	2.449
8	218.571	0.989	1.069	0.080	0.000	8.092	2.828
10	218.571	0.989	1.069	0.080	0.000	10.116	3.162

Table F6: Kinetic adsorption model for catalyst PBC at phenol concentration of 250mg/l

t(hrs)	C_t(mg/l)	q_t(mg/g)	q_e(mg/g)	q_e-q_t(mg/g)	log(q_e-q_t)(mg/g)	t/q_t(min.g/mg)	$t^{1/2}$($min^{1/2}$)
0	243.286	0.000	1.760	1.760	0.246		
1	224.857	0.737	1.760	1.023	0.010	1.357	1.000
2	220.428	0.914	1.760	0.846	-0.073	2.187	1.414
4	208.286	1.400	1.760	0.360	-0.444	2.857	2.000
6	199.286	1.760	1.760	0.000	0.000	3.409	2.449
8	199.286	1.760	1.760	0.000	0.000	4.545	2.828
10	199.286	1.760	1.760	0.000	0.000	5.682	3.162

Table F7: Kinetic adsorption model for catalyst PB-5 at phenol concentration of 250mg/l

t(hrs)	C_t(mg/l)	q_t(mg/g)	q_e(mg/g)	q_e-q_t(mg/g)	log(q_e-q_t)(mg/g)	t/q_t(min.g/mg)	$t^{1/2}$($min^{1/2}$)
0	243.286	0.000	2.669	2.669	0.426	0	0
1	220.857	0.897	2.669	1.771	0.248	1.115	1.000
2	210.571	1.309	2.669	1.360	0.134	1.528	1.414
4	189.857	2.137	2.669	0.531	-0.275	1.872	2.000
6	176.571	2.669	2.669	0.000	0.000	2.248	2.449
8	176.571	2.669	2.669	0.000	0.000	2.998	2.828
10	176.571	2.669	2.669	0.000	0.000	3.747	3.162

Table F8: Kinetic adsorption model for catalyst PB-60 at phenol concentration of 250mg/l

t(hrs)	C_t(mg/l)	q_t(mg/g)	q_e(mg/g)	q_e-q_t(mg/g)	log(q_e-q_t)(mg/g)	t/q_t(min.g/mg)	$t^{1/2}$($min^{1/2}$)
0	243.286	0.000	5.263	5.263	0.721	0	0
1	189.714	2.143	5.263	3.120	0.494	0.467	1.000
2	164.429	3.154	5.263	2.109	0.324	0.634	1.414
4	132.571	4.429	5.263	0.834	-0.079	0.903	2.000
6	111.714	5.263	5.263	0.000	0.000	1.140	2.449
8	111.714	5.263	5.263	0.000	0.000	1.520	2.828
10	111.714	5.263	5.263	0.000	0.000	1.900	3.162

Table F9: Kinetic adsorption model for catalyst PB at phenol concentration of 125mg/l

t(hrs)	C_t(mg/l)	q_t(mg/g)	q_e(mg/g)	q_e-q_t(mg/g)	log(q_e-q_t)(mg/g)	t/q_t(min.g/mg)	$t^{1/2}$($min^{1/2}$)
0	129.714	0.000	0.503	0.503	-0.299	0	0
1	126.714	0.120	0.583	0.463	-0.335	8.333	1.000
2	122.286	0.297	0.583	0.286	-0.544	6.731	1.414
4	119.000	0.429	0.583	0.154	-0.812	9.333	2.000
6	117.143	0.503	0.583	0.080	0.000	11.932	2.449
8	117.143	0.503	0.583	0.080	0.000	15.909	2.828
10	117.143	0.503	0.583	0.080	0.000	19.886	3.162

Table F10: Kinetic adsorption model for catalyst PBC at phenol concentration of 125mg/l

t(hrs)	C_t(mg/l)	q_t(mg/g)	q_e(mg/g)	q_e-q_t(mg/g)	log(q_e-q_t)(mg/g)	t/q_t(min.g/mg)	$t^{1/2}$($min^{1/2}$)
0	129.714	0.000	1.131	1.131	0.054		
1	117.000	0.509	1.131	0.623	-0.206	1.966	1.000
2	112.571	0.686	1.131	0.446	-0.351	2.917	1.414
4	107.429	0.891	1.131	0.240	-0.620	4.487	2.000
6	101.429	1.131	1.131	0.000	0.000	5.303	2.449
8	101.429	1.131	1.131	0.000	0.000	7.071	2.828
10	101.429	1.131	1.131	0.000	0.000	8.838	3.162

Table F11: Kinetic adsorption model for catalyst PB-5 at phenol concentration of 125mg/l

t(hrs)	C_t(mg/l)	q_t(mg/g)	q_e(mg/g)	q_e-q_t(mg/g)	log(q_e-q_t)(mg/g)	t/q_t(min.g/mg)	$t^{1/2}$($min^{1/2}$)
0	129.714	0.000	1.737	1.737	0.240		
1	112.714	0.680	1.737	1.057	0.024	1.471	1.000
2	102.857	1.074	1.737	0.663	-0.179	1.862	1.414
4	94.143	1.423	1.737	0.314	-0.503	2.811	2.000
6	86.286	1.737	1.737	0.000	0.000	3.454	2.449
8	86.286	1.737	1.737	0.000	0.000	4.605	2.828
10	86.286	1.737	1.737	0.000	0.000	5.757	3.162

Table F12: Kinetic adsorption model for catalyst PB-60 at phenol concentration of 125mg/l

t(hrs)	C_t(mg/l)	q_t(mg/g)	q_e(mg/g)	q_e-q_t(mg/g)	log(q_e-q_t)(mg/g)	t/qt(min.g/mg)	$t^{1/2}$($min^{1/2}$)
0	129.714	0.000	3.166	3.166	0.500	0	0
1	97.000	1.309	3.166	1.857	0.269	0.764	1.000
2	78.714	2.040	3.166	1.126	0.051	0.980	1.414
4	60.429	2.771	3.166	0.394	-0.404	1.443	2.000
6	50.571	3.166	3.166	0.000	0.000	1.895	2.449
8	50.571	3.166	3.166	0.000	0.000	2.527	2.828
10	50.571	3.166	3.166	0.000	0.000	3.159	3.162

Table F13: Kinetic adsorption model for catalyst PB at phenol concentration of 62.5mg/l

t(hrs)	C_t(mg/l)	q_t(mg/g)	q_e(mg/g)	q_e-q_t(mg/g)	log(q_e-q_t)(mg/g)	t/q_t(min.g/mg)	$t^{1/2}$($min^{1/2}$)
0	68.286	0.000	0.448	0.448	-0.349	-	0.000
1	63.429	0.194	0.448	0.254	-0.596	5.147	1.000
2	60.143	0.326	0.448	0.122	-0.913	6.140	1.414
4	58.143	0.406	0.448	0.042	-1.374	9.859	2.000
6	57.086	0.448	0.448	0.000	0.000	13.393	2.449
8	57.086	0.448	0.448	0.000	0.000	17.857	2.828
10	57.086	0.448	0.448	0.000	0.000	22.321	3.162

Table F14: Kinetic adsorption model for catalyst PBC at phenol concentration of 62.5mg/l

t(hrs)	C_t(mg/l)	q_t(mg/g)	q_e(mg/g)	q_e-q_t(mg/g)	log(q_e-q_t)(mg/g)	t/q_t(min.g/mg)	$t^{1/2}$($min^{1/2}$)
0	68.286	0.000	0.686	0.686	-0.164		0.000
1	59.429	0.354	0.686	0.331	-0.480	2.823	1.000
2	55.857	0.497	0.686	0.189	-0.725	4.023	1.414
4	52.571	0.629	0.686	0.057	-1.243	6.364	2.000
6	51.143	0.686	0.686	0.000	0.000	8.750	2.449
8	51.143	0.686	0.686	0.000	0.000	11.667	2.828
10	51.143	0.686	0.686	0.000	0.000	14.583	3.162

Table F15: Kinetic adsorption model for catalyst PB-5 at phenol concentration of 62.5mg/l

t(hrs)	C_t(mg/l)	q_t(mg/g)	q_e(mg/g)	q_e-q_t(mg/g)	log(q_e-q_t)(mg/g)	t/q_t(min.g/mg)	$t^{1/2}$($min^{1/2}$)
0	68.286	0.000	0.989	0.989	-0.005		0.000
1	57.000	0.451	0.989	0.537	-0.270	2.215	1.000
2	50.106	0.727	0.989	0.261	-0.583	2.750	1.414
4	45.557	0.909	0.989	0.079	-1.100	4.400	2.000
6	43.571	0.989	0.989	0.000	0.000	6.069	2.449
8	43.571	0.989	0.989	0.000	0.000	8.092	2.828
10	43.571	0.989	0.989	0.000	0.000	10.116	3.162

Table F16: Kinetic adsorption model for catalyst PB-60 at phenol concentration of 62.5mg/l

t(hrs)	C_t(mg/l)	q_t(mg/g)	q_e(mg/g)	q_e-q_t(mg/g)	log(q_e-q_t)(mg/g)	t/q_t(min.g/mg)	$t^{1/2}$($min^{1/2}$)
0	68.286	0.000	1.789	1.789	0.253	-	0.000
1	46.157	0.885	1.789	0.903	-0.044	1.130	1.000
2	35.637	1.306	1.789	0.483	-0.316	1.531	1.414
4	26.857	1.657	1.789	0.131	-0.881	2.414	2.000
6	23.571	1.789	1.789	0.000	0.000	3.355	2.449
8	23.571	1.789	1.789	0.000	0.000	4.473	2.828
10	23.571	1.789	1.789	0.000	0.000	5.591	3.162

Table F17: Equilibrium adsorption isotherm model for catalyst PB.

Ads Conc.	C_e(mg/l)	q_e(mg/g)	$1/C_e$(l/mg)	$1/q_e$(g/mg)	lnC_e(mg/l)	lnq_e(mg/g)
500mg/l	381.286	1.937	0.003	0.516	5.944	0.661
250mg/l	218.571	0.989	0.005	1.012	5.387	-0.011
125mg/l	115.143	0.583	0.009	1.716	4.746	-0.540
62.5mg/l	57.086	0.448	0.018	2.232	4.045	-0.803

Table F18: Equilibrium adsorption isotherm model for catalyst PBC.

Ads Conc.	C_e(mg/l)	q_e(mg/g)	$1/C_e$(l/mg)	$1/q_e$(g/mg)	lnC_e(mg/l)	lnq_e(mg/g)
500mg/l	370.714	2.360	0.003	0.424	5.915	0.859
250mg/l	199.286	1.760	0.005	0.568	5.295	0.565
125mg/l	103.429	1.051	0.010	0.951	4.639	0.050
62.5mg/l	51.143	0.686	0.020	1.458	3.935	-0.377

*T*able F19: Equilibrium adsorption isotherm model for catalyst PB-5.

Ads Conc.	C_e(mg/l)	q_e(mg/g)	$1/C_e$(l/mg)	$1/q_e$(g/mg)	lnC_e(mg/l)	lnq_e(mg/g)
500mg/l	318.571	4.446	0.003	0.225	5.764	1.492
250mg/l	176.571	2.669	0.006	0.375	5.174	0.982
125mg/l	86.286	1.737	0.012	0.576	4.458	0.552
62.5mg/l	40.571	1.109	0.025	0.902	3.703	0.103

Table F20: Equilibrium adsorption isotherm model for catalyst PB-60

Ads Conc.	C_e(mg/l)	q_e(mg/g)	$1/C_e$(l/mg)	$1/q_e$(g/mg)	$\ln C_e$(mg/l)	$\ln q_e$(mg/g)
500mg/l	216.857	8.514	0.005	0.117	5.379	2.142
250mg/l	111.714	5.263	0.009	0.190	4.716	1.661
125mg/l	50.571	3.166	0.020	0.316	3.923	1.152
62.5mg/l	23.571	1.789	0.042	0.559	3.160	0.581

APPENDIX G

Below are the tables for the calculation of Langmuir-Hinshelwood kinetic model for all the catalysts.

Table G1: Langmuir-Hinshelwood kinetic model for catalyst PB at reaction time of 30mins.

ro	Co	1/ro	1/Co
0.333	393.000	3.000	0.00254
0.348	215.000	2.877	0.00465
0.310	112.143	3.231	0.00892
0.238	49.857	4.200	0.02006

Table G2: Langmuir-Hinshelwood kinetic model for catalyst PB at reaction time of 90mins.

ro	Co	1/ro	1/Co
0.200	393.000	5.000	0.00254
0.170	215.000	5.888	0.00465
0.160	112.143	6.238	0.00892
0.110	49.857	9.130	0.02006

Table G3: Langmuir-Hinshelwood kinetic model for catalyst PB at reaction time of 120mins.

ro	Co	1/ro	1/Co
0.176	393.000	5.676	0.00254
0.173	215.000	5.793	0.00465
0.142	112.143	7.059	0.00892
0.087	49.857	11.507	0.02006

Table G4: Langmuir-Hinshelwood kinetic model for catalyst PBC at reaction time of 30mins.

ro	Co	1/ro	1/Co
1.224	370.714	0.817	0.00270
1.252	199.286	0.798	0.00502
0.762	101.429	1.313	0.00986
0.462	51.143	2.165	0.01955

Table G5: Langmuir-Hinshelwood kinetic model for catalyst PBC at reaction time of 90mins.

ro	Co	1/ro	1/Co
0.741	370.714	1.349	0.00270
0.606	199.286	1.649	0.00502
0.375	101.429	2.669	0.00986
0.219	51.143	4.565	0.01955

Table G6: Langmuir-Hinshelwood kinetic model for catalyst PBC at reaction time of 120mins.

ro	Co	1/ro	1/Co
0.932	370.714	1.073	0.00270
0.567	199.286	1.765	0.00502
0.326	101.429	3.066	0.00986
0.212	51.143	4.719	0.01955

Table G7: Langmuir-Hinshelwood kinetic model for catalyst PB-5 at reaction time of 30mins.

ro	Co	1/ro	1/Co
2.043	322.571	0.490	0.00310
1.348	173.571	0.742	0.00576
0.971	86.286	1.029	0.01159
0.505	43.571	1.981	0.02295

Table G8: Langmuir-Hinshelwood kinetic model for catalyst PB-5 at reaction time of 90mins.

ro	Co	1/ro	1/Co
0.997	322.571	1.003	0.00310
0.717	173.571	1.394	0.00576
0.444	86.286	2.250	0.01159
0.249	43.571	4.013	0.02295

Table G9: Langmuir-Hinshelwood kinetic model for catalyst PB-5 at reaction time of 120mins.

ro	Co	1/ro	1/Co
1.107	322.571	0.903	0.00310
0.685	173.571	1.461	0.00576
0.368	86.286	2.718	0.01159
0.237	43.571	4.221	0.02295

Table G10: Langmuir-Hinshelwood kinetic model for catalyst PB-60 at reaction time of 30mins.

ro	Co	1/ro	1/Co
2.976	236.857	0.336	0.00422
1.952	111.714	0.512	0.00895
0.971	50.571	1.029	0.01977
0.505	23.571	1.981	0.04242

Table G11: Langmuir-Hinshelwood kinetic model for catalyst PB-60 at reaction time of 90mins.

ro	Co	1/ro	1/Co
1.159	236.857	0.863	0.00422
0.681	111.714	1.469	0.00895
0.381	50.571	2.625	0.01977
0.186	23.571	5.385	0.04242

Table G12: Langmuir-Hinshelwood kinetic model for catalyst PB-60 at reaction time of 120mins.

ro	Co	1/ro	1/Co
1.206	236.857	0.829	0.00422
0.645	111.714	1.550	0.00895
0.344	50.571	2.907	0.01977
0.175	23.571	5.714	0.04242

Table G13: Kinetic model for catalyst PB-60 at various solution pH.

Irrad. Time(mins)/pH	**C@pH11**	**C@pH9**	**C@pH5**	**lnC@pH11**	**lnC@pH9**	**lnC@pH5**
0	259.714	277.571	302.571	5.560	5.626	5.712
30	176.429	125.000	101.429	5.173	4.828	4.619
90	163.143	92.714	62.143	5.095	4.530	4.129
120	149.143	75.429	46.000	5.005	4.323	3.829

Table G14: Kinetic model for catalyst PB-60 at various sorbent dose.

Irrad. Time(mins)/pH	C@1.5g	C@2.0g	C@2.5g	C@3.0g	lnC@1.5g	lnC@2.0g	lnC@2.5g	lnC@3.0g
0	272.571	262.857	236.857	258.286	5.608	5.572	5.467	5.554
30	240.857	243.143	188.000	219.857	5.484	5.494	5.236	5.393
90	230.286	200.429	122.000	157.857	5.439	5.300	4.804	5.062
120	207.714	163.286	97.857	132.571	5.336	5.096	4.584	4.887

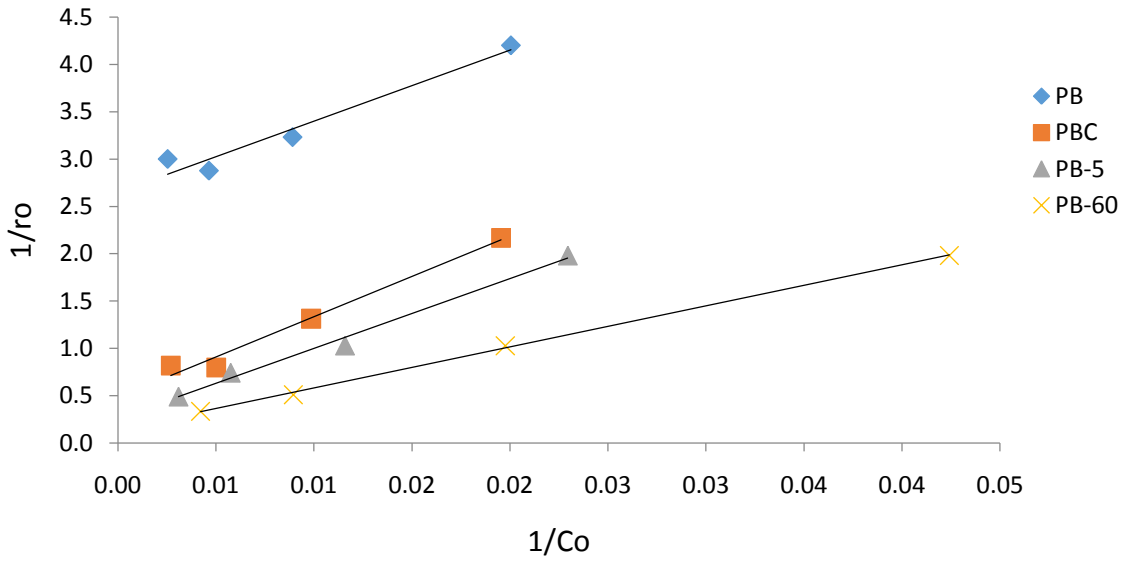


Fig. G1 Langmuir-Hinshelwood kinetic model for photocatalytic degradation of phenol using PB, PBC, PB-5 and PB-60

1. *Langmuir adsorption isotherm for the raw and acid treated clays*

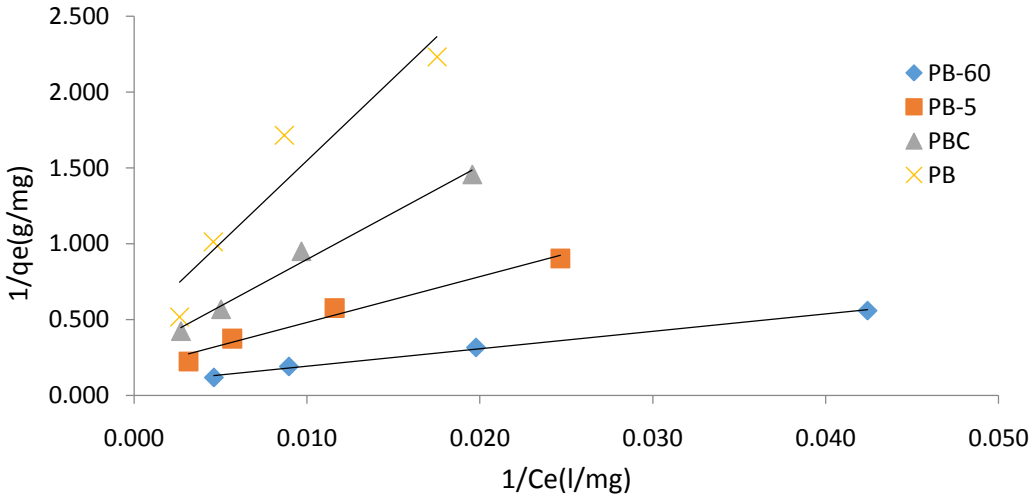


Fig. G2 Langmuir adsorption isotherms for the raw and treated Pindiga clays

2. *Freundlich adsorption isotherm for the raw and acid treated clays*

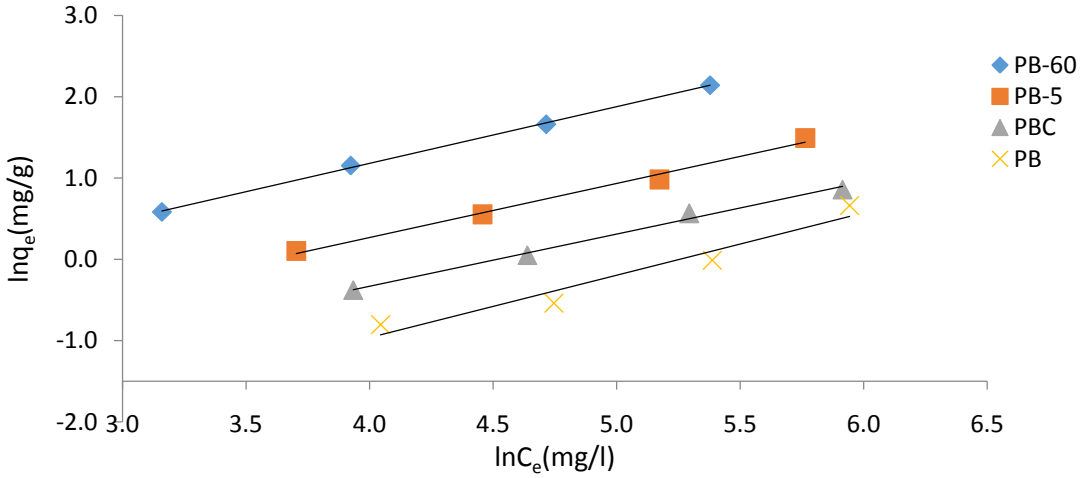


Fig. G3 Freundlich adsorption isotherms for the raw and treated Pindiga clays

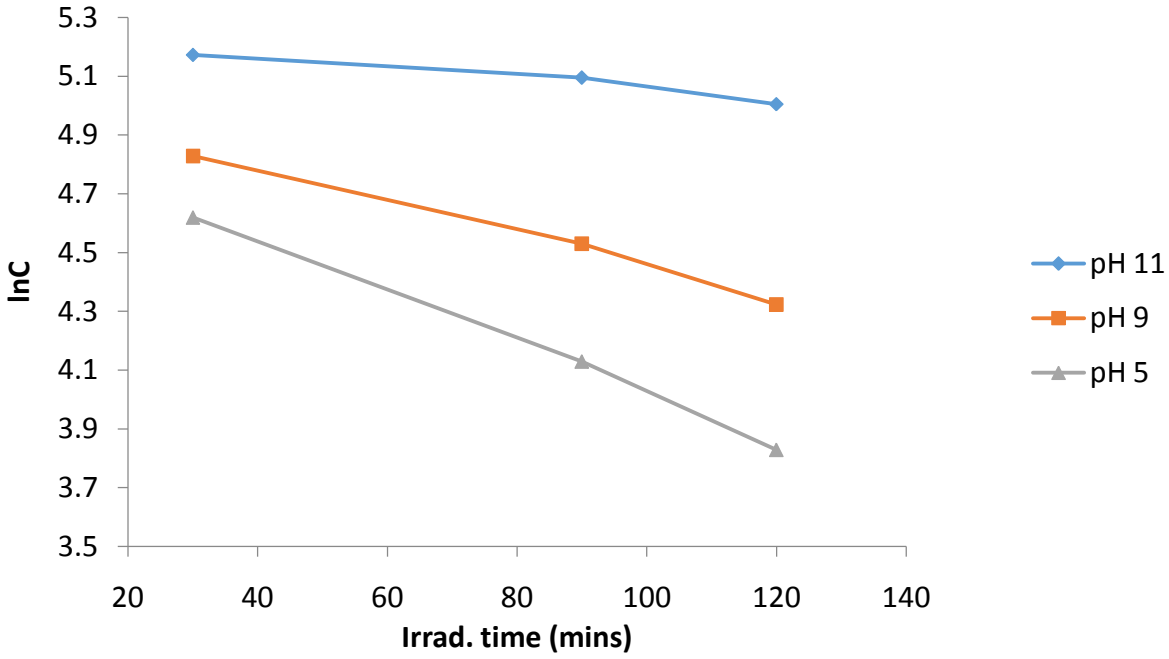


Fig. G2 Effect of solution pH on the photocatalytic degradation of phenol by PB-60 at phenol concentration of 500mg/*l*

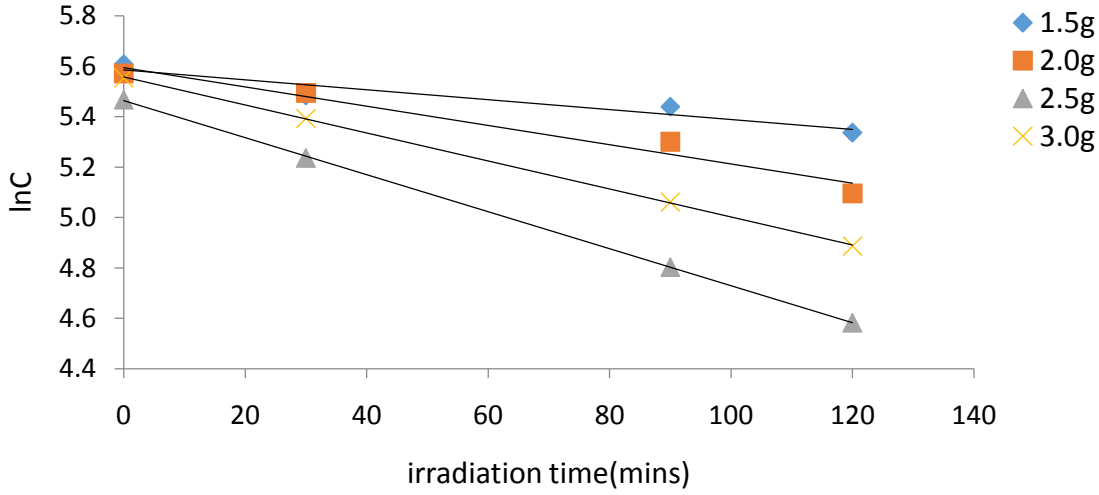


Fig. G3 Effect of catalyst dosage on the photocatalytic degradation of phenol with phenol concentration of 500mg/l by PB-60.

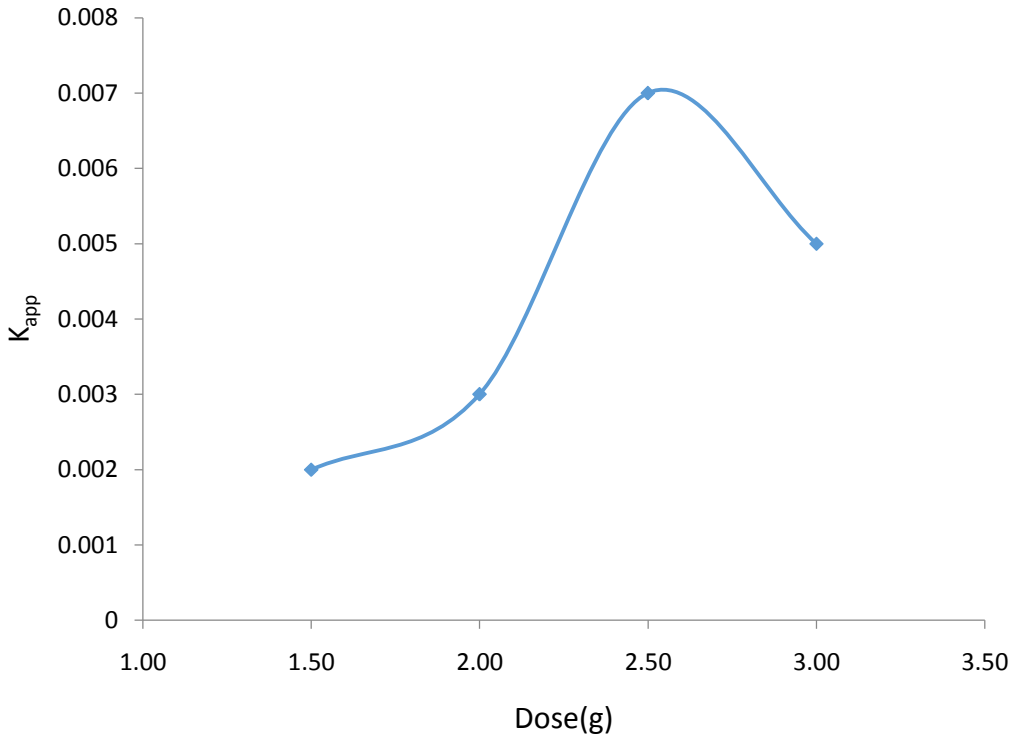


Fig. G4 Effect of catalyst dosage on the photocatalytic degradation of phenol with phenol concentration of 500mg/l by PB-60.